MAGNETOTELLURIC SURVEY

ON THE

MT. SPURR GEOTHERMAL EXPLORATION PROJECT

ALASKA

FOR

ORMAT TECHNOLOGIES INC.

DATA ACQUISITION AND PROCESSING

ZONGE JOB# 2010.118

ISSUE DATE: 27 DECEMBER 2011

ZONGE GEOSCIENCES INC.
924 Greg Street
Sparks, Nevada 89431

TABLE OF CONTENTS

INTRODUCTION **1**

DATA ACQUISITION **3**

INSTRUMENTATION **4**

SURVEY CONTROL **4**

DATA PROCESSING **5**

STATIC CORRECTIONS **5**

1-D INVERSION **6**

MT PARAMETER DEFINITIONS AND COMPUTATIONS **7**

DATA QUALITY **10**

DATA PRESENTATION **11**

SAFETY AND ENVIRONMENTAL ISSUES **12**

REFERENCES. **13**

APPENDIX A: DATA PLOTS **14**

APPENDIX B: MT DATA CURVES **52**

APPENDIX C: LOGISTICS **66**

APPENDIX D: MT STATION LOCATIONS **70**

APPENDIX E: INSTRUMENT SPECIFICATIONS **72**

APPENDIX F: OVERVIEW OF MAGNETOTELLURICS **75**

APPENDIX G: GEOMAGNETIC INDICES **81**

APPENDIX H: FILE STRUCTURES **82**

LIST OF FIGURES

Figure 1. Mt. Spurr, Alaska location map. 2
Figure 2: MT station location map. 2
Figure 3: MT field configuration. 3
Figure 4: MT Station Locations. 15
Figure 5: Contour map of determinant resistivity at 128 Hz. 16
Figure 6: Contour map of determinant phase at 128 Hz. 17
Figure 7: Contour map of Tipper magnitude at 128 Hz. 18
Figure 8: Contour map of determinant resistivity at 8 Hz. 19
Figure 9: Contour map of determinant phase at 8 Hz. 20
Figure 10: Contour map of Tipper magnitude at 8 Hz. 21
Figure 11: Contour map of determinant resistivity at 1 Hz. 22
Figure 12: Contour map of determinant phase at 1 Hz. 23
Figure 13: Contour map of Tipper magnitude at 1Hz. 24
Figure 14: Contour map of determinant resistivity at 0.125 Hz. 25
Figure 15: Contour map of determinant phase at 0.125Hz. 26
Figure 16: Contour map of Tipper magnitude at 0.125 Hz. 27
Figure 17: MT station location map, showing profiles. 28
Figure 18: Observed Zxy, Profile 1. 29
Figure 19: Observed Zyx, Profile 1. 30
Figure 20: Observed Zxy, Profile 2. 31
Figure 21: Observed Zyx, Profile 2. 32
Figure 22: Observed Zxy, Profile 3. 33
Figure 23: Observed Zyx, Profile 3. 34
Figure 24: Observed Zxy, Profile 4. 35
Figure 25: Observed Zyx Profile 4. 36
Figure 26: Observed Zxy, Profile 5. 37
Figure 27: Observed Zyx, Profile 5. 38
Figure 28: Observed Zxy, Profile 6. 39
Figure 29: Observed Zyx, Profile 6. 40

Figure 30: Section of 1D inversion results, Profile 1..... 41
Figure 31: Section of 1D inversion results, Profile 2..... 42
Figure 32: Section of 1D inversion results, Profile 3..... 43
Figure 33: Section of 1D inversion results, Profile 4..... 44
Figure 34: Section of 1D inversion results, Profile 5..... 45
Figure 35: Section of 1D inversion results, Profile 6..... 46
Figure 36: Contour map of 1D inversion results, 0m elevation..... 47
Figure 37: Contour map of 1D inversion results, -400m elevation. 48
Figure 38: Contour map of 1D inversion results, -800m elevation. 49
Figure 39: Contour map of 1D inversion results. -1400m elevation. 50
Figure 40: Contour map of 1D inversion results, -2200m elevation. 51

MAGNETOTELLURIC SURVEY

ON THE

MOUNT SPURR PROJECT

INTRODUCTION

Zonge Geosciences, Inc. performed a magnetotelluric (MT) survey on the Mt. Spurr, Geothermal Exploration Project, Alaska, for ORMAT Technologies Inc. This survey was conducted during the period of 12 July 2010 to 31 August 2010 and is covered under Zonge job number 2010.118. Daily field activities are summarized in the logistics report in Appendix B.

The general location of Mt. Spurr is shown in Figure 1. Full tensor magnetotelluric data were acquired at 49 stations in the survey area. Mt. Spurr (61^{o}17'59" N, 152^{o}15'05"W) is the highest volcano in the Aleutian Volcanic Arc. It is currently classified as non-active (USGS Code Green). The survey area is located along the mountain's southern flank. Station locations are shown in Figure 2. The objective of the survey was to investigate the resistivity structure beneath the area of interest to help guide exploration for a geothermal resource.

Zonge's Geophysical Field Supervisor for this project was Jerrod Davis. Data processing was conducted by Nicole Pendrigh, Geophysicist for Zonge Geosciences Inc.

This report covers data acquisition and processing and includes one-dimensional inversion results.

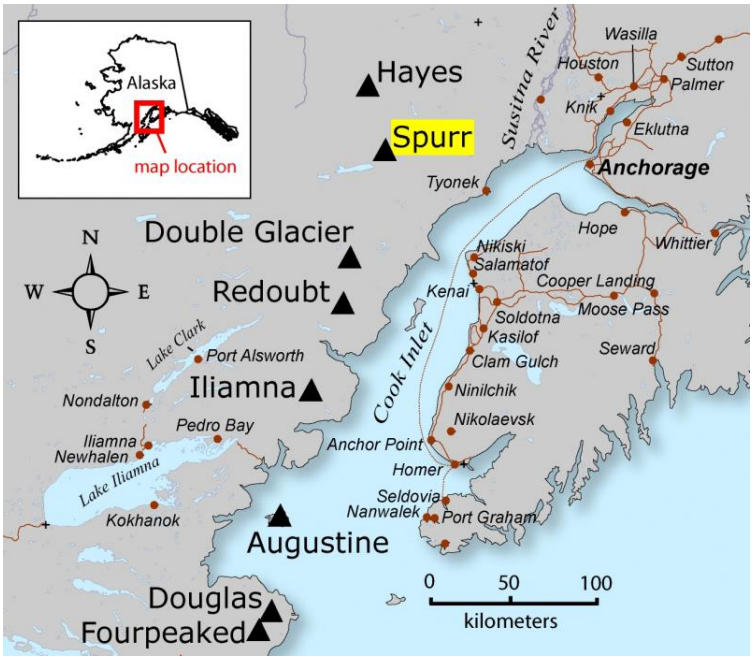

Figure 1. Mt. Spurr, Alaska location map.

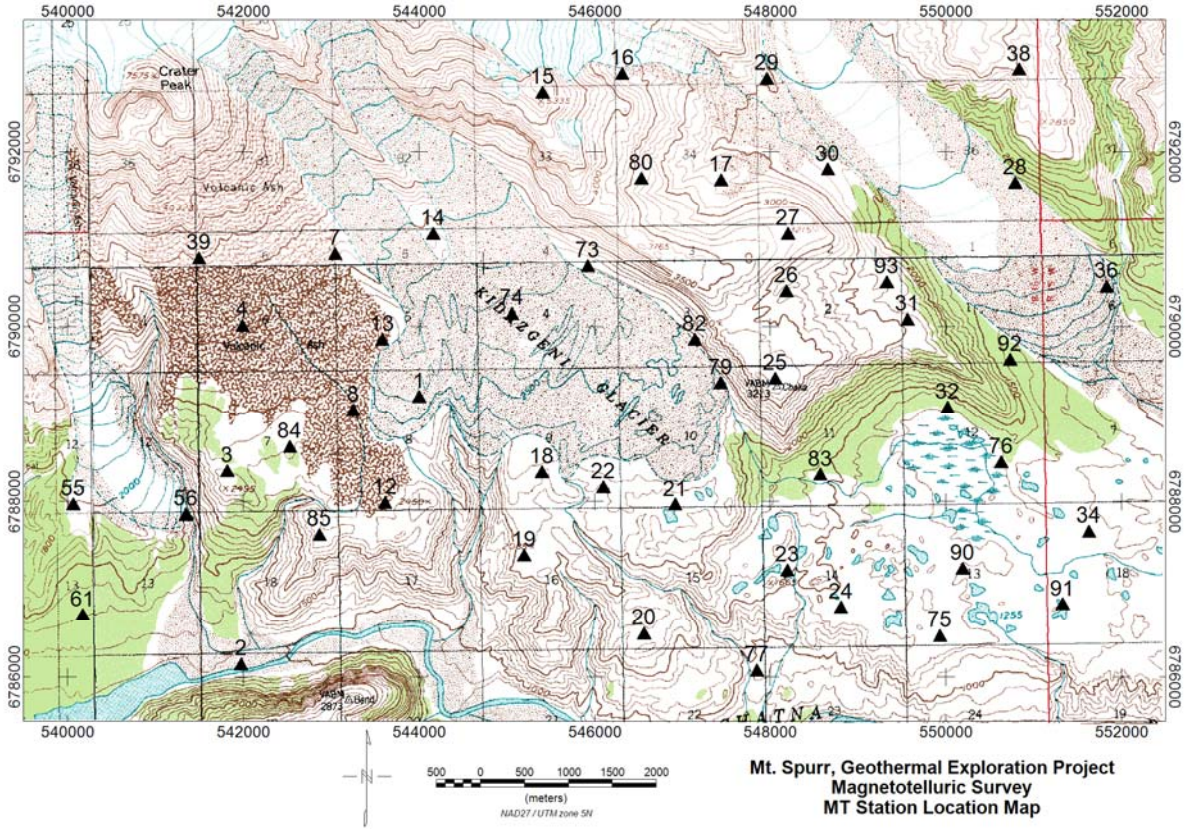

Figure 2: MT station location map.

DATA ACQUISITION

Full-tensor MT data were acquired at 49 stations in the Mt. Spurr area. Each station consisted of two orthogonal electric-field dipoles, Ex and Ey, which were each 100 m long, and two horizontal magnetic antennas Hx and Hy, oriented in the East and North directions respectively, as shown in Figure 3. In addition a third magnetic antenna (Hz) was oriented vertically. Time-series data were recorded and post-acquisition processed over frequency bands ranging from 0.0029 to 1024 hertz. The 49 MT stations were referenced to an MT station at a remote location in order to achieve greater signal-to-noise (Gamble et al, 1985). Initially the survey was designed so that two receivers would operate in widely-separated portions of the survey area, which was planned to extend approximately twice as far to the west. The intent was for mutual remote-referencing between these receivers. As operations began, constraints on helicopter operation due to weather resulted in the receivers being limited to the eastern half of the planned survey area. A third GDP receiver was established as a remote reference at a site near the village of Tyonek on August 1 and was relocated to a more accessible site on August 8.

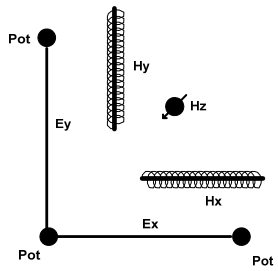

Figure 3: MT field configuration.

Transient electromagnetic (TEM) data were also acquired at the 49 MT sites to provide information to correct for MT static shift caused by near-surface resistivity variations. A 100m transmitter loop was used, with the Ex and Ey dipoles forming two sides of the square transmitter loop. Measurements of the decaying magnetic field (dB/dt) were made in the center of the loop.

Mt. Spurr proved a challenging operating environment due to extremes of weather, topography and vegetation. Crew activity was delayed or prevented on numerous days due to grounding of the helicopter in dense fog. Crews were stranded on a few occasions and spent the

night away from camp. Much of the area was densely covered with trees and shrubs, nearly impenetrable and without nearby landing zones for the helicopter. Vegetation is estimated to be the single biggest factor in determining the location of the MT stations. Very steep topography, unstable ground, flowing water and swamps provided additional constraints on the station locations.

INSTRUMENTATION

Data were acquired with three Zonge model GDP-32/II multiple purpose receivers, serial numbers 3220, 32287, 32258. The Zonge GDP-32/II instrument is a backpack-portable, 16 bit, microprocessor-controlled receiver that can gather data on as many as eight channels simultaneously. The GDP receivers were synchronized via GPS timing. The electric-field signal was measured using non-polarizing ceramic Cu-$CuSO_4$ porous-pot electrodes connected to the receiver with insulated 14-gauge wire. Magnetic field measurements were made with Zonge ANT/4 mu-metal-cored antennas, serial numbers, 1044, 1114, 1184, 1464, 1534, 1544, 1554, and 1564.

Electric and magnetic fields were amplified and conditioned by Zonge SC8 signal-conditioning preamplifiers, serial numbers SC31, SC33 and SC60, followed by amplification, analog-to-digital conversion, processing and storage as time-series in the GDP-32/II receiver.

TEM measurements were made with the GDP-32II receiver with a Zonge TEM3 coil and a Zonge ZT-20 battery-powered TEM transmitter.

A complete listing of instrument specifications can be found in Appendix E

SURVEY CONTROL

Zonge personnel established survey control for this project. Stations were located using Garmin hand-held GPS model GPSMAP 60CSx. These GPS receivers are Wide Area Augmentation System (WAAS) enabled and typical field accuracy is 2-5 meters. The UTM Zone 5N NAD83 metric coordinate system was used for this survey. Station locations and date of data acquisition are tabulated in Appendix D.

DATA PROCESSING

The MT data processing flow includes the following steps using Zonge's integrated suite of MT/AMT processing and inversion programs:

1. Fourier transform time-series data into the frequency domain with cascade decimation. Apply magnetic field antenna and analog gain calibration factors (MTFT).
2. Group frequency domain data by frequency and presort by coherence (MTEDIT).
3. Apply robust processing to estimate apparent resistivity, phase, coherence, and error (MTEDIT).
4. Interactively review unaveraged data with apparent resistivity versus frequency sounding curve and complex plane point-cloud plots to de-weight noisy outlier data before final averaging. Repeat values for each station are then averaged and written to ASCII avg-format files (MTEDIT).
5. Interactive data review of averaged impedance data for individual sounding curves to set or clear skip flags marking outlier points in the averaged data (ASTATIC).
6. Compute tensor parameters including tipper, skew, determinant resistivity and phase, and plot impedance polar diagrams (NSSKEW).
7. Determinant resistivity data are static-corrected using TEM, in-loop sounding data (ASTATIC).
8. Perform one-dimensional, smooth-model inversion for each station (SCSINV).

8 Plot maps and sections of data and inversion-resistivity.

STATIC CORRECTIONS

TEM in-loop sounding data were transformed into an equivalent frequency-domain MT sounding using a smooth layered-earth model to link TEM and MT data (Sternberg et al, 1988; Pellerin and Hohmann, 1990). The TEM transient is first converted to a smooth layered-earth model using the smooth-model TEM inversion program STEMINV. The program first sets

model layer thicknesses by calculating source-field penetration depths for each TEM time window. Layer resistivities are then iteratively adjusted until the calculated TEM response for the model is as close as possible to observed TEM data, consistent with smooth resistivity variation from one layer to the next. The resulting resistivity model was used to generate Cagniard resistivity and impedance phase values over a range of frequencies consistent with the depth of investigation of the transient sounding. The converted TEM data were combined with the determinant resistivity and the determinant resistivity was shifted to match the TEM curve in the range of frequency overlap. In many cases the TEM data were not parallel with the MT data and the match was made to maximize the agreement over the frequency range considered to be the best quality.

1-D INVERSION

Ranganayaki (1984) concluded that determinant apparent resistivity and impedance phase were the best summary parameters to use for one-dimensional, layered-earth modeling in areas with complex two- and three-dimensional geology in the absence of more sophisticated inversion algorithms or sufficient data density.

The static-corrected determinant resistivity and impedance phase data for each station were inverted to one-dimensional resistivity-depth sections using Zonge's 1-D MT inversion algorithm, SCSINV. The determinant data were edited to remove the high skew data at low frequency, where the determinant 1D approximation may produce questionable results. Data with a skew of greater than approximately 0.35 were removed from the dataset prior to inversion. In many cases this limited the data to frequencies above 0.1 Hz. For some stations with low signal and poor quality within the dead band, this severely limited the depth of the 1D inversion results.

The smooth-model 1-D inversion uses an iterative procedure to improve the match between measured field data and values calculated using a layered-earth forward model algorithm. At each iteration, layer resistivities are adjusted to improve the fit with field data, while maintaining a smoothly varying layer-to-layer resistivity structure. The results of the smooth-model inversion are intentionally gradational, rather than showing abrupt changes in the

subsurface resistivity. This approach allows automated imaging without a-priori information about geologic structure.

Plots showing the inversion results for each station, with curves showing inversion results and observed and calculated resistivity are provided on the accompanying data CD. The 1-D depth inversion results for several stations are projected onto the six profile lines and contoured to produce resistivity-depth sections. Inversion results for individual stations are combined and output as .csv files containing x, y, z and inversion resistivity for several elevation intervals.

MT PARAMETER DEFINITIONS AND COMPUTATIONS

Impedance estimates for each pair of electric and magnetic field components are calculated during the robust impedance processing stage. The impedance tensor $\overline{\overline{\mathbf{Z}}}$ relates horizontal electric and magnetic field components as

$$\begin{bmatrix} E_x \\ E_y \end{bmatrix} = \begin{bmatrix} Z_{xx} & Z_{xy} \\ Z_{yx} & Z_{yy} \end{bmatrix} \cdot \begin{bmatrix} H_x \\ H_Y \end{bmatrix}$$

or equivalently

$$E_x = Z_{xx} \cdot H_x + Z_{xy} \cdot H_y \text{ and } E_y = Z_{yx} \cdot H_x + Z_{yy} \cdot H_y .$$

Note that since E_x and E_y are associated with two different equations, estimates of Z_{xx} and Z_{xy} are separate from estimates of Z_{yx} and Z_{yy}.

Impedance magnitudes are transformed to Cagniard apparent resistivity values

$$\rho_{xy} = \frac{1}{\omega \cdot \mu} \left| Z_{xy} \right|^2 \text{ (ohm - meters)}$$

where ω is radial frequency in radians/second, μ is magnetic permeability in henries/m, and Z_{xy} is electrical impedance in ohms (Cagniard, 1953). The magnetic permeability is usually taken as the magnetic permeability of free space, μ_0.

Similarly, Z_{xx}, Z_{yx} and Z_{yy} magnitudes can be scaled to ρ_{xx}, ρ_{yx} and ρ_{yy}. The accepted scientific convention is to use SI units with electric field values in V/m and magnetic field values

in A/m. But since geophysical signal strengths are so low, it is convenient to scale E-field values to nanoVolts/meter (nV/m) and H-field values to picoTesla (pT). Note that although pT values should be annotated as B-field magnetic flux density, H-field labels and pT units are used in most of Zonge's documentation and plot annotation.

Impedances are complex, therefore they have both magnitude |Z| and phase ϕ:

$$\phi_{xy} = \text{phase}\left(Z_{xy}\right) = 1000 \cdot \arctan\left(\frac{\text{imag}(Z_{xy})}{\text{real}(Z_{xy})}\right) \text{ mrad}.$$

Impedance phase is related to the change in apparent resistivity as a function of frequency:

$$\phi = 1000\frac{\pi}{4}\left(1 + \frac{\partial \log(\rho)}{\partial \log(f)}\right) \text{ mrad}.$$

Impedance phase is a measure of the slope of the apparent resistivity sounding curve, adding information about sounding curve shape at each data point. Plots of apparent resistivity sounding curves, produced by Zonge, often include impedance phase information represented as a vector posted at each data point. If impedance phase values are consistent with apparent resistivity curve shape, the posted vectors are tangent to the sounding curve.

In addition to apparent resistivity and impedance phase representations of each impedance tensor element, additional derived parameters can be constructed (Vozoff, 1987, Simpson and Bahr, 2005), of which a subset is described below.

The impedance tensor coordinate system can be rotated to generate an impedance tensor for an arbitrary (x, y) electromagnetic component orientation. Impedance tensor rotation is used to estimate electrical strike by finding an (x, y) orientation for which the magnitude of the tensor's diagonal trace is minimized, in effect identifying the EM component orientation for which the geological structure appears to be most two-dimensional. In this fashion, the strike direction θ_{min} is the E_x azimuth that minimizes $|Z_{xx}|^2 + |Z_{yy}|^2$ and maximizes $|Z_{xy}|^2 + |Z_{yx}|^2$. (Tensor parameters are output in Tensor_MT_Data.csv and the quantity θ_{min} is denoted MaxResEAzm.). It should be noted that the strike direction calculated in this manner is non-unique to 90 degrees.

In addition to information describing the electrical strike, parameters derived from the impedance tensor can be used to estimate the degree of multidimensionality, namely with the rotationally-invariant parameter skew:

$$skew = \frac{\left|Z_{xx} + Z_{yy}\right|}{\left|Z_{xy} - Z_{yx}\right|}$$

In one- and two-dimensional geology, the skew is near 0. Values of 0.2 or less have been used to imply one- or two-dimensional geologic structure, while areas with skew values greater than 0.3 indicate measurements near the corners of three-dimensional structure. Simpson and Bahr, (2005) argue that while values of 0.2 and greater are indicators of influence of 3D structure, values of less 0.2 cannot be used to infer that the geologic structure is two-dimensional. Skew values are tabulated in the Det.csv file and included on the CD-ROM.

Rotationally-invariant versions of the apparent resistivity and phase can be used to average the multidimensional information into single pseudosections and plan view presentations. The determinant apparent resistivity and phase combine impedance tensor elements into a single apparent resistivity and impedance phase values:

$$\rho_{\det} = \frac{1}{\omega \cdot \mu}\left|Z_{\det}\right|^2 \text{ (ohm - meters)}$$

$$\phi_{\det} = 1000 \cdot \text{atan}\left(\frac{imag\left(Z_{\det}\right)}{real\left(Z_{\det}\right)}\right) \text{ (mrad)}$$

where $Z_{det} = (Z_{xx}Z_{yy}\text{-}Z_{xy}Z_{yx})^{1/2}$.

Small-scale, near-surface resistivity structure and topography can cause a frequency independent effect termed “static offset” or “static shift”. Static offsets shift the entire apparent resistivity sounding curve up or down without changing sounding curve shape (in log(frequency) versus log(apparent resistivity) plots.

Tensor parameters are calculated using Zonge’s NSSKEW program module and are output in the Tensor_MT_Data.csv file which is included on the data CD.

Impedance polar diagrams are presented in map view plots along with the determinant resistivity for selected frequencies. The outer curve of this plot represents the magnitude of $|Z_{xy}|$ as it is rotated through 360 degrees in 4 degree increments. The inner curve represents the

magnitude of the diagonal element $|Z_{xx}|$ as described above. A circular polarization is usually considered as evidence of 1-D structure.

More detail on the MT method can be found in Appendix F: Overview of magnetotellurics. This section also includes more information on tipper quantities and phase tensors.

DATA QUALITY

Several measures of data quality are recorded in the provided averaged data files. Natural source signal strengths were sufficient to get good quality data over most of the survey's AMT and MT frequency range extending from .0029 to approximately 1000 hertz. The magnetotelluric data collected during this survey range from poor to very good. Weather systems caused noise sources on several days.

Initial remote referencing was done by mutual reference between the two operating GPS receivers. Due to access issues it was determined that the survey area would need to be smaller and that the receivers would operate closer together than originally planned. A remote reference was established approximately 26 km from the site on August 1. Data quality was markedly better as a result of these efforts.

Station 36, had no usable data in the 10 to 0.1 Hz. range and is not used for most products. Stations 2, 12, 15, 19, 21, 30 and 38 had low quality over portions of the recording range and were selectively edited or deleted from the data used for some products.

Geomagnetic activity, the source of the MT signal below approximately 1 Hz., ranged from quiet to a NOAA Geomagnetic Storm Level of G2 during the course of the survey. A tabulation of the geomagnetic indices for the duration of the survey is included in Appendix G. Stations 13, 61, 74, 75, 84, 92 and 93 were acquired during periods of low geomagnetic activity. The relatively long overnight recording times resulted in usable data for these stations.

DATA PRESENTATION

Figures are included as image files on the Data CD and are included in Appendix A as fit-to-page plots.

Plots of the Cagniard resistivity and impedance phase for the components as acquired, are shown in Appendix B and are also included as .png image files on the data CD. A discussion of the tensor MT parameters is included in Appendix F.

Figures 2 and 4 show the location of the MT stations on a USGS topographic base map.

Plan maps showing contours of determinant resistivity, determinant phase, and Tipper magnitude are shown for frequencies of 0.125, 1, 8 and 128 hertz in Figures 5 through 16. Polar diagrams are shown for each station on these maps. Figure 17 shows the station location map with a series of profiles for which nearby stations have been projected. Figures 18 through 29 show sections of the resistivity and phase versus frequency for the Zxy and Zyx (Ex/Hy and Ey/Hx) components along these profiles.

Figures 30 through 35 show results of one-dimensional smooth-model inversion of the impedance determinant data for each of these profiles and are presented as inversion resistivity versus depth sections. Plan maps of the inversion results are presented for selected elevations in Figures 36 through 40.

A .csv file (Tensor_MT_Data.csv) is provided which contains the MT impedance data and tensor computations. A description of the contents is included with this file on the CD-ROM. Digital data files and images are included on the data CD-ROM. File structure of the zonge .avg file format is described in Appendix H.

SAFETY AND ENVIRONMENTAL ISSUES

No health, safety incidents or accidents occurred during the course of this survey. No environmental damage was sustained as a direct result of the survey progress. There was no ground vehicular use during this survey.

Respectfully submitted,

Les P. Beard
Senior Geophysicist

Chester S. Lide
Managing Geophysicist

Gary Oppliger
Senior Geophysicist

ZONGE GEOSCIENCES INC.

REFERENCES.

Cagniard, L., 1953, Basic theory of the magnetotelluric method of geophysical prospecting, Geophysics, 18, 605-635.

Gamble, T.D., Gaubau, W.M., and Clarke, J., 1979, Magnetotellurics with a remote magnetic reference: Geophysics, 44, 53-68.

Pellerin, L. and Hohmann, G.W., 1990, Transient electromagnetic inversion: a remedy for magnetotelluric static shifts, Geophysics, 55, 1242-1250.

Ranganayaki, R.P., 1984, An interpretive analysis of magnetotelluric data, Geophysics, 49, 1730-1748.

Simpson, F., and Bahr, K., 2005, Practical Magnetotellurics, Cambridge University Press, Cambridge, UK.

Sternberg, B.K., Washburne, J.C., and Pellerin, L., 1988, Correction for the static shift in magnetotellurics using transient electromagnetic soundings, Geophysics, 53, 1459-1468.

Vozoff, K., 1987, The magnetotelluric method, in Nabighian, M.N., ed. Electromagnetic methods in applied geophysics, Vol. 2, Society of Exploration Geophysicists, 641-711.

Wannamaker, P.E., Hohmann, G.W., and Ward, S.H., 1984, Magnetotelluric responses of three-dimensional bodies in layered earths, Geophysics, 49, 1517-1533.

APPENDIX A: DATA PLOTS

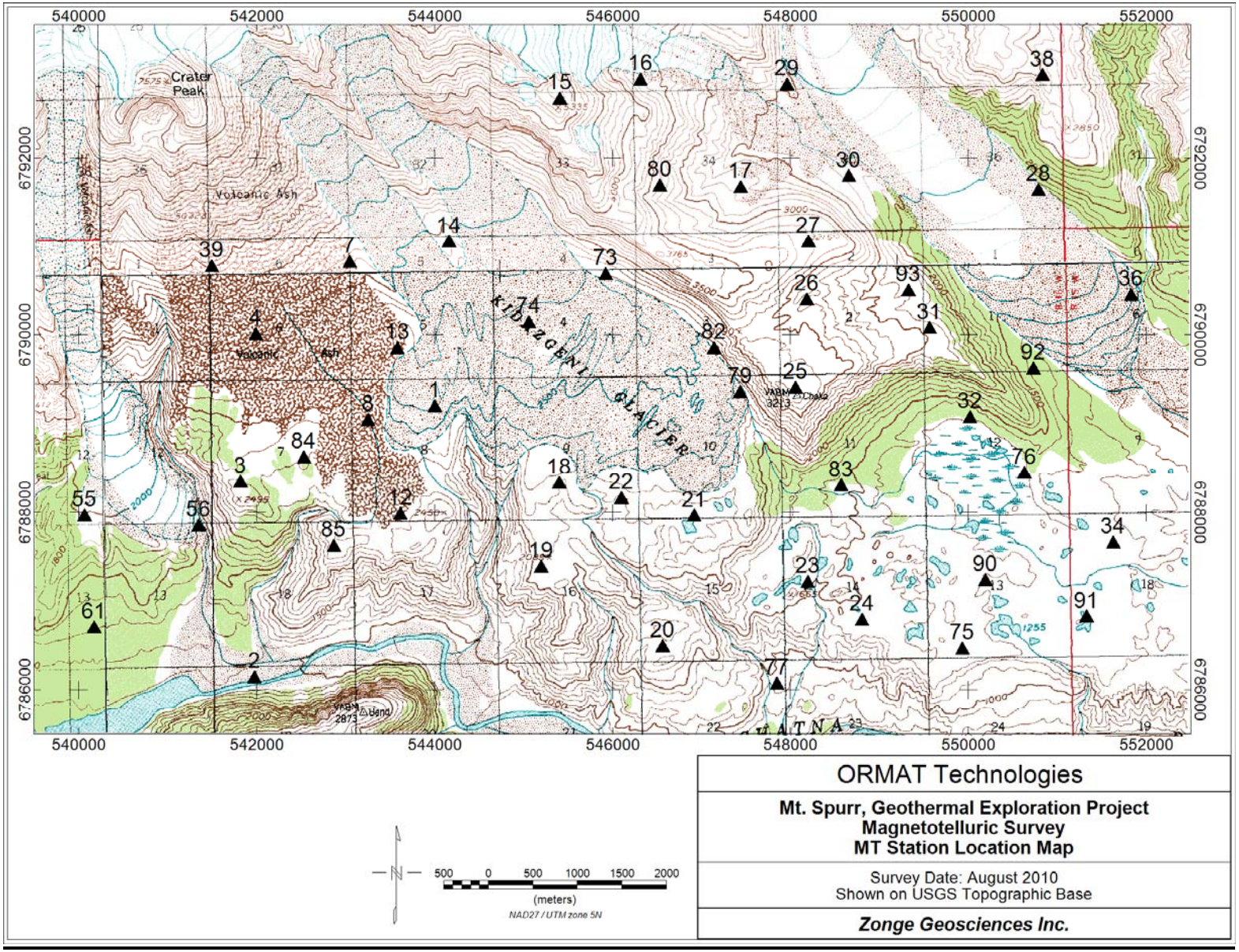

Figure 4: MT Station Locations.

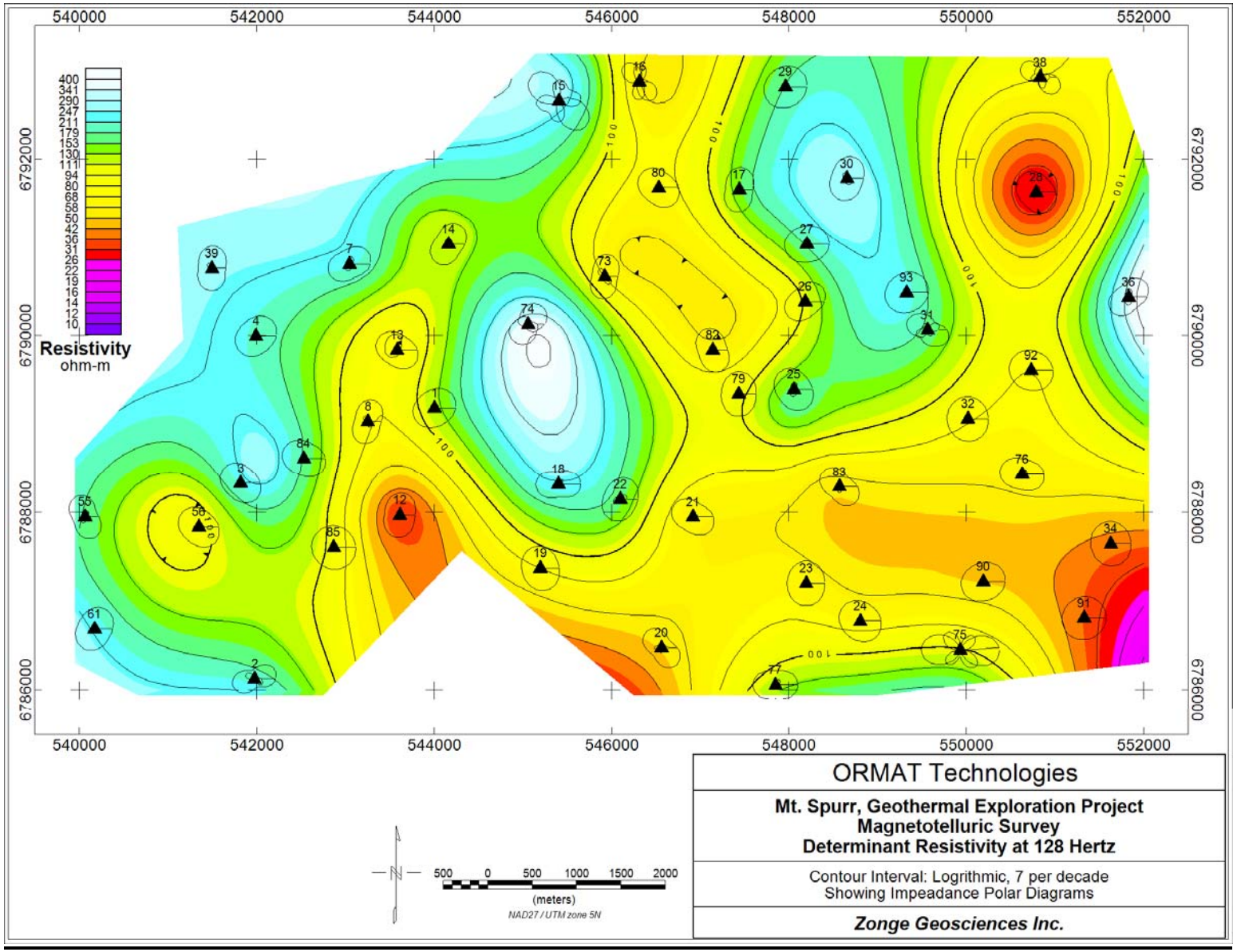

Figure 5: Contour map of determinant resistivity at 128 Hz.

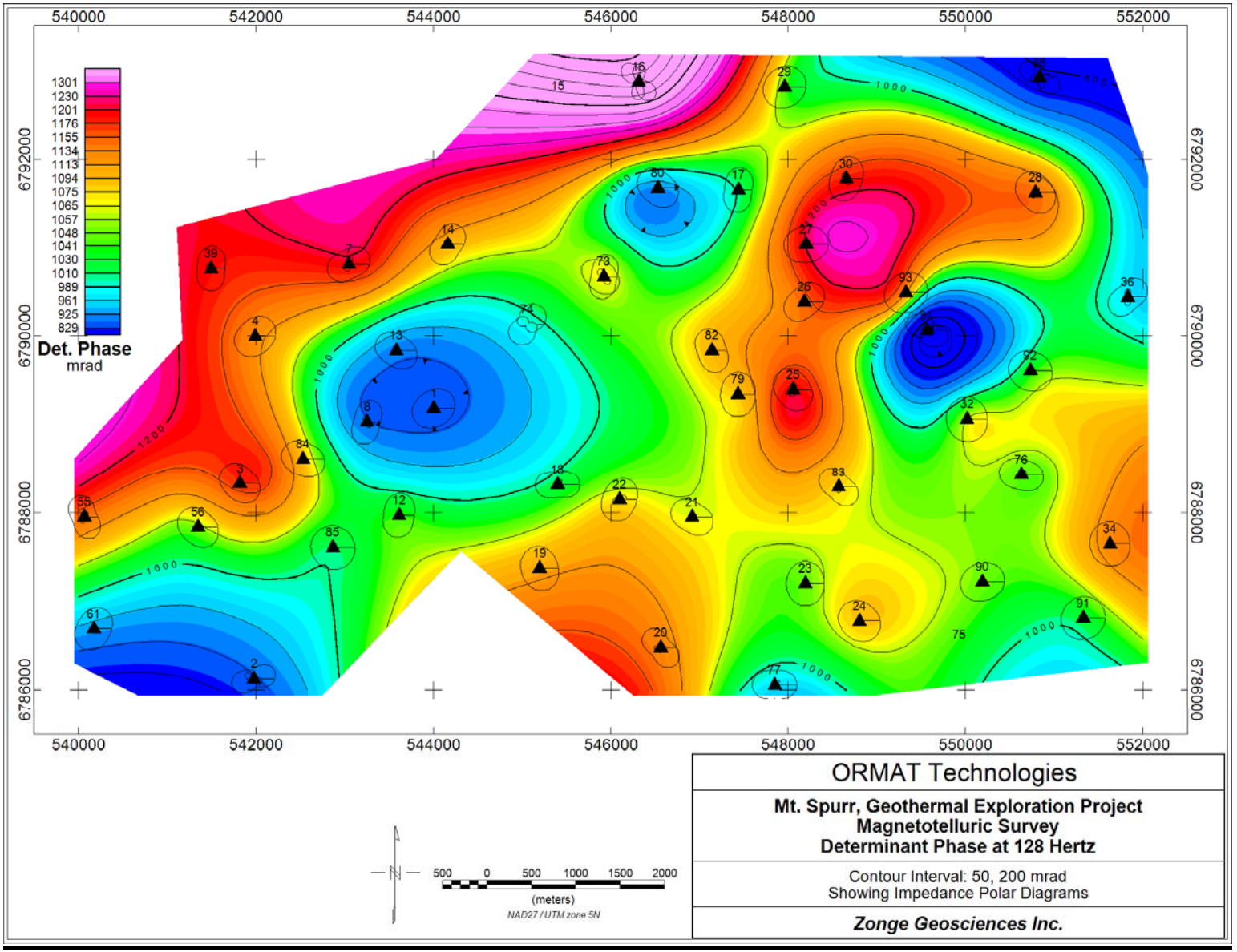

Figure 6: Contour map of determinant phase at 128 Hz.

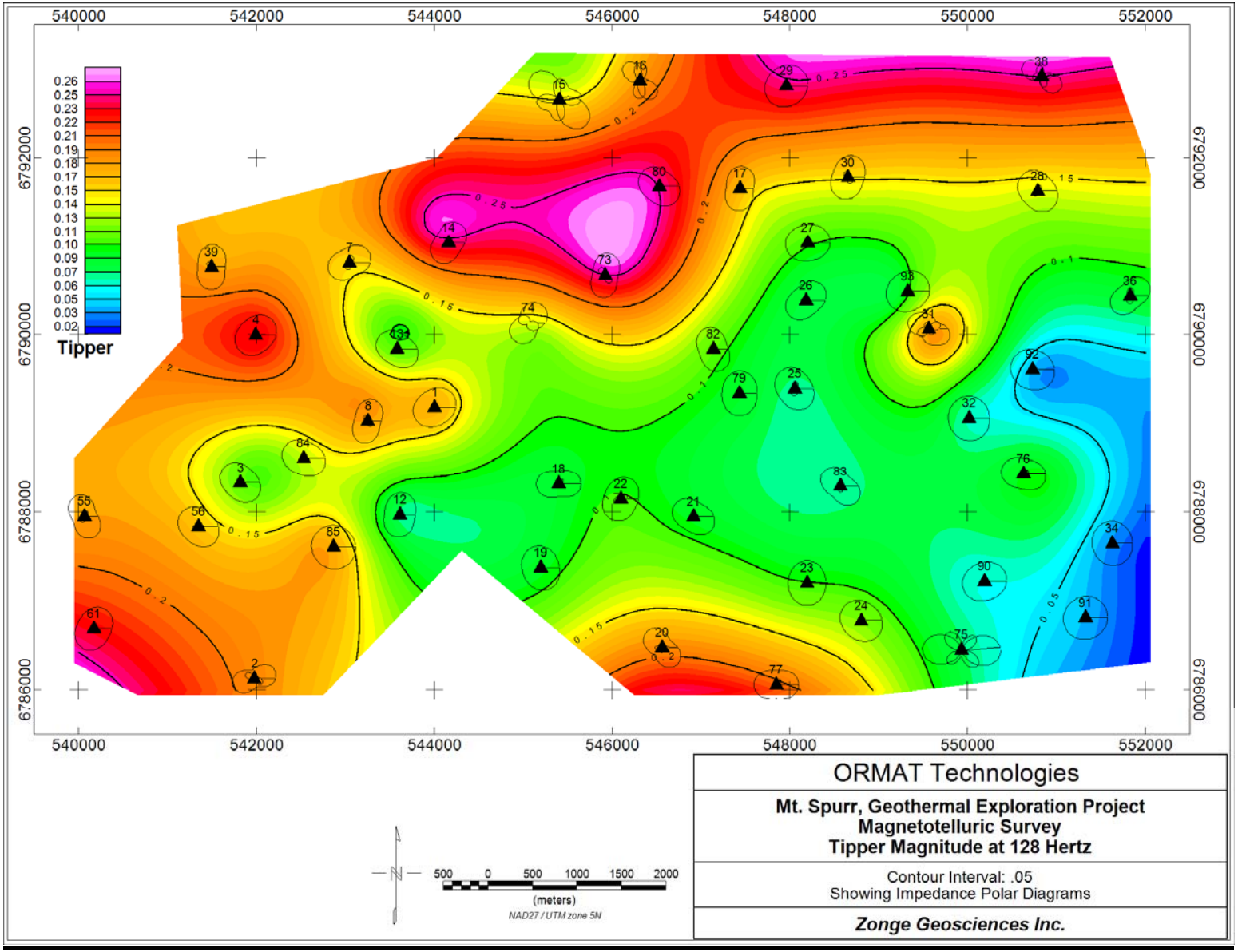

Figure 7: Contour map of Tipper magnitude at 128 Hz.

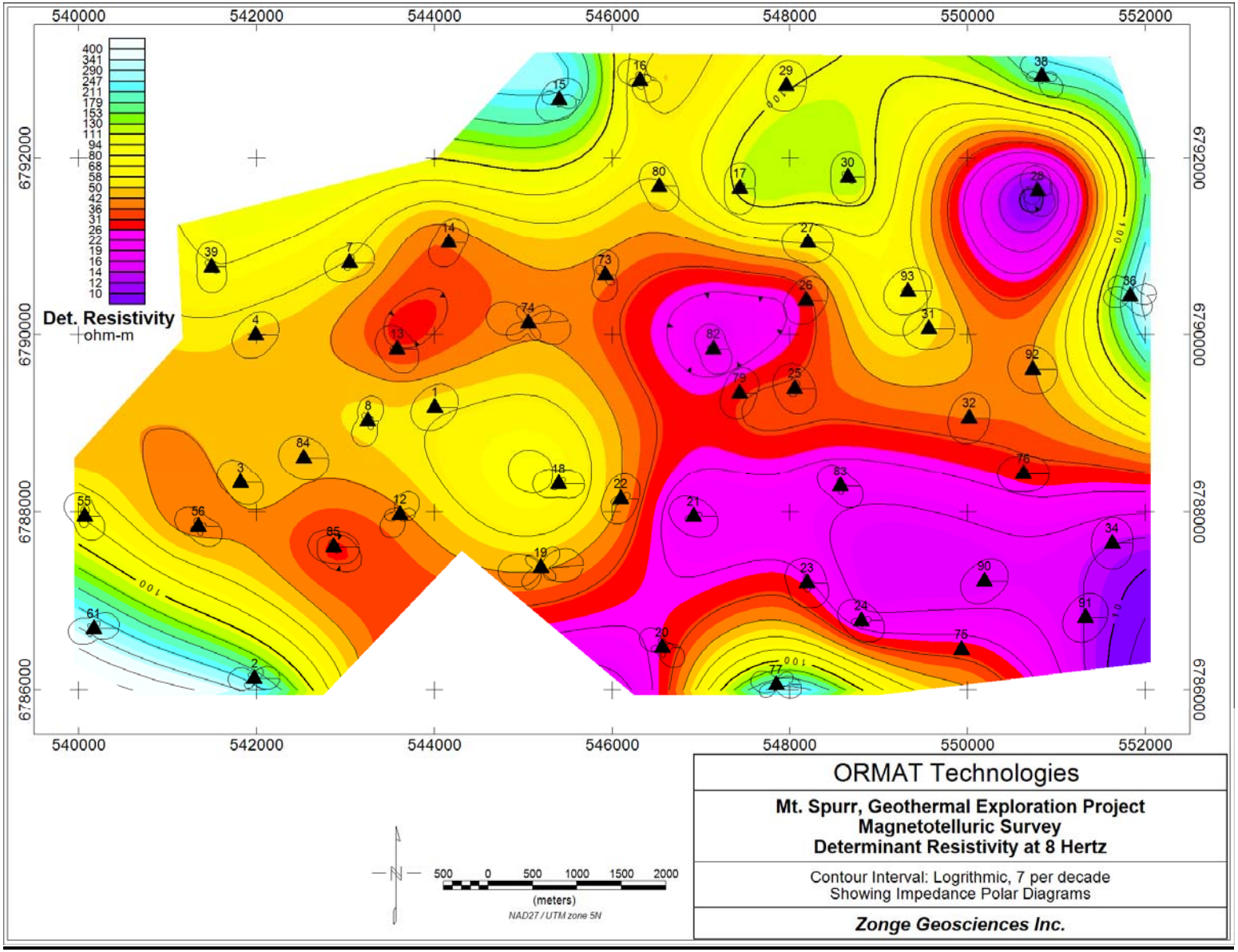

Figure 8: Contour map of determinant resistivity at 8 Hz.

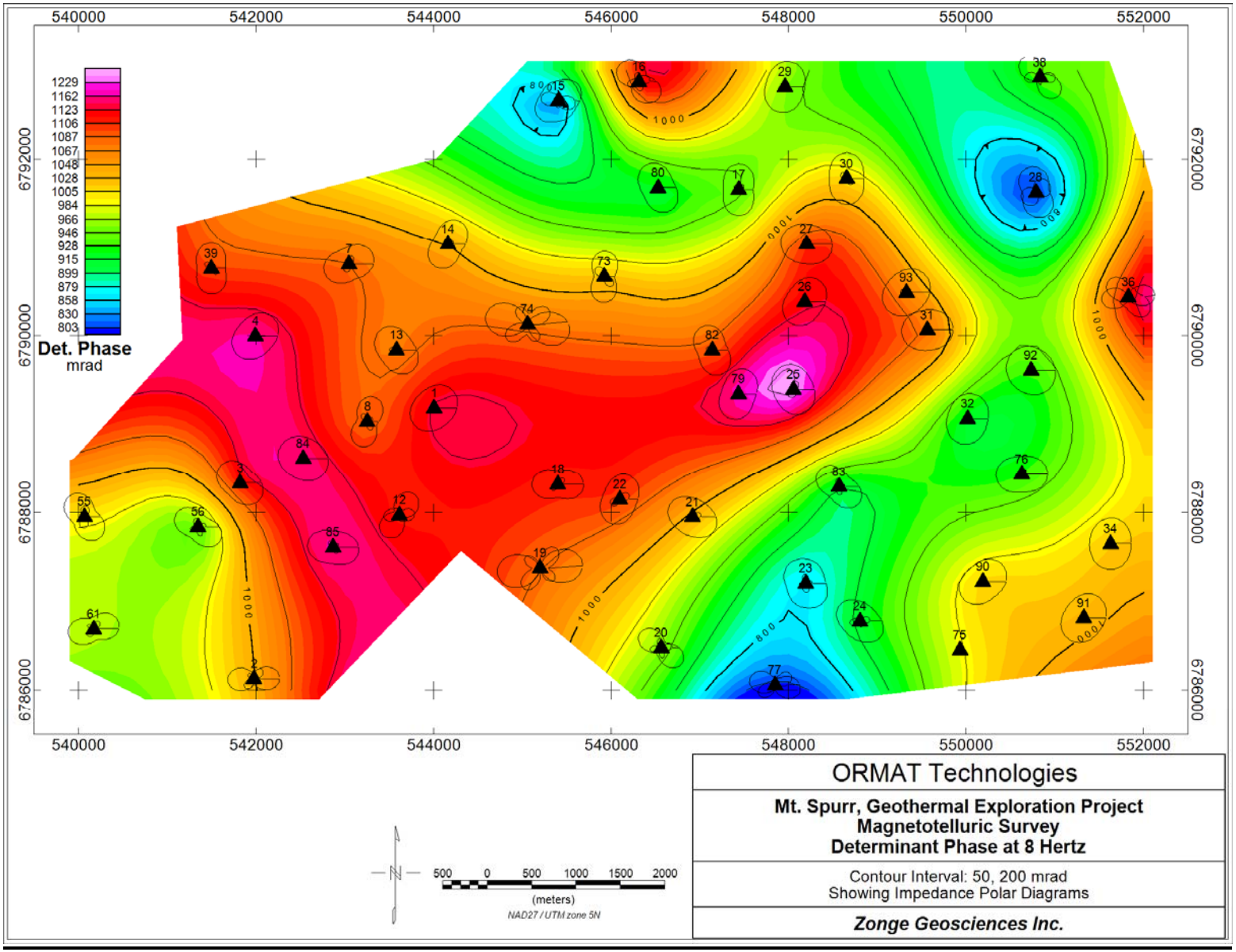

Figure 9: Contour map of determinant phase at 8 Hz.

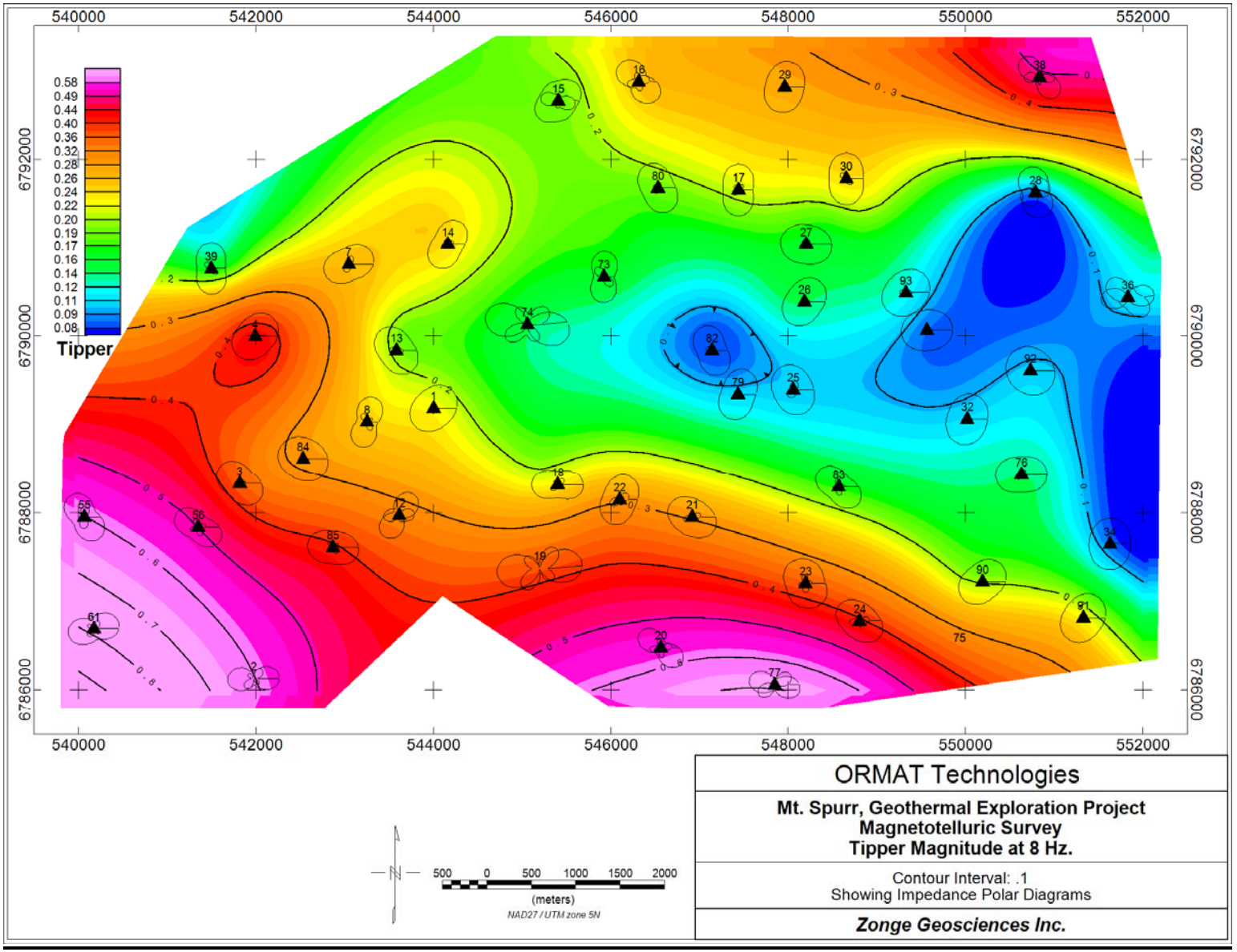

Figure 10: Contour map of Tipper magnitude at 8 Hz.

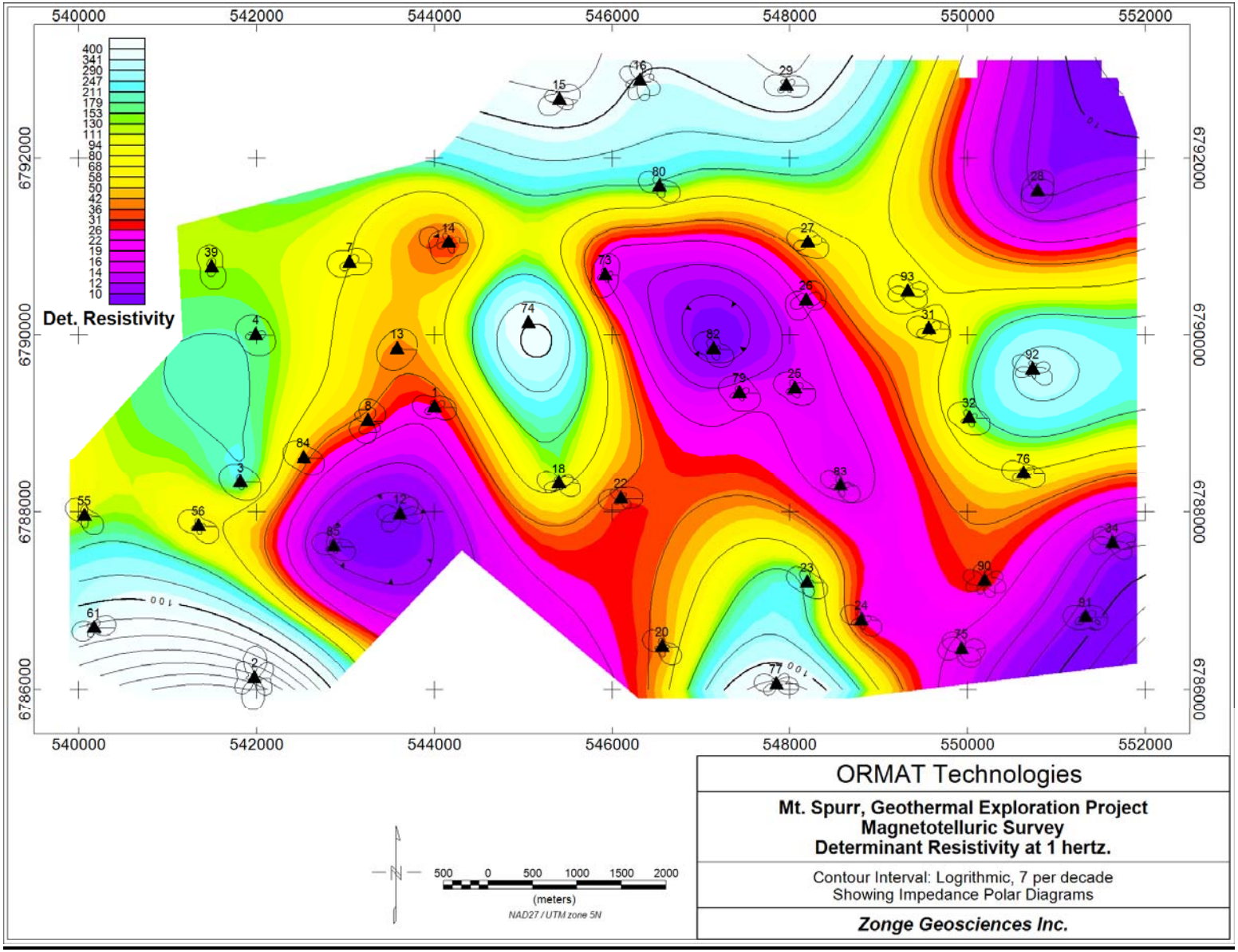

Figure 11: Contour map of determinant resistivity at 1 Hz.

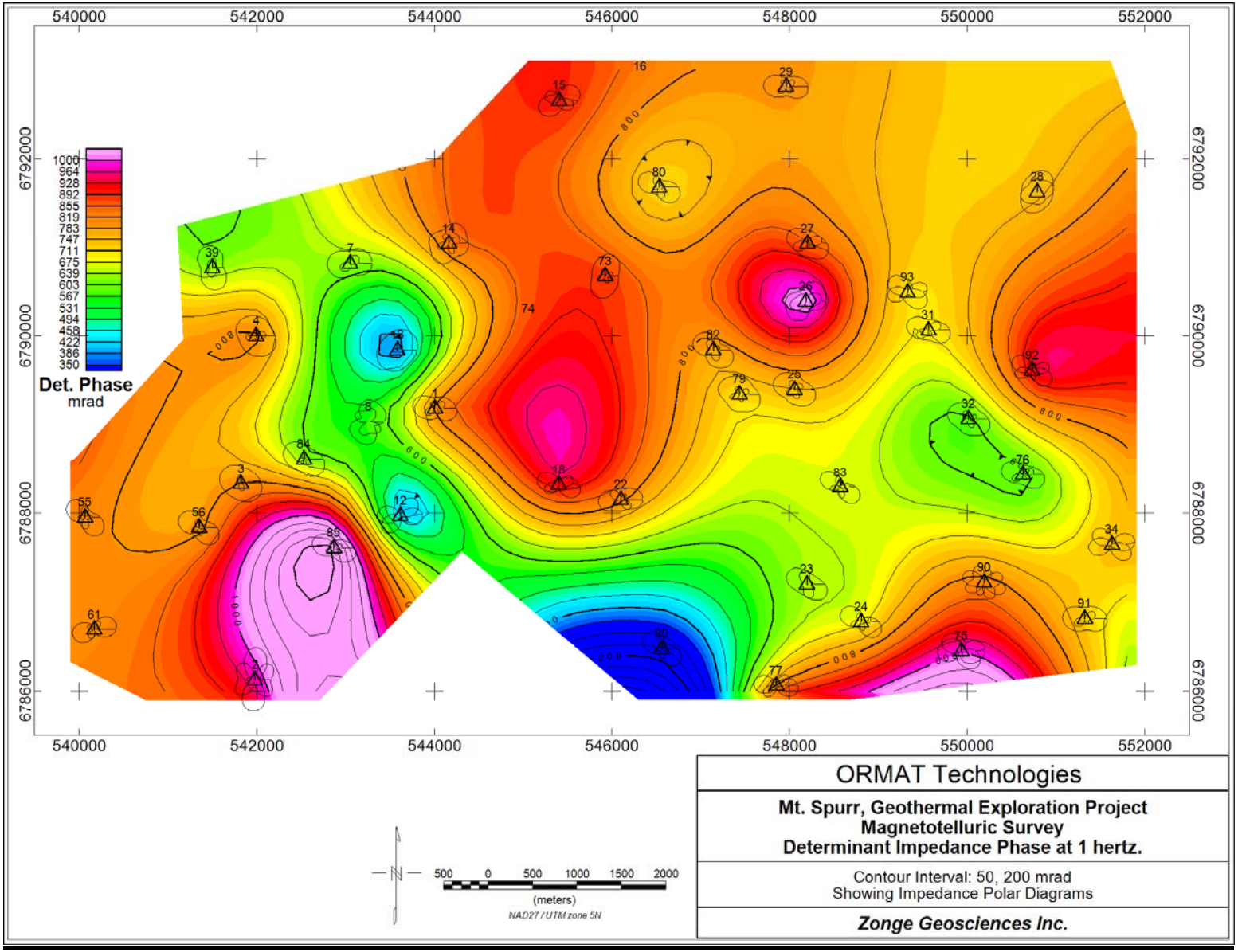

Figure 12: Contour map of determinant phase at 1 Hz.

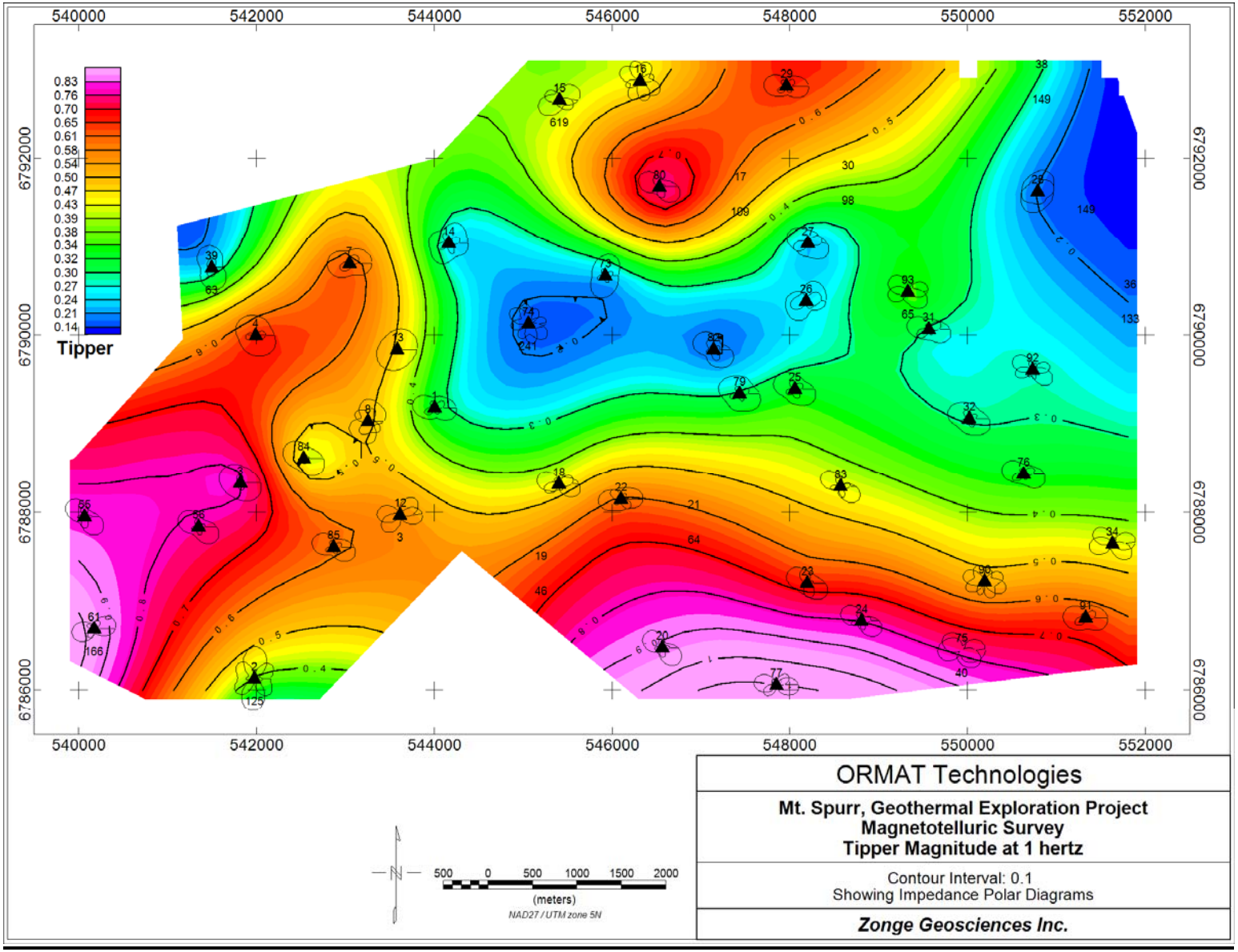

Figure 13: Contour map of Tipper magnitude at 1Hz.

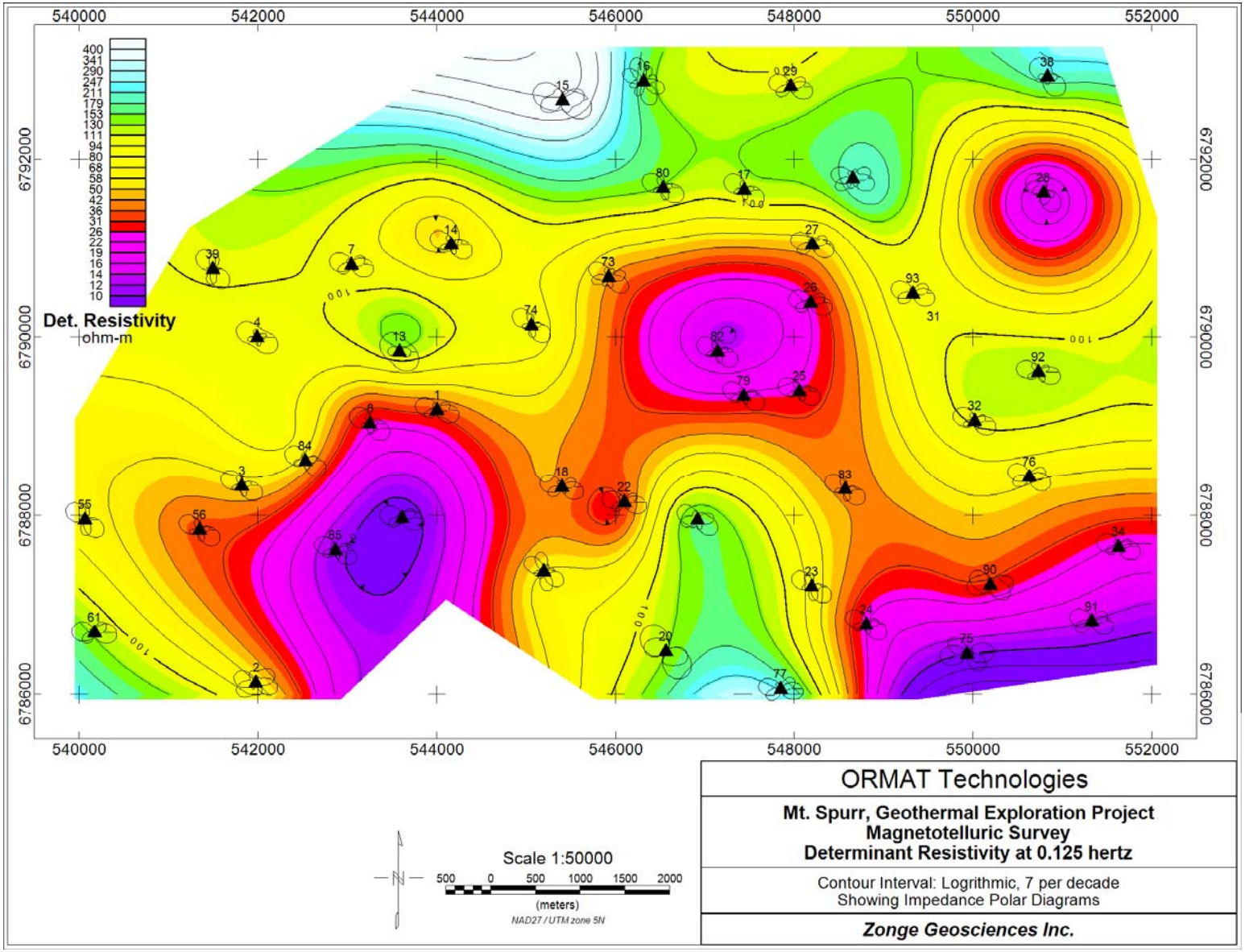

Figure 14: Contour map of determinant resistivity at 0.125 Hz.

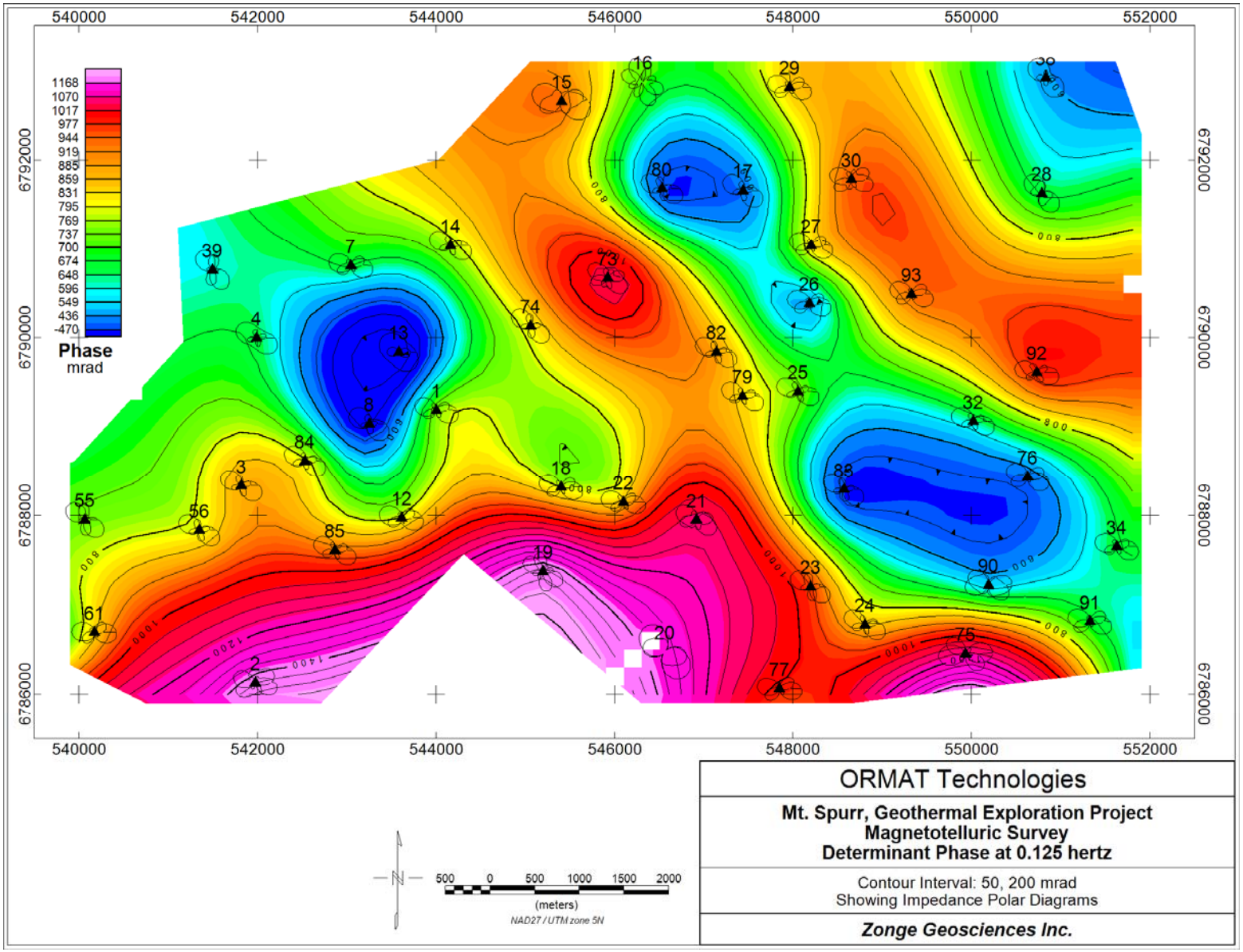

Figure 15: Contour map of determinant phase at 0.125Hz.

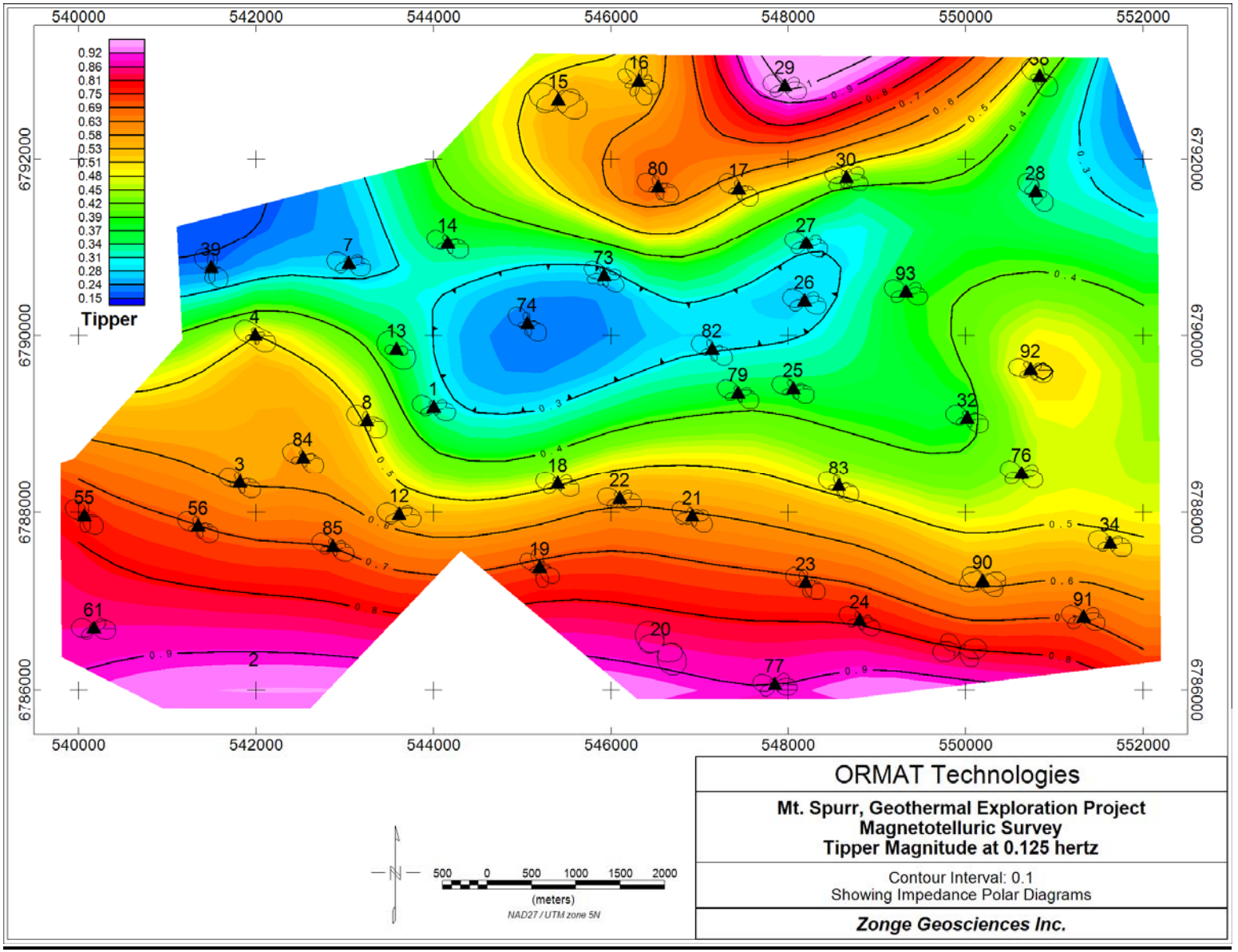

Figure 16: Contour map of Tipper magnitude at 0.125 Hz.

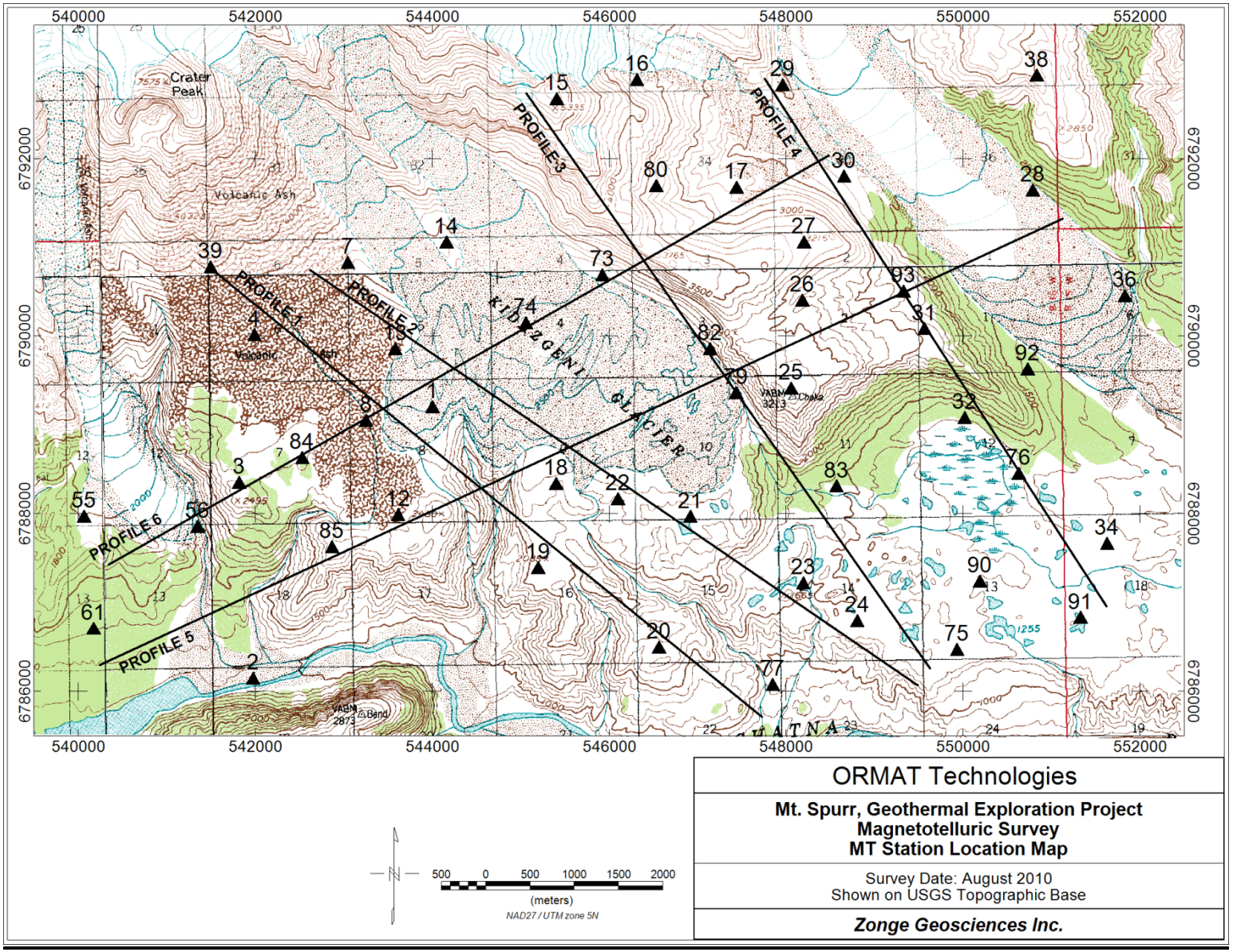

Figure 17: MT station location map, showing profiles.

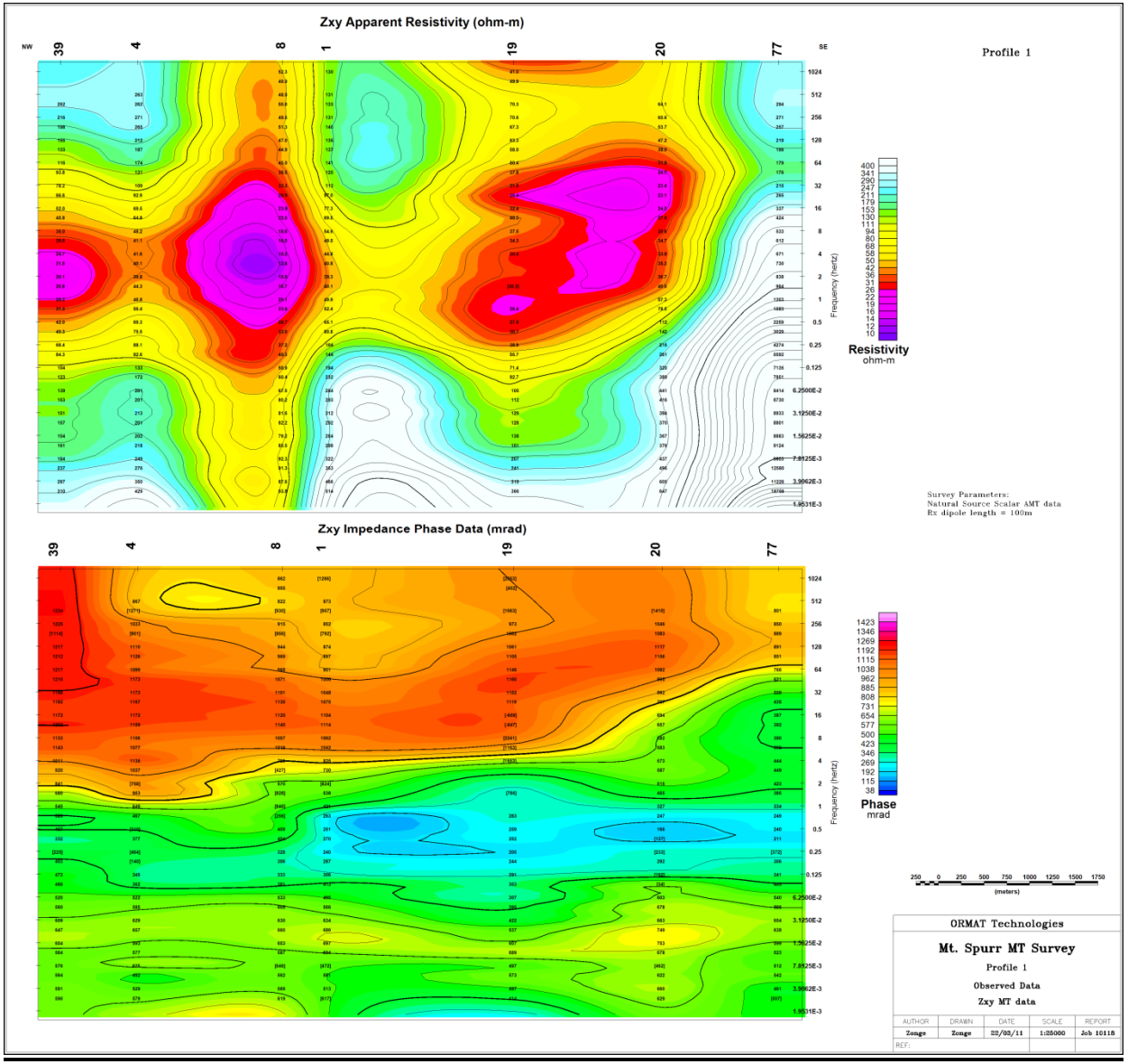

Figure 18: Observed Zxy, Profile 1.

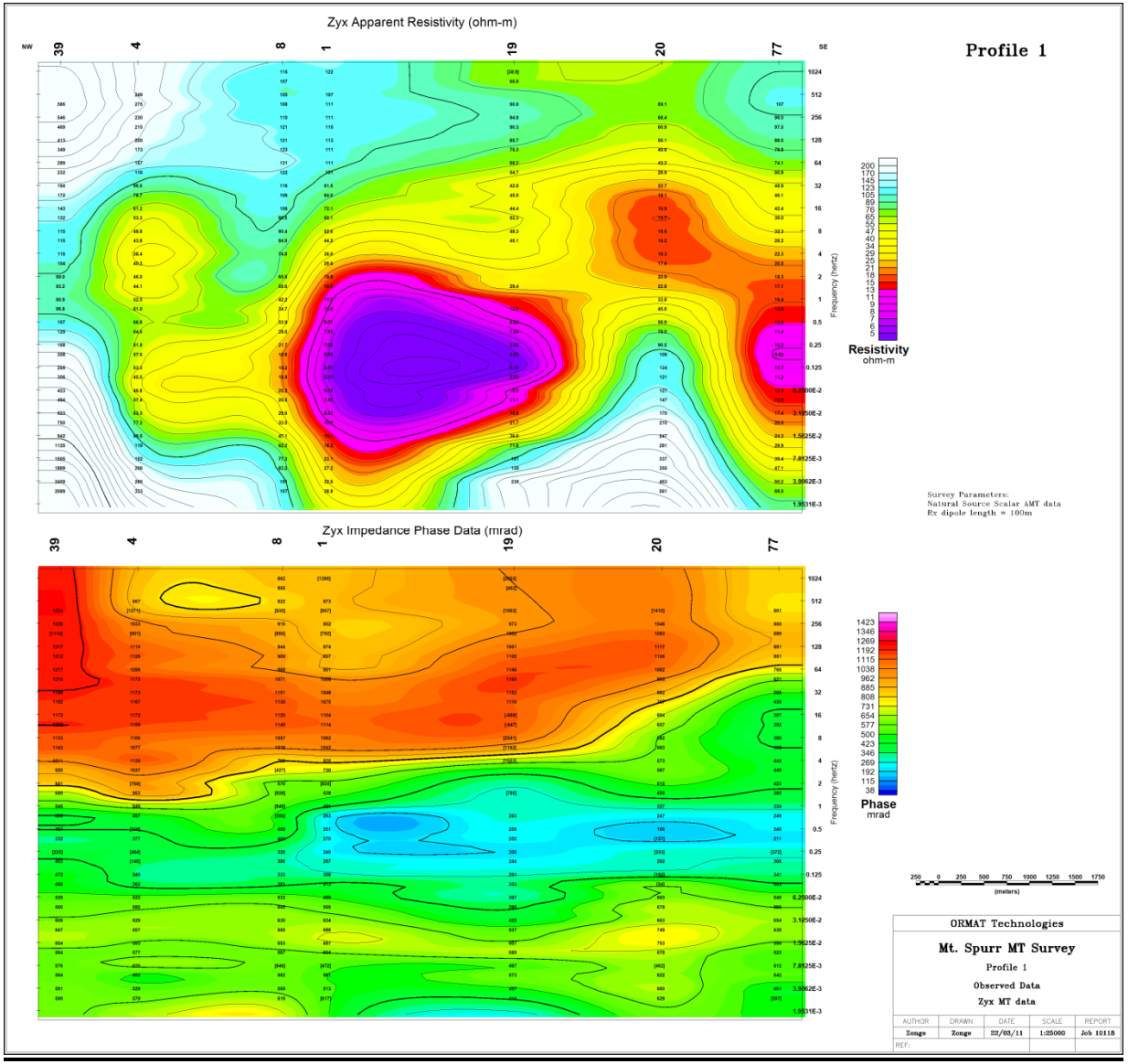

Figure 19: Observed Zyx, Profile 1.

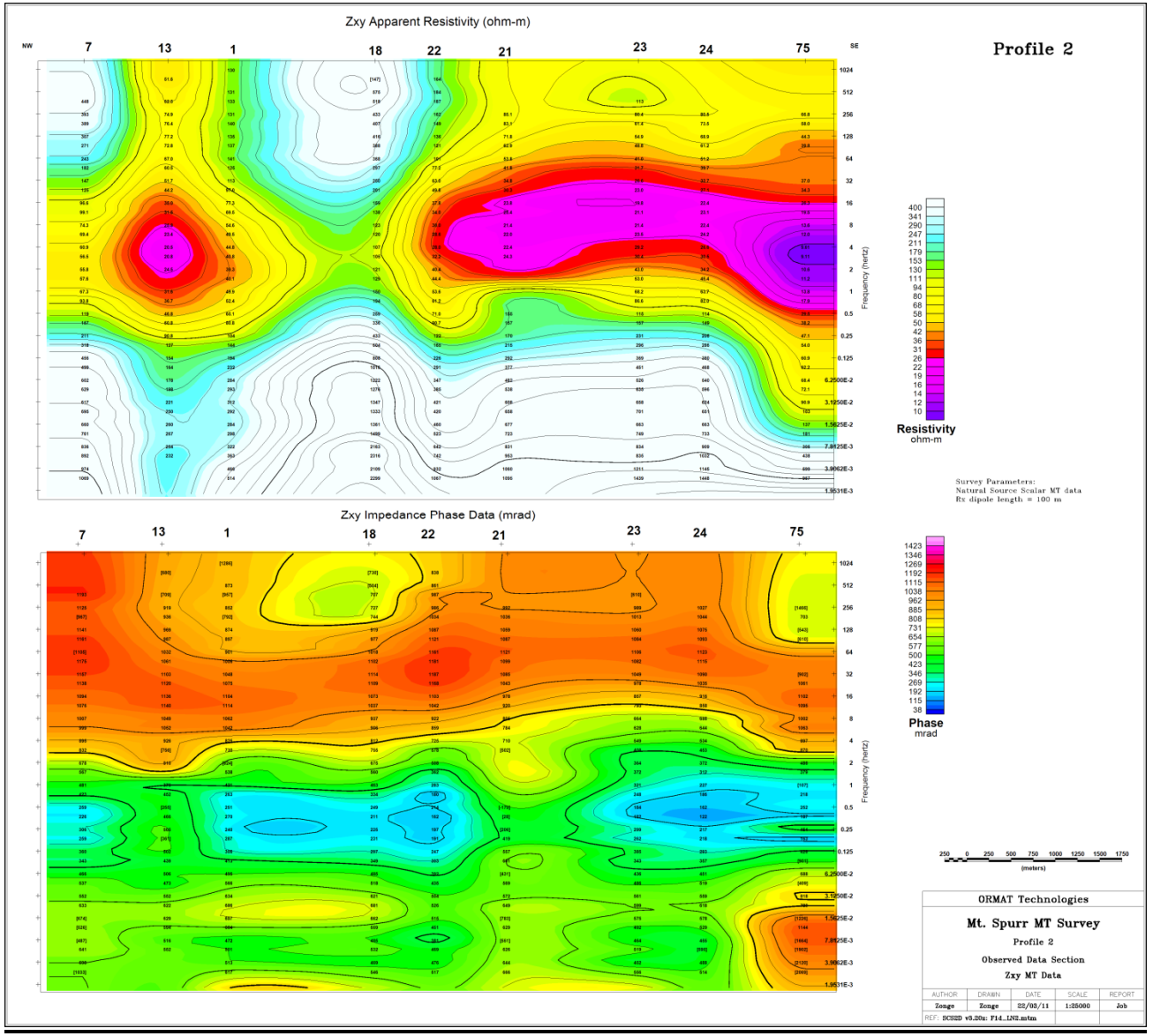

Figure 20: Observed Zxy, Profile 2.

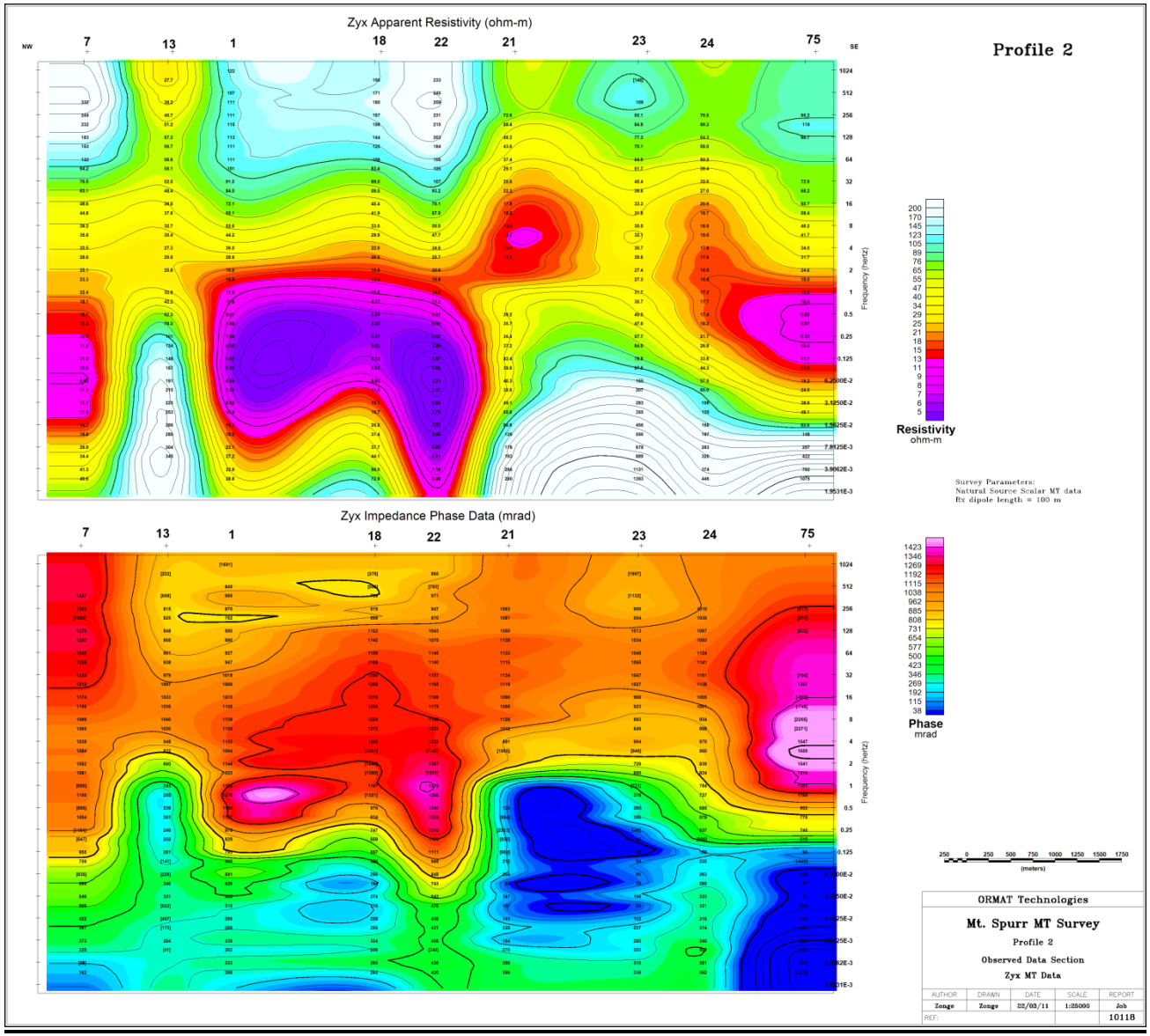

Figure 21: Observed Zyx, Profile 2.

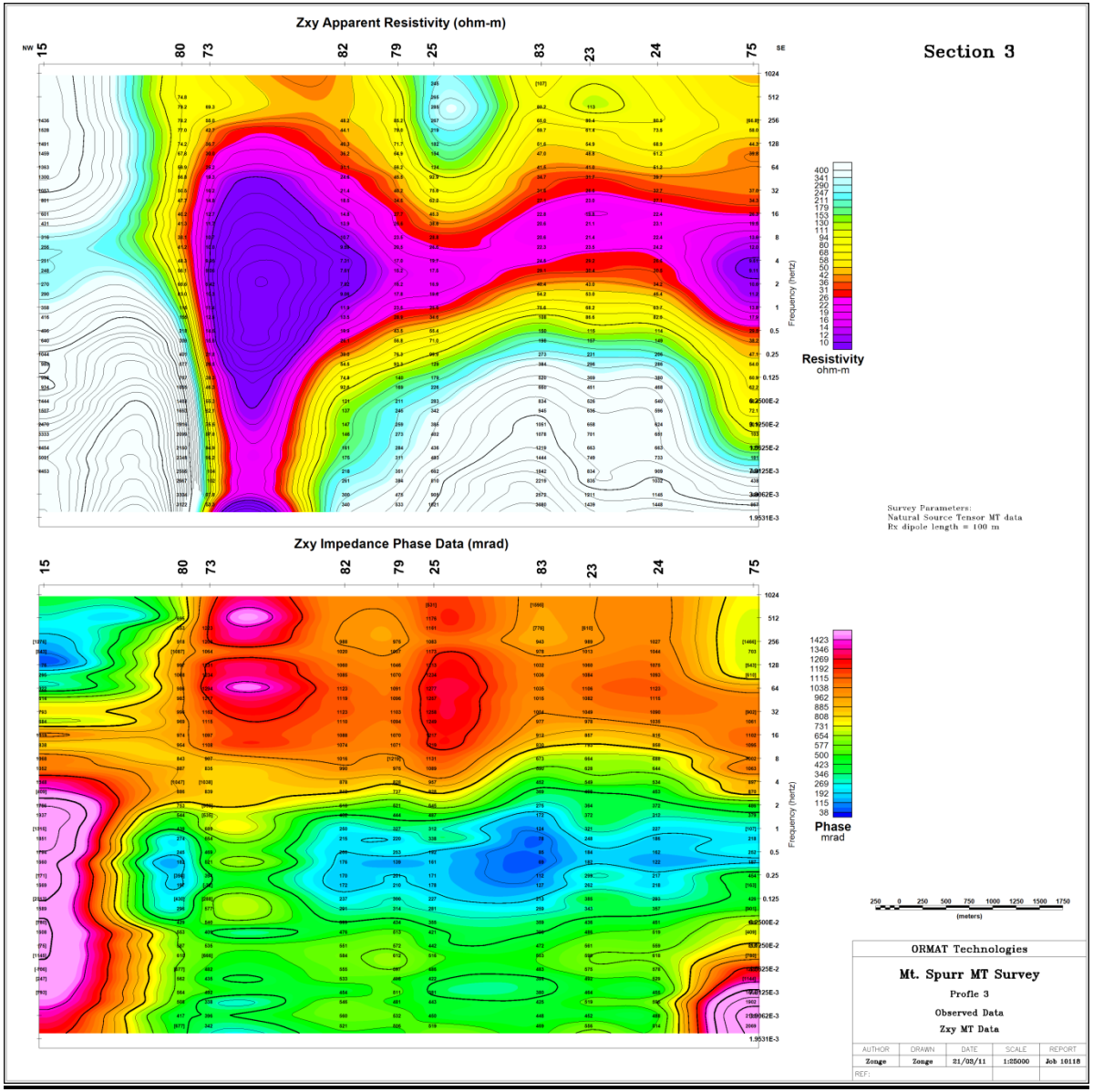

Figure 22: Observed Zxy, Profile 3.

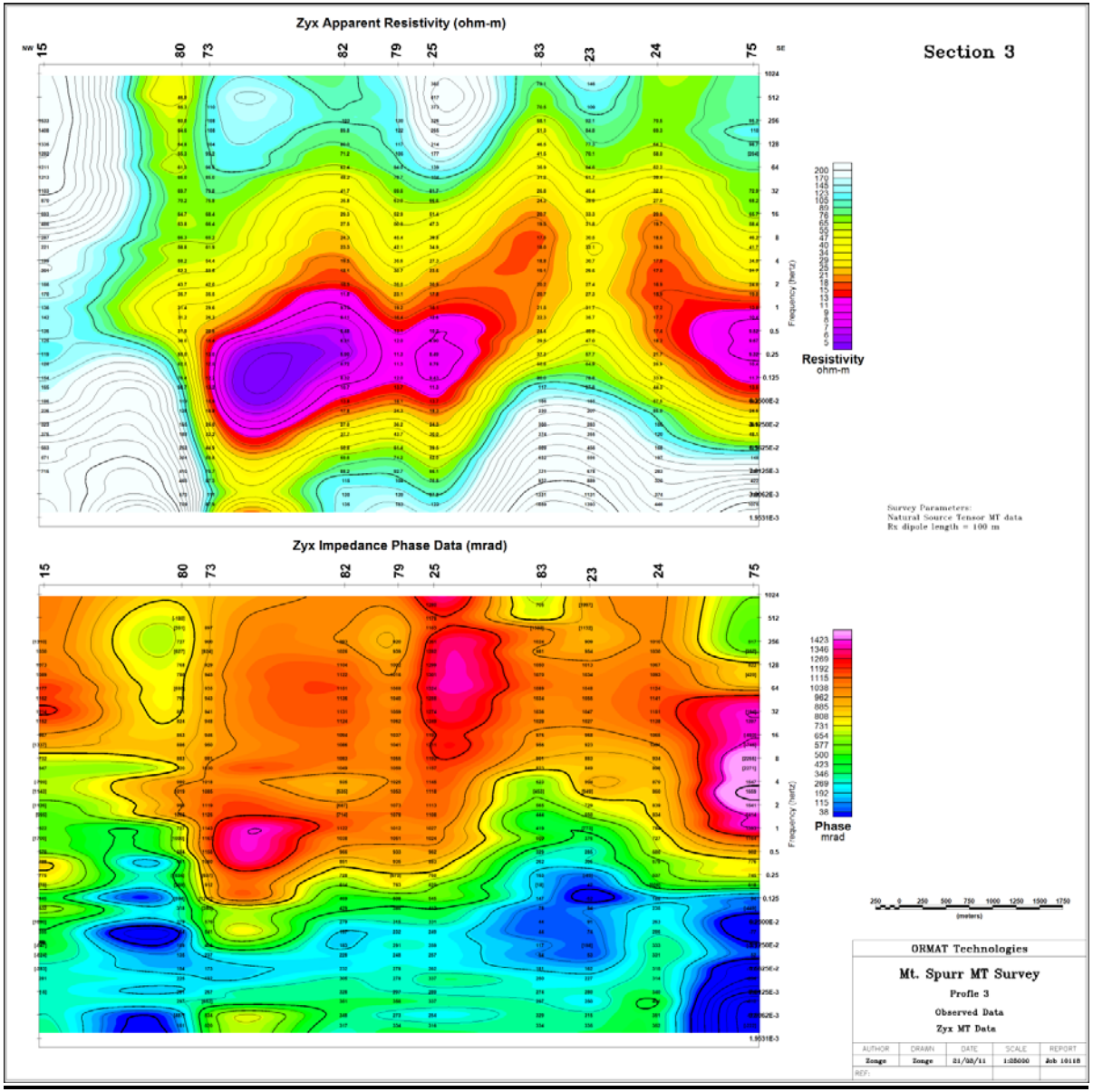

Figure 23: Observed Zyx, Profile 3.

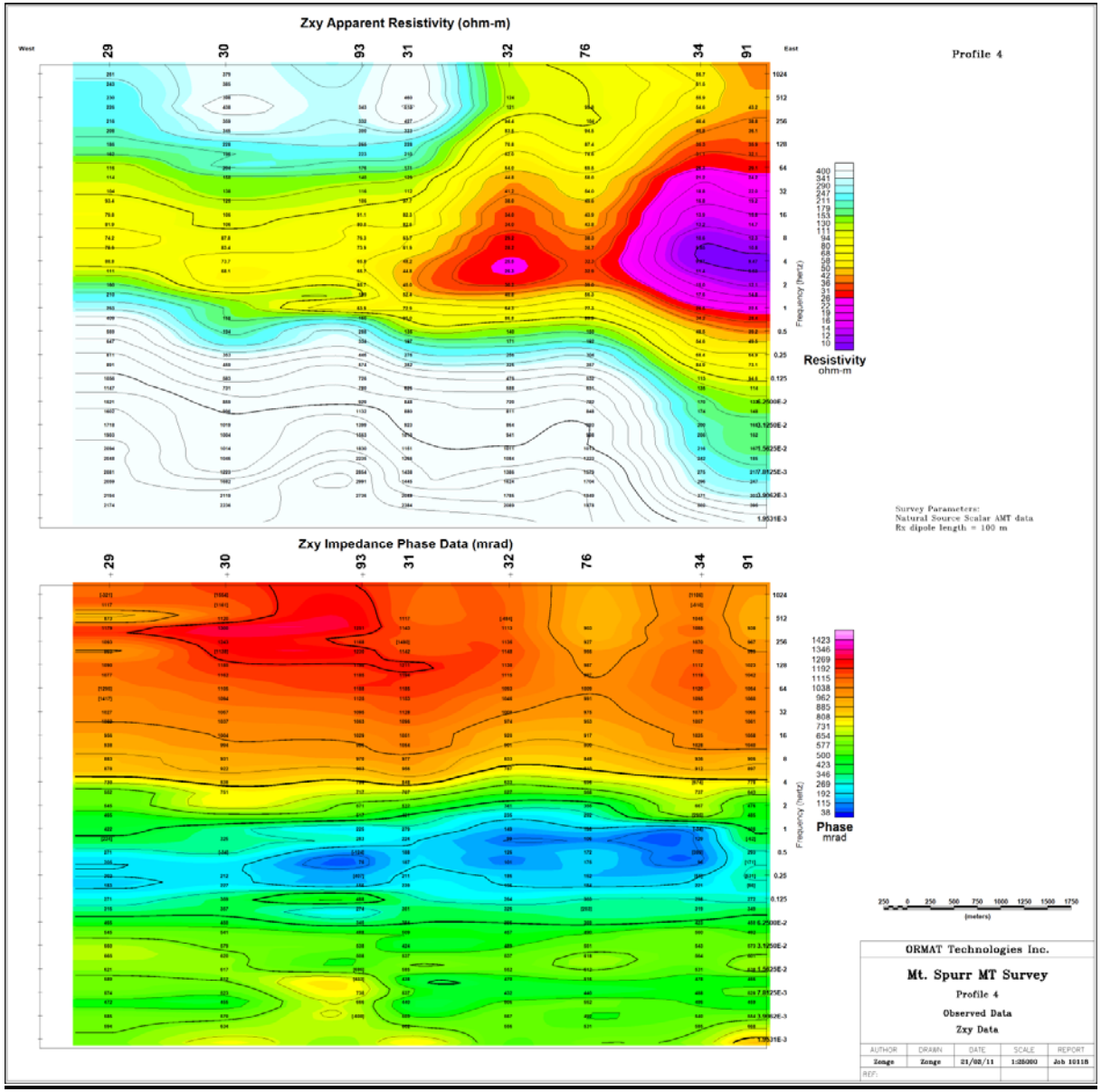

Figure 24: Observed Zxy, Profile 4.

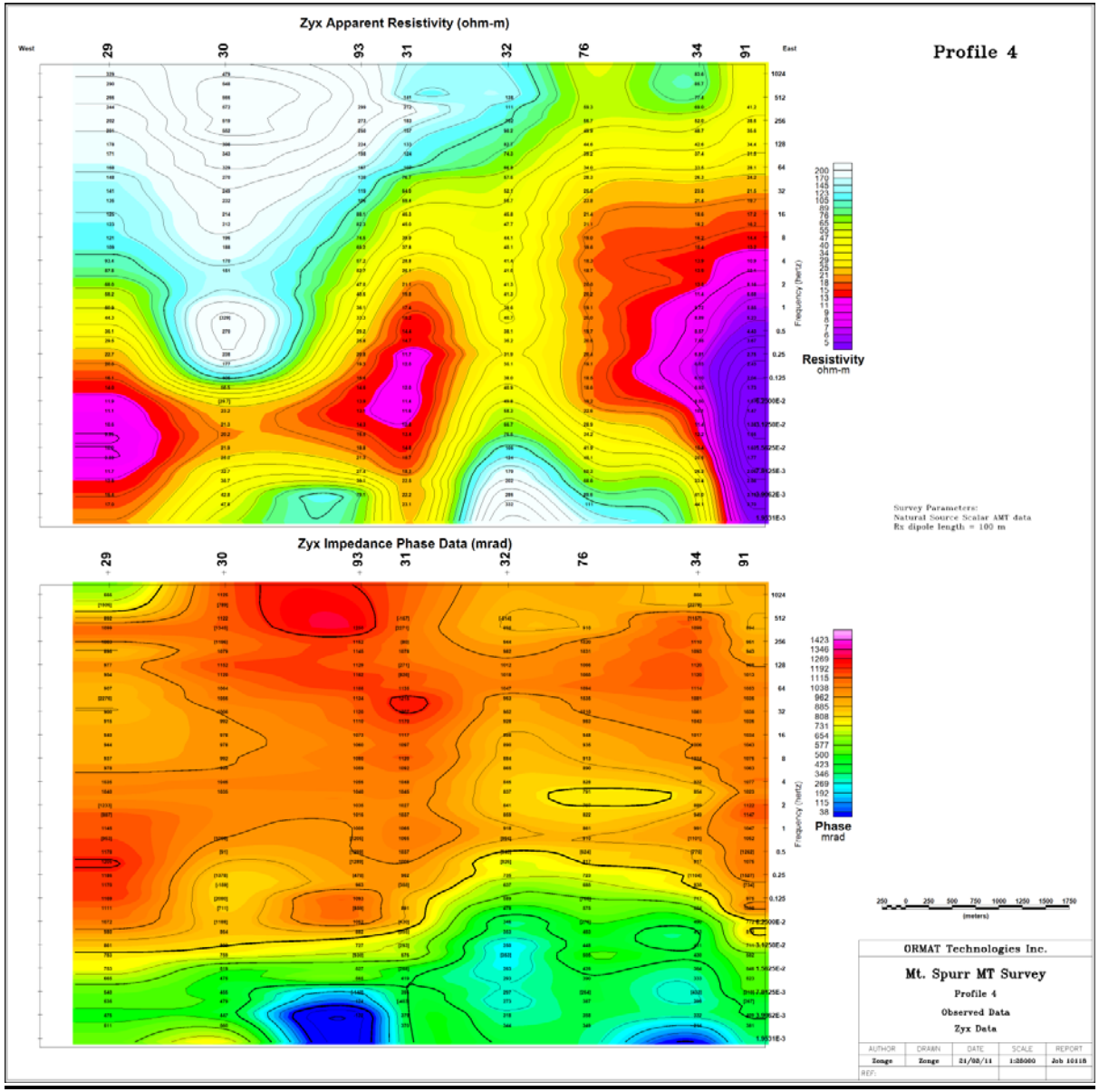

Figure 25: Observed Zyx Profile 4.

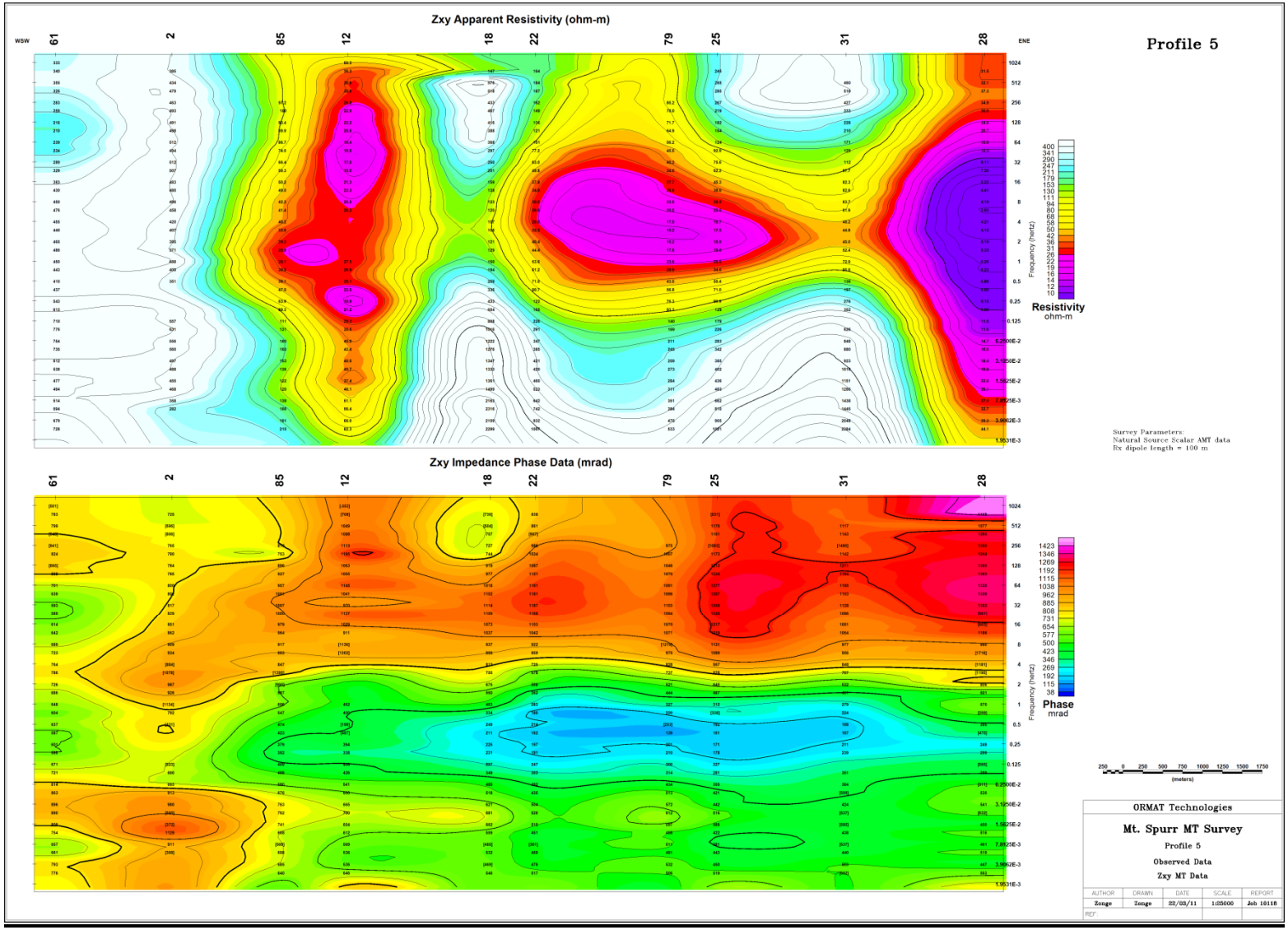

Figure 26: Observed Zxy, Profile 5.

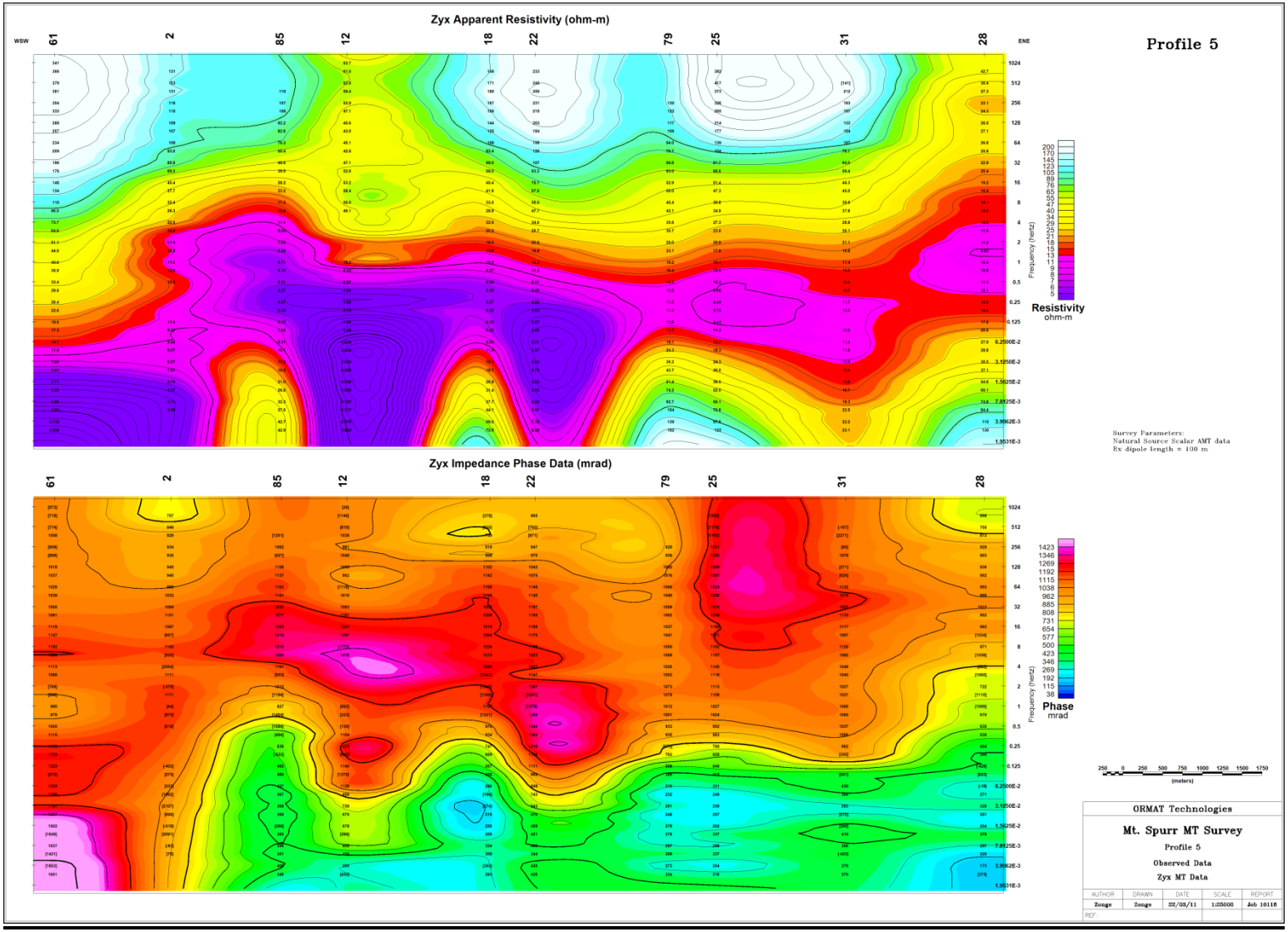

Figure 27: Observed Zyx, Profile 5.

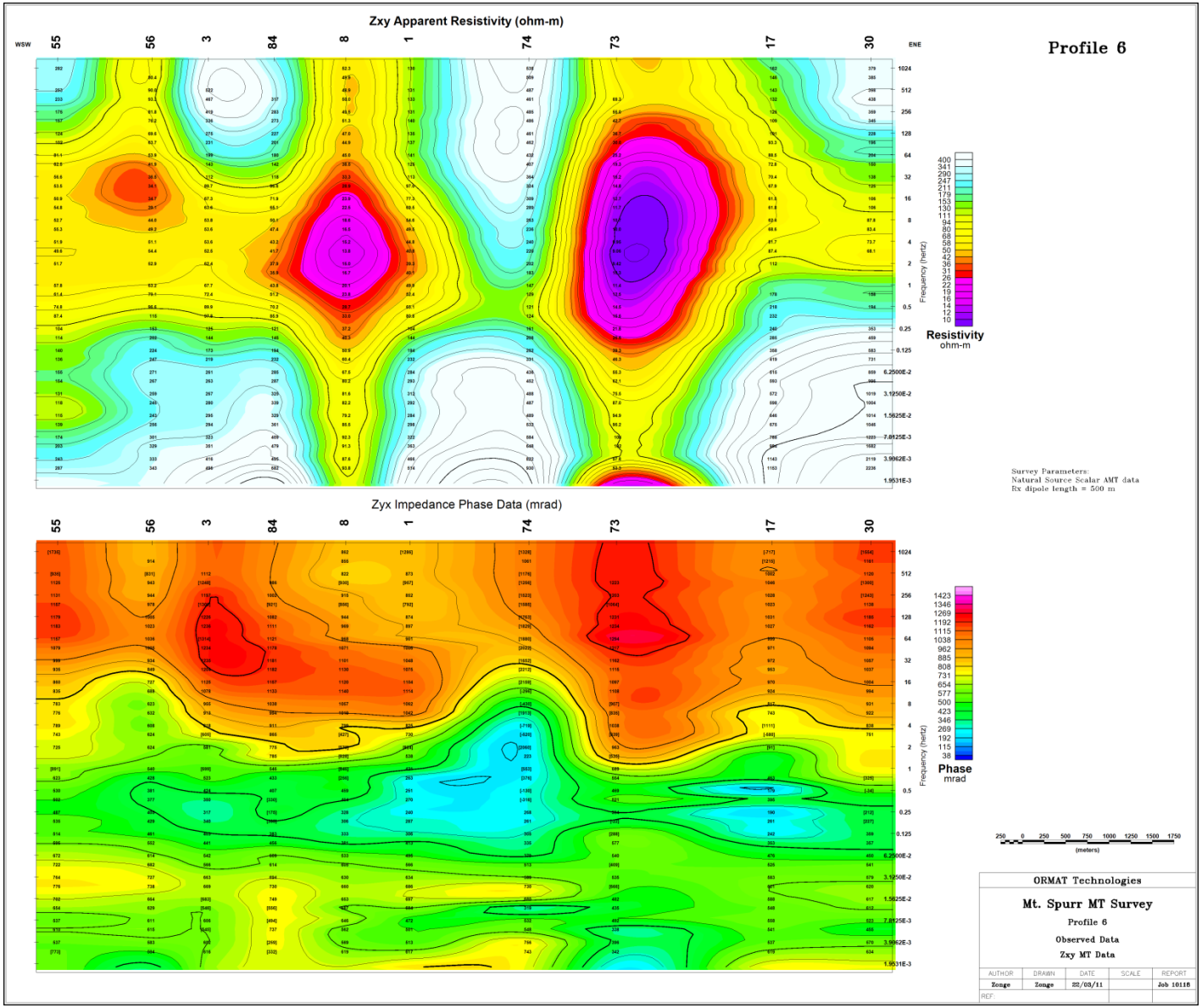

Figure 28: Observed Zxy, Profile 6.

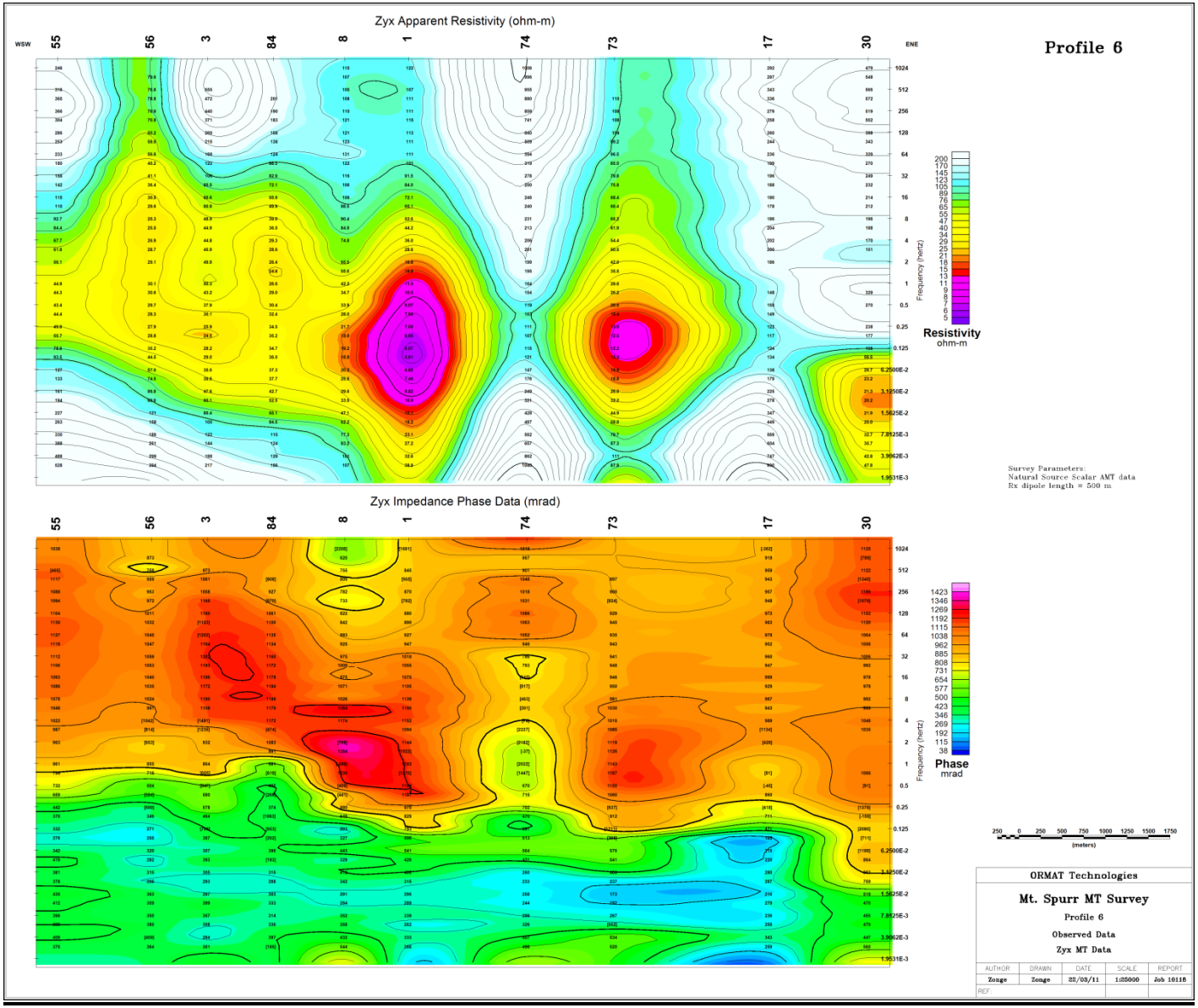

Figure 29: Observed Zyx, Profile 6.

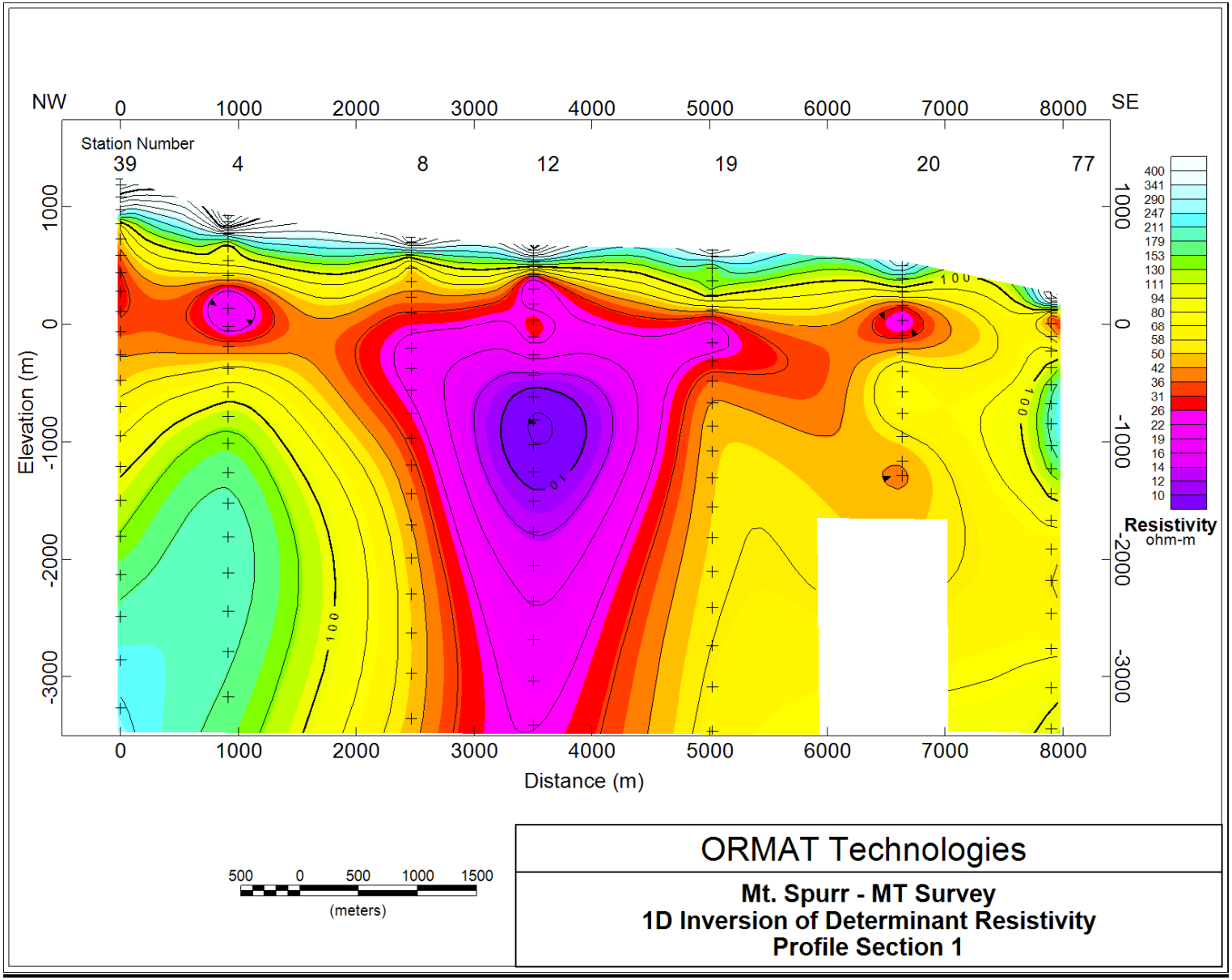

Figure 30: Section of 1D inversion results, Profile 1.

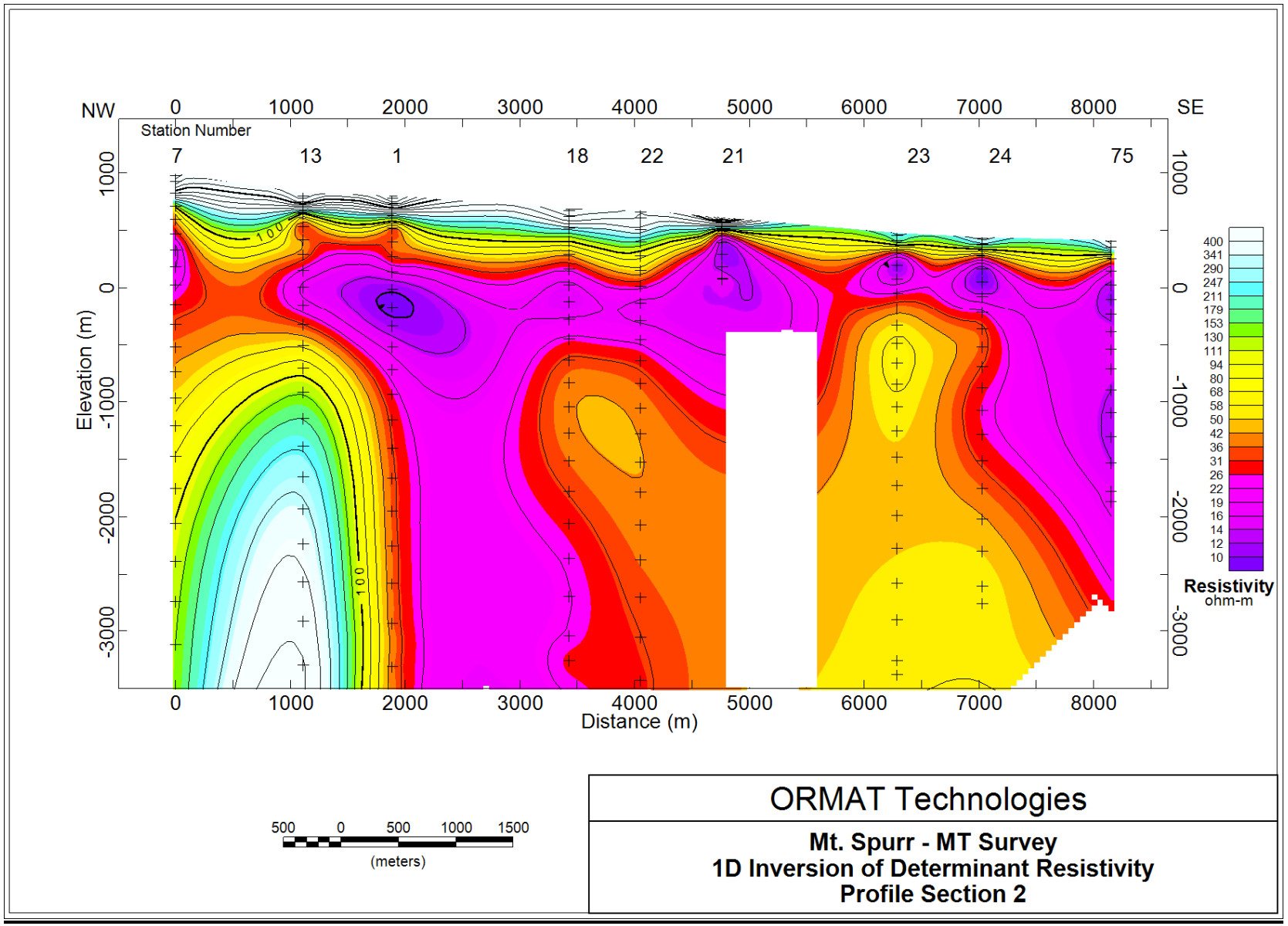

Figure 31: Section of 1D inversion results, Profile 2.

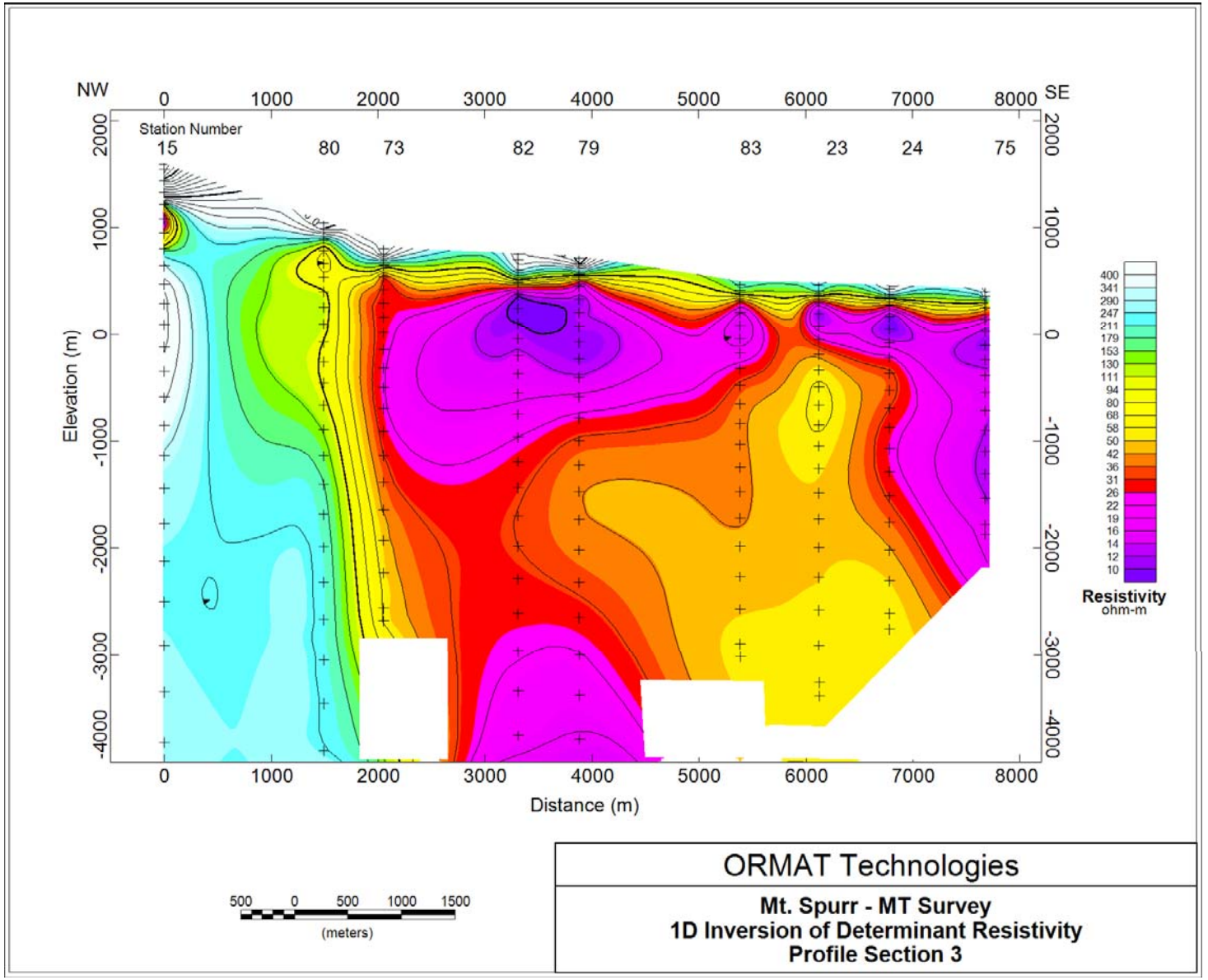

Figure 32: Section of 1D inversion results, Profile 3.

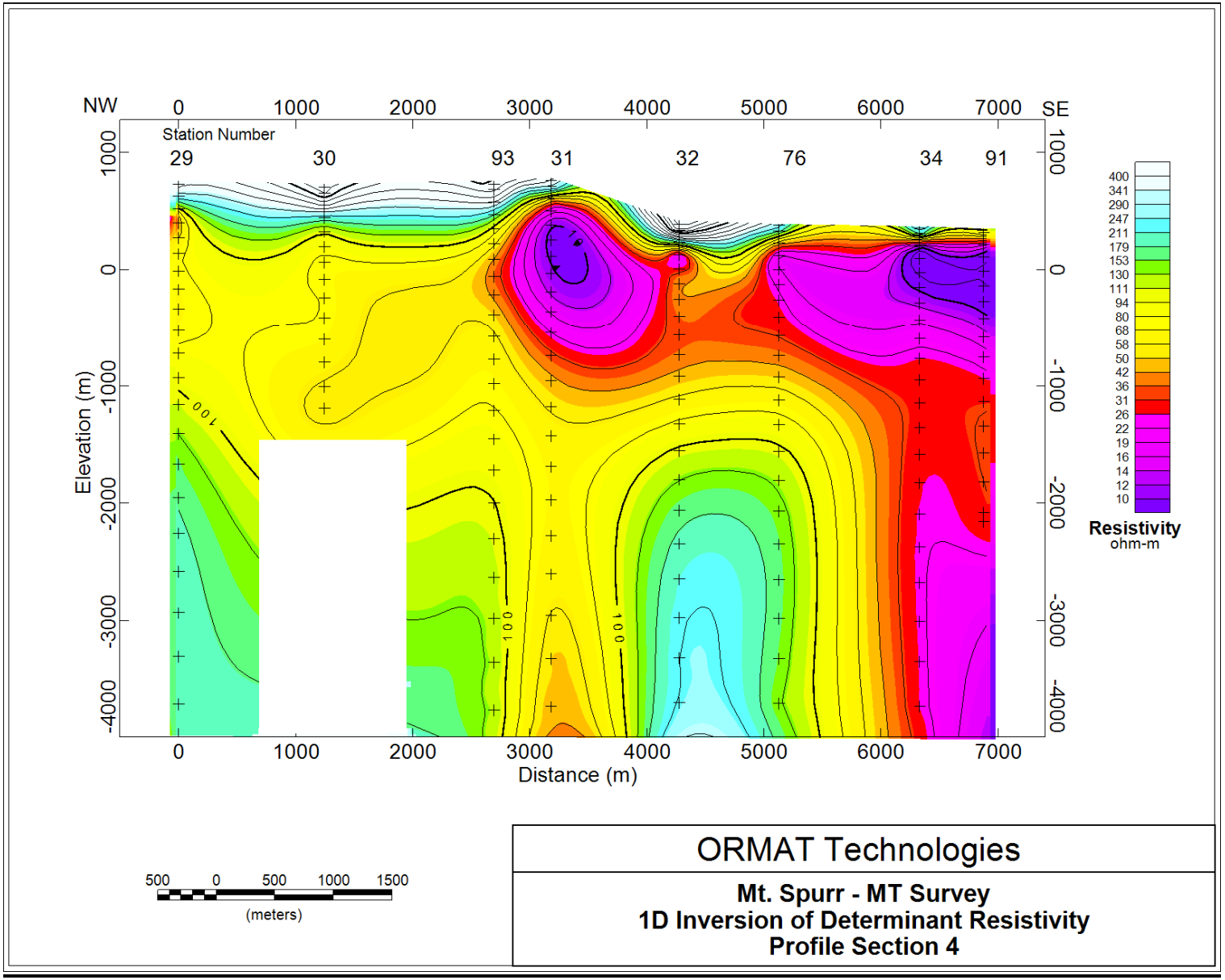

Figure 33: Section of 1D inversion results, Profile 4.

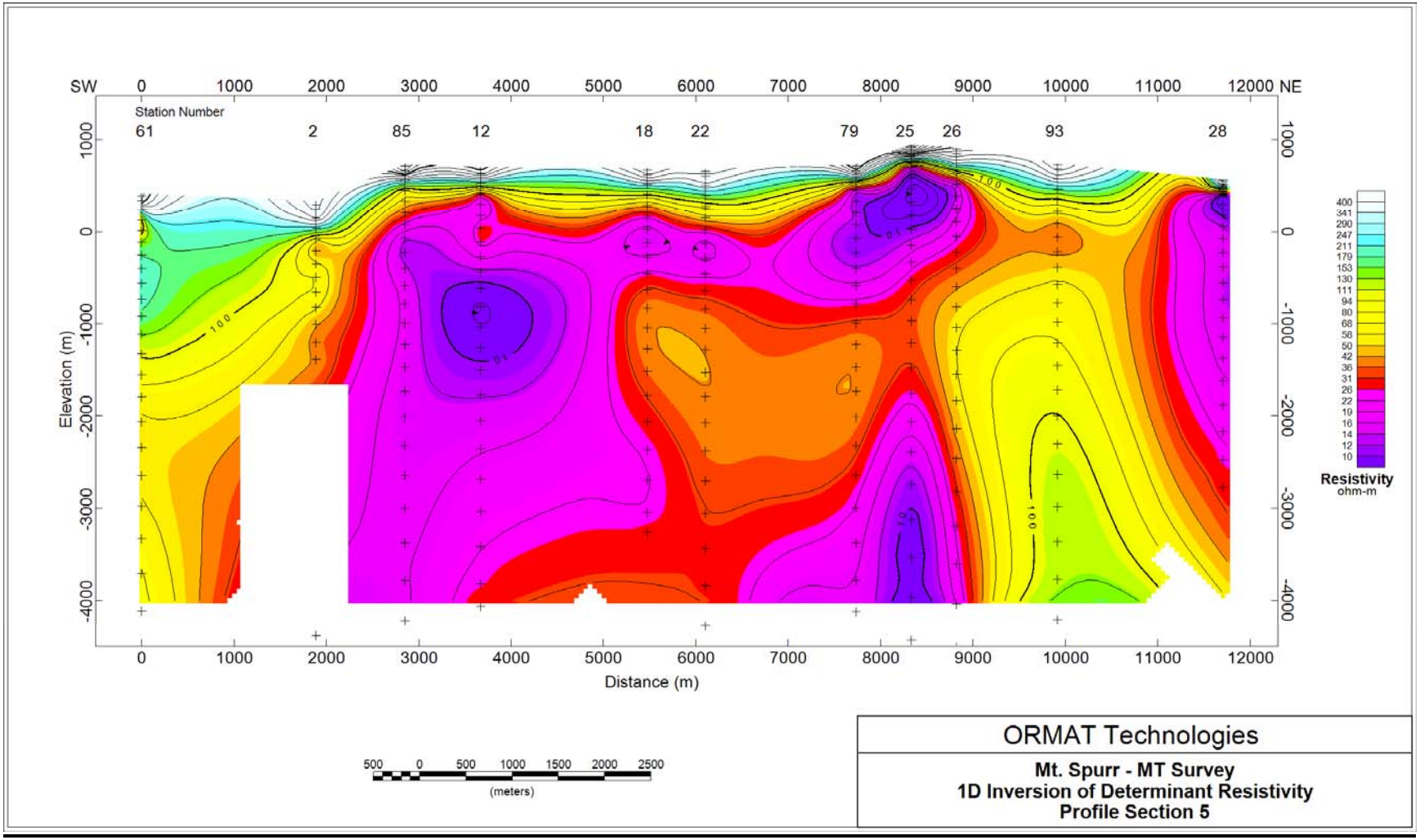

Figure 34: Section of 1D inversion results, Profile 5.

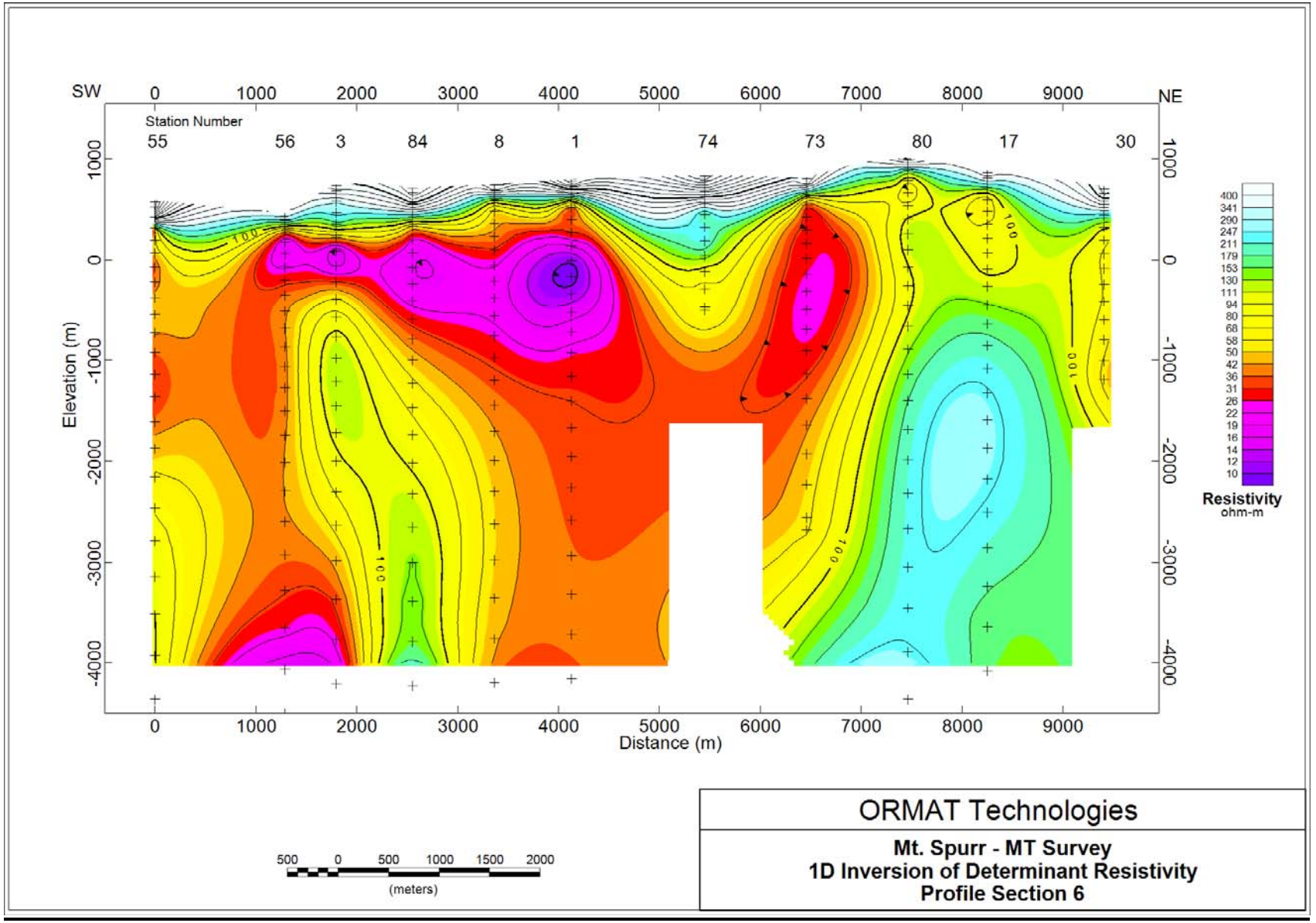

Figure 35: Section of 1D inversion results, Profile 6.

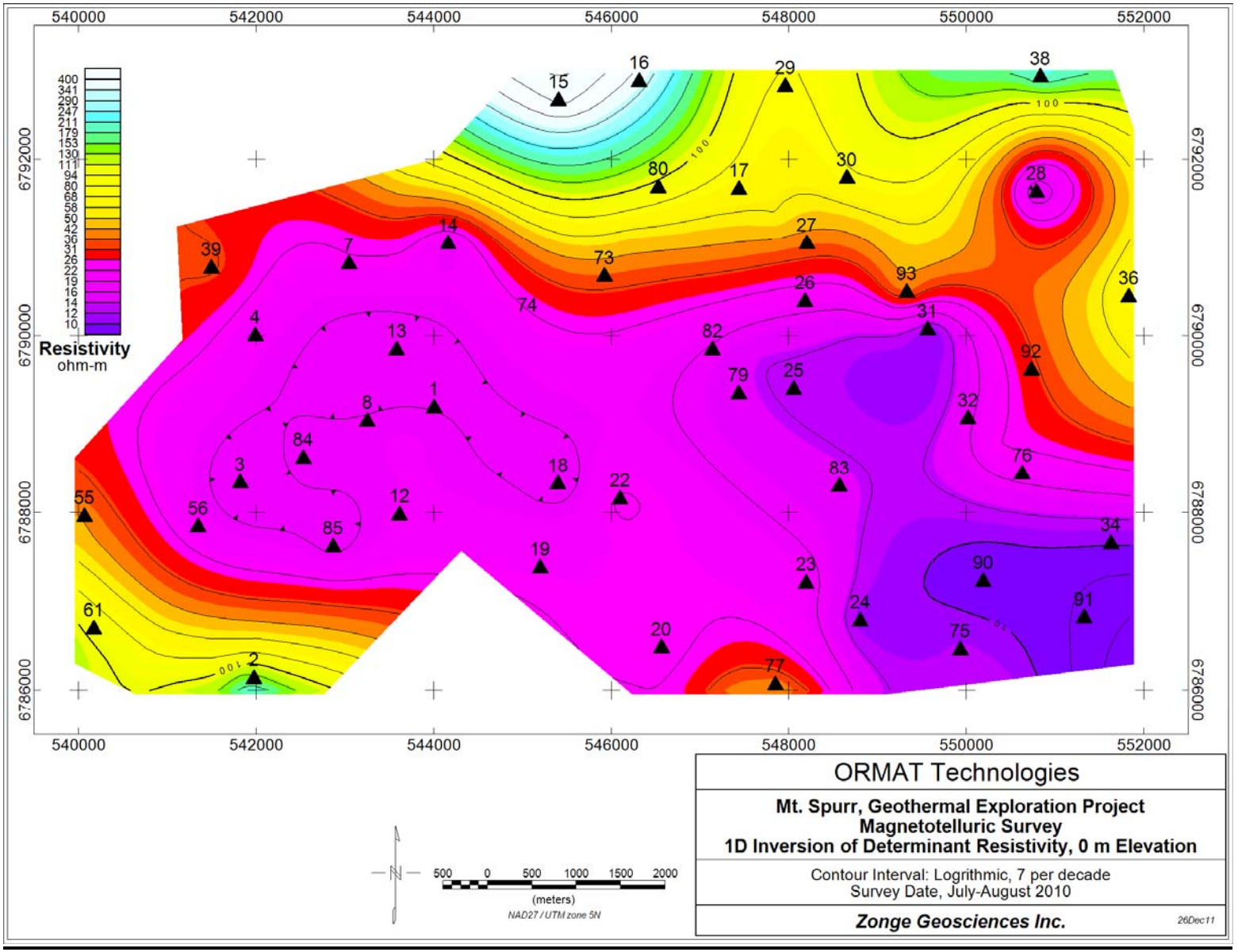

Figure 36: Contour map of 1D inversion results, 0m elevation.

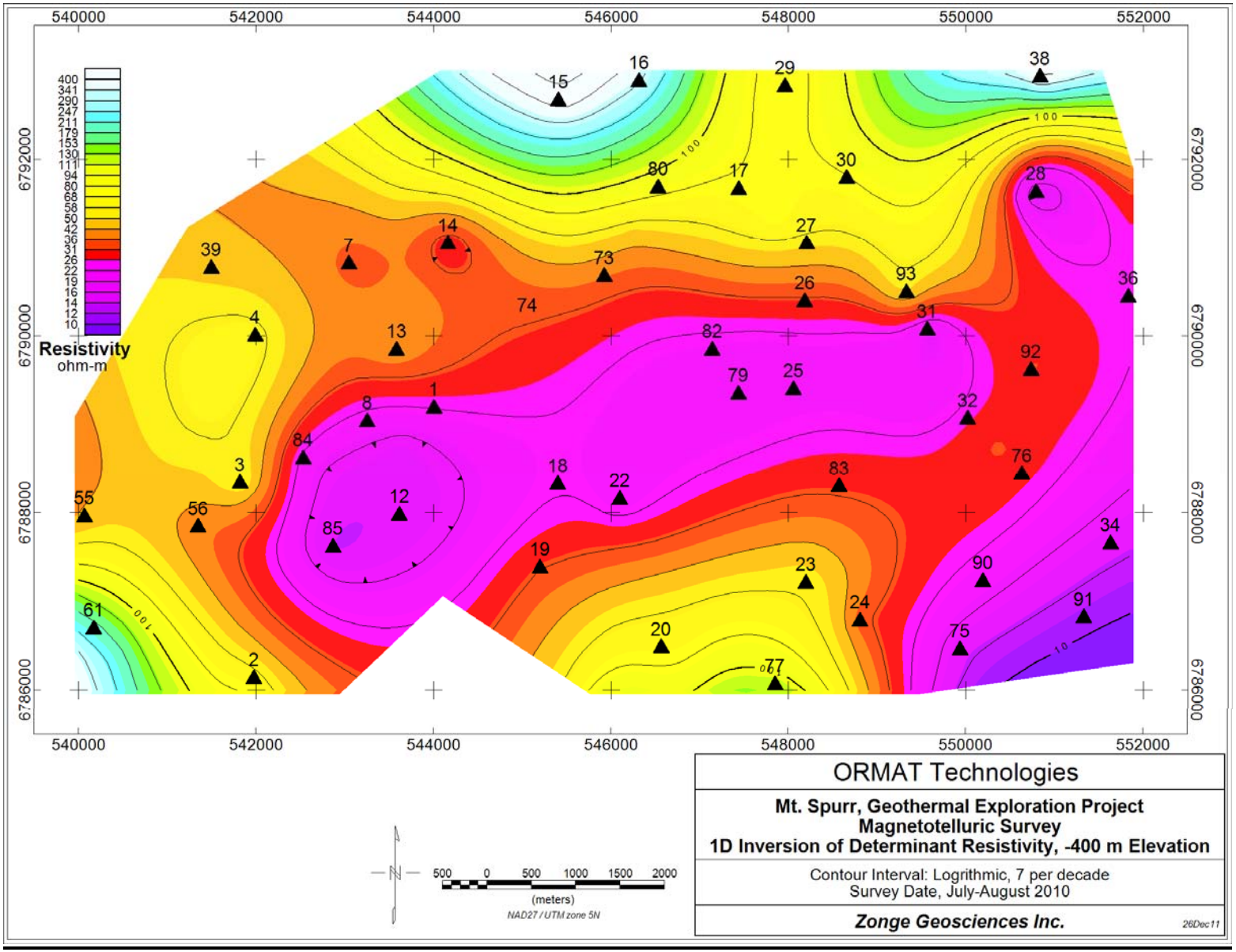

Figure 37: Contour map of 1D inversion results, -400m elevation.

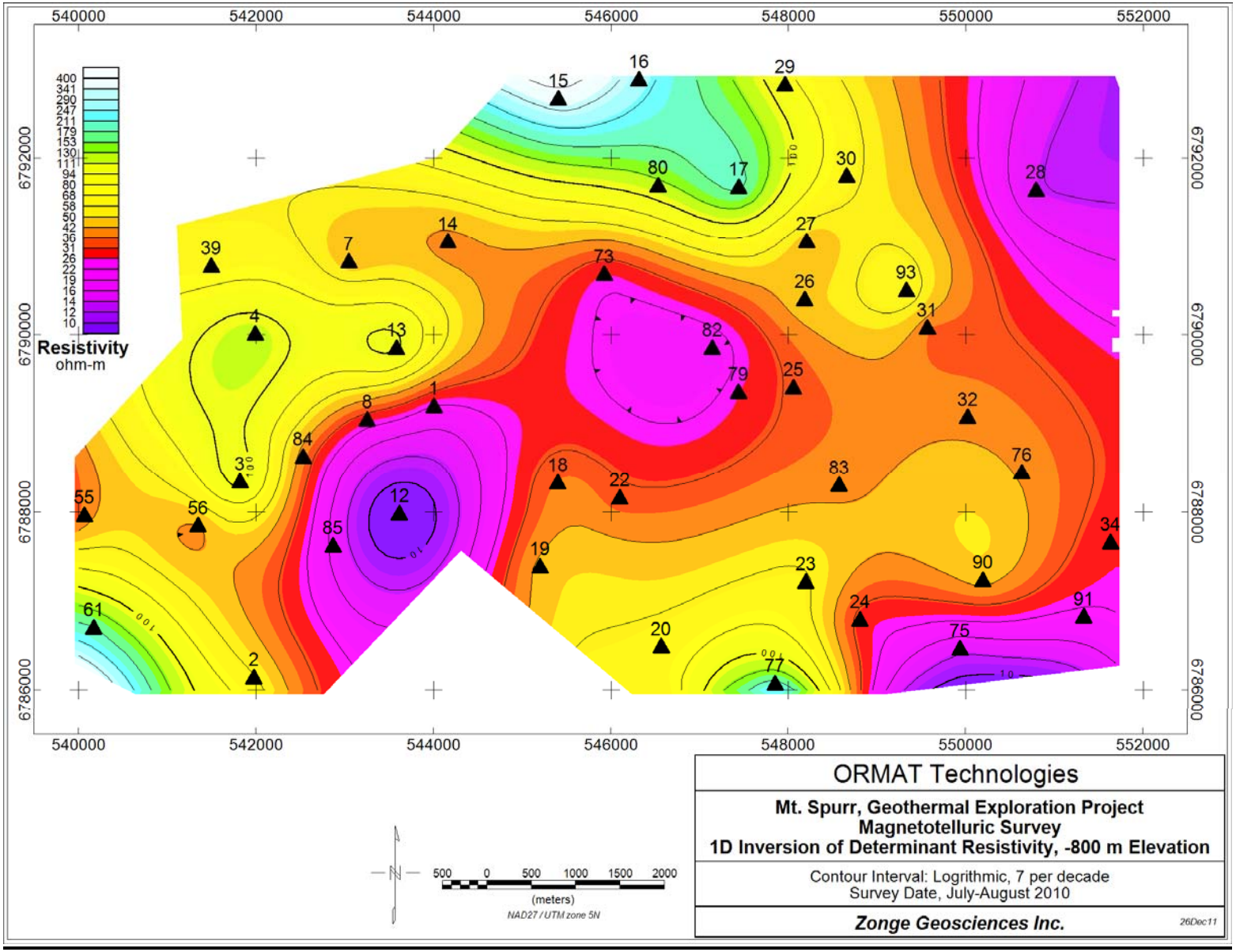

Figure 38: Contour map of 1D inversion results, -800m elevation.

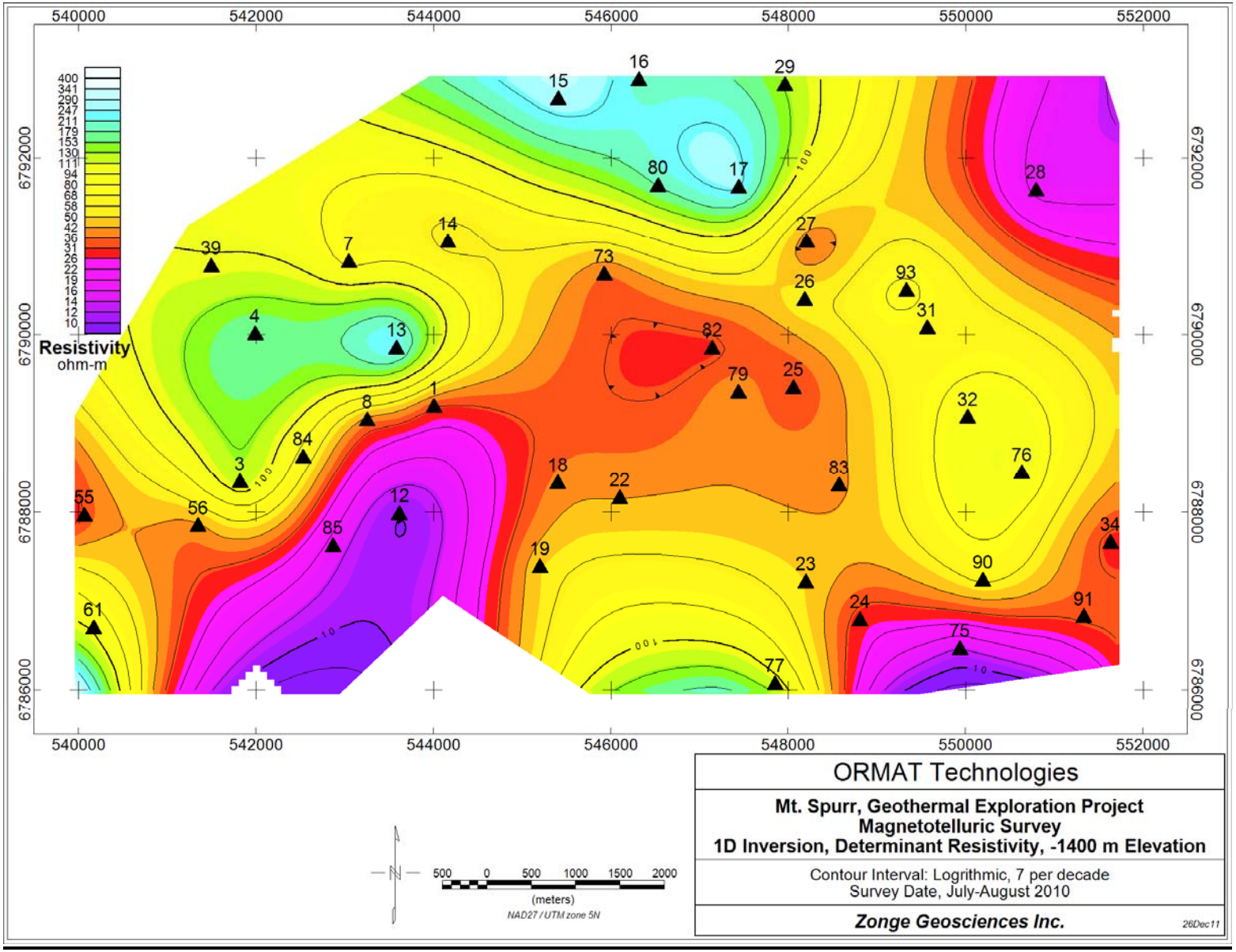

Figure 39: Contour map of 1D inversion results. -1400m elevation.

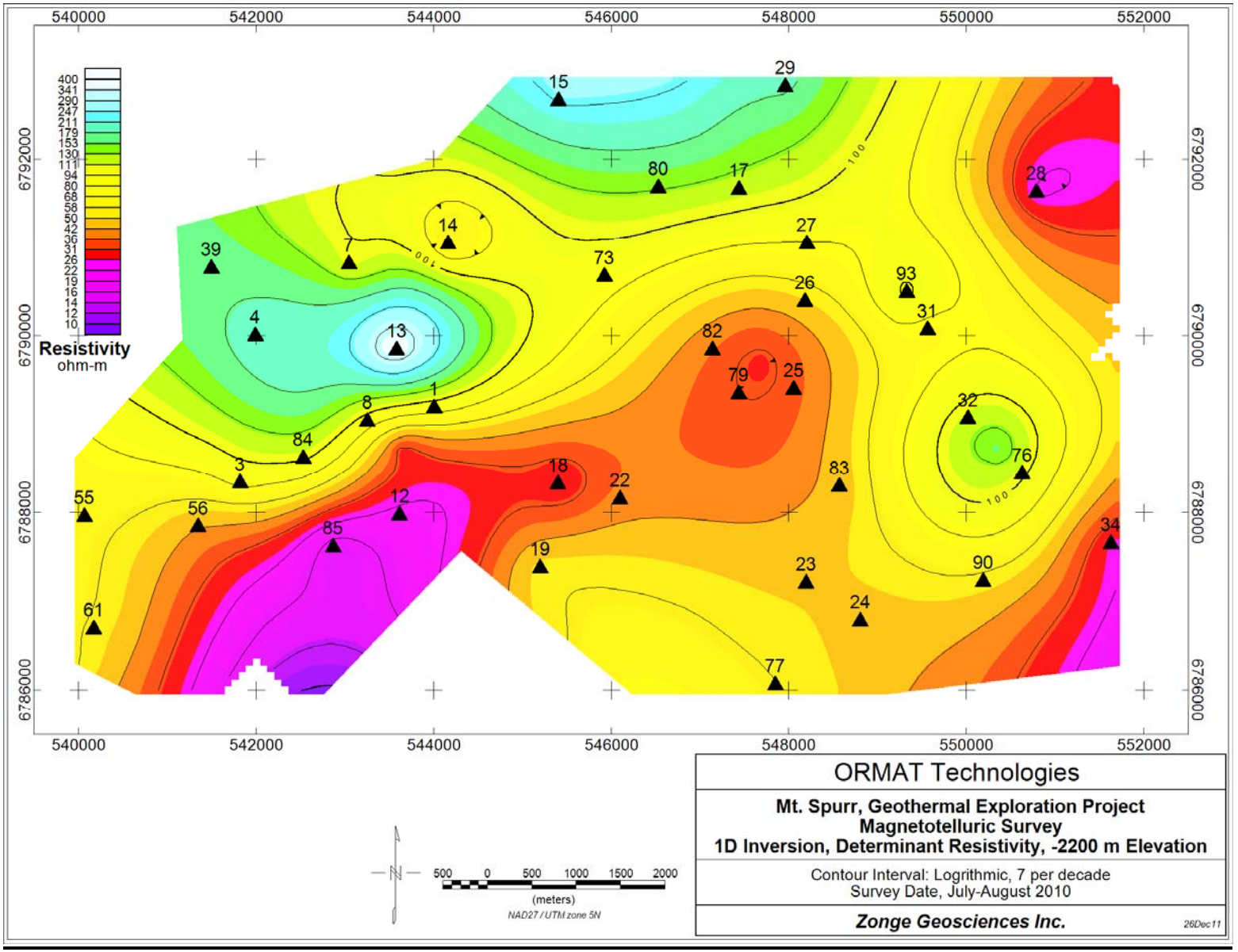

Figure 40: Contour map of 1D inversion results, -2200m elevation.

APPENDIX B: MT DATA CURVES

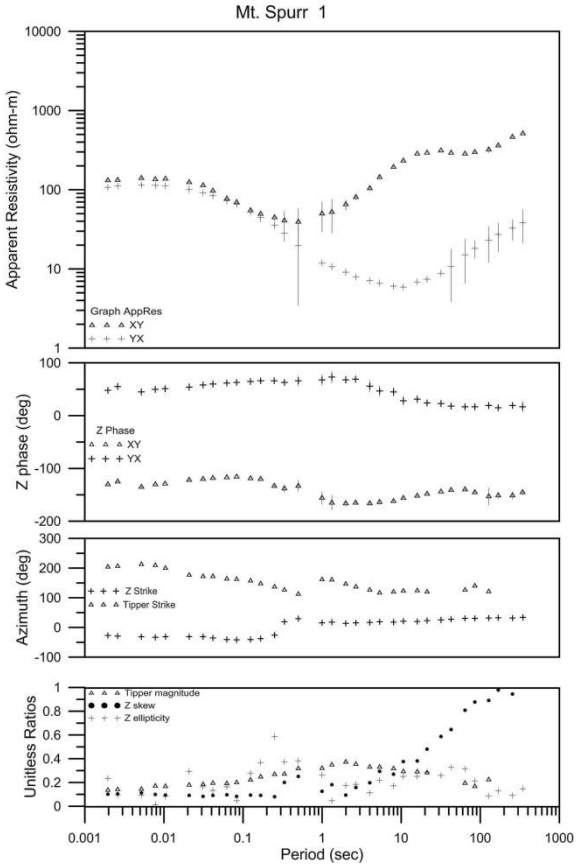
Mt. Spurr 1
Apparent Resistivity (ohm-m)
Graph AppRes
XY
YX
Z phase (deg)
Z Phase
XY
YX
Azimuth (deg)
Z Strike
Tipper Strike
Unitless Ratios
Tipper magnitude
Z skew
Z ellipticity
Period (sec)

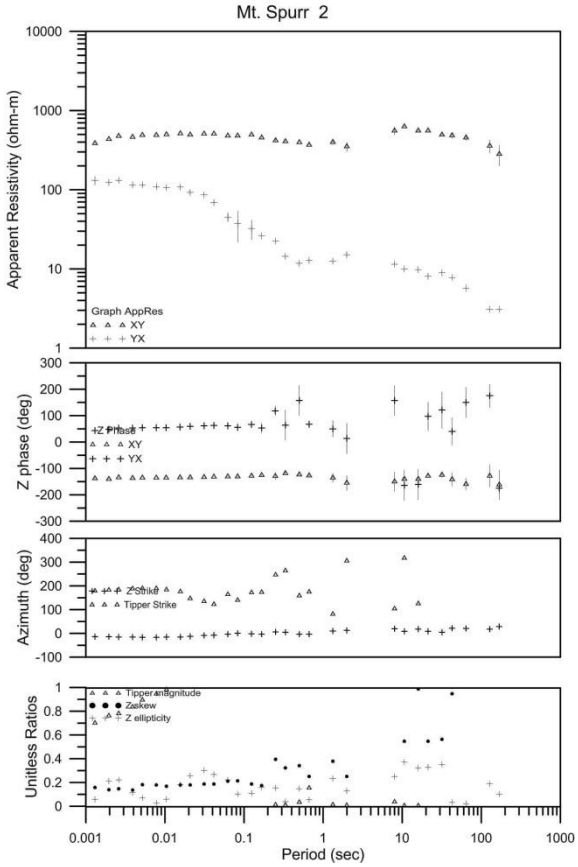
Mt. Spurr 2
Apparent Resistivity (ohm-m)
Graph AppRes
XY
YX
Z phase (deg)
Z Phase
XY
YX
Azimuth (deg)
Z Strike
Tipper Strike
Unitless Ratios
Tipper magnitude
Z skew
Z ellipticity
Period (sec)

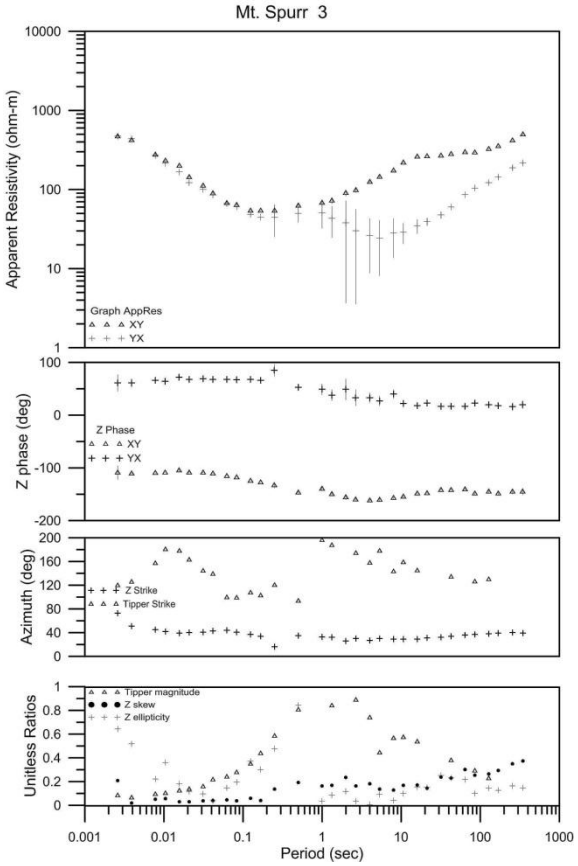
Mt. Spurr 3
Apparent Resistivity (ohm-m)
Graph AppRes
XY
YX
Z phase (deg)
Z Phase
XY
YX
Azimuth (deg)
Z Strike
Tipper Strike
Unitless Ratios
Tipper magnitude
Z skew
Z ellipticity
Period (sec)

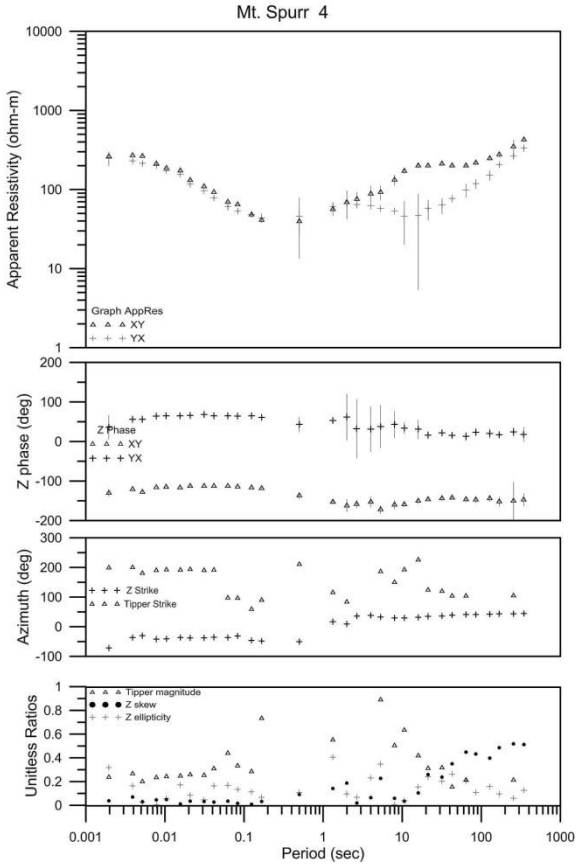
Mt. Spurr 4
Apparent Resistivity (ohm-m)
Graph AppRes
XY
YX
Z phase (deg)
Z Phase
XY
YX
Azimuth (deg)
Z Strike
Tipper Strike
Unitless Ratios
Tipper magnitude
Z skew
Z ellipticity
Period (sec)

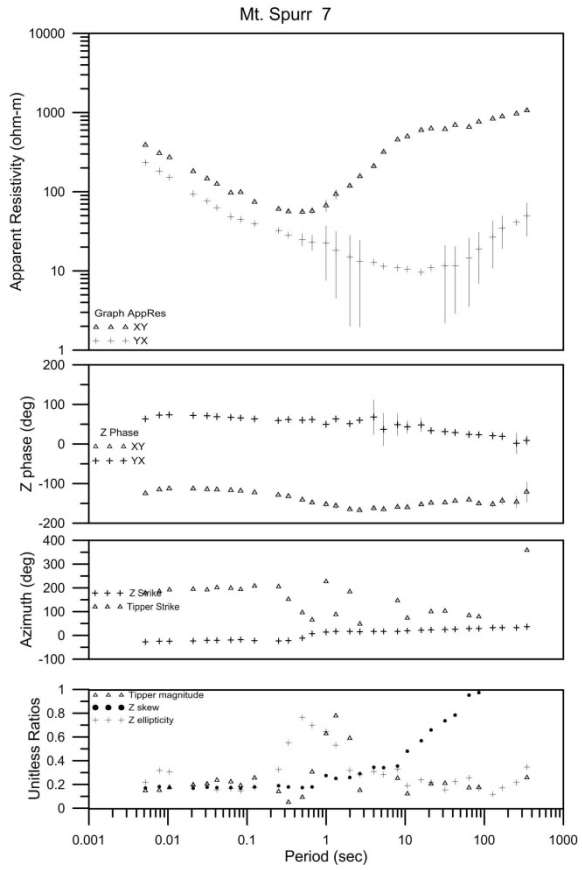
Mt. Spurr 7
Apparent Resistivity (ohm-m)
Graph AppRes
XY
YX
Z phase (deg)
Z Phase
Azimuth (deg)
Z Strike
Tipper Strike
Unitless Ratios
Tipper magnitude
Z skew
Z ellipticity
Period (sec)

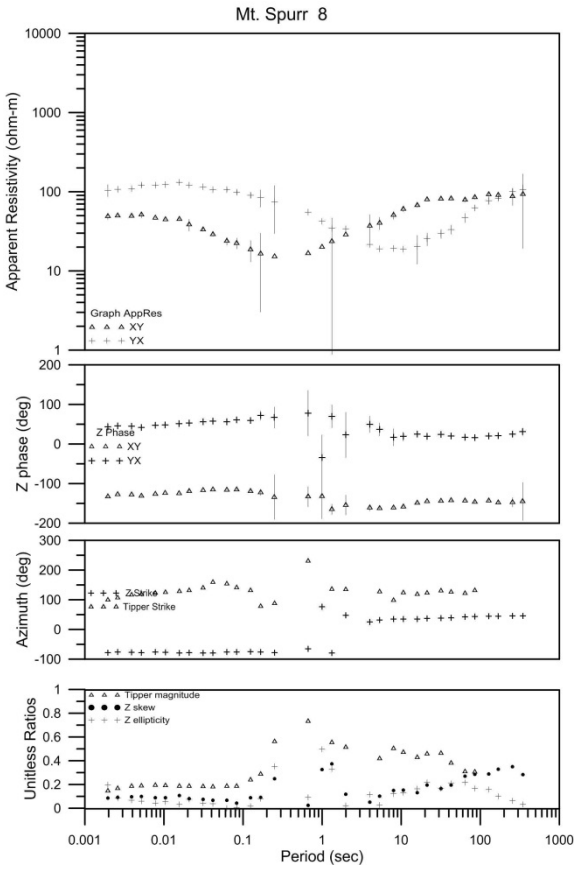
Mt. Spurr 8
Apparent Resistivity (ohm-m)
Graph AppRes
XY
YX
Z phase (deg)
Z Phase
Azimuth (deg)
Z Strike
Tipper Strike
Unitless Ratios
Tipper magnitude
Z skew
Z ellipticity
Period (sec)

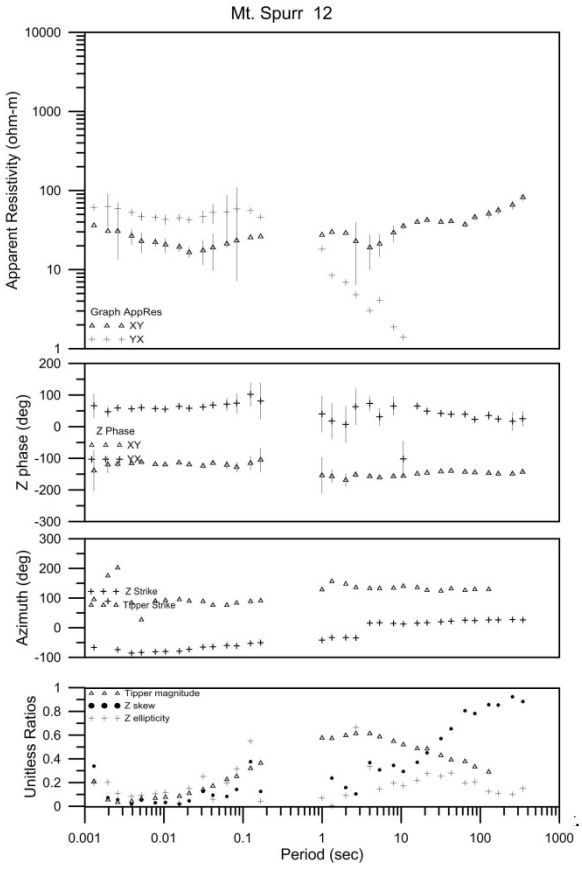
Mt. Spurr 12
Apparent Resistivity (ohm-m)
Graph AppRes
XY
YX
Z phase (deg)
Z Phase
Azimuth (deg)
Z Strike
Tipper Strike
Unitless Ratios
Tipper magnitude
Z skew
Z ellipticity
Period (sec)

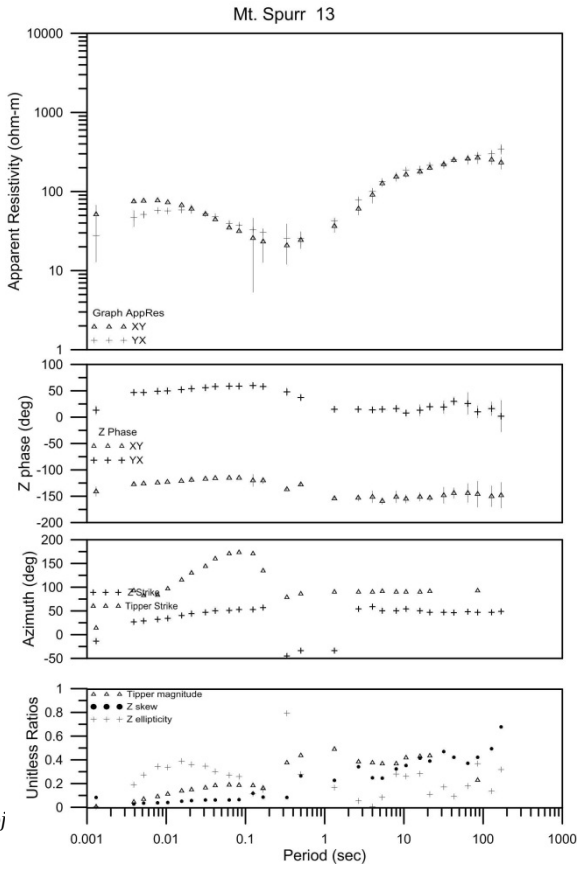
Mt. Spurr 13
Apparent Resistivity (ohm-m)
Graph AppRes
XY
YX
Z phase (deg)
Z Phase
Azimuth (deg)
Z Strike
Tipper Strike
Unitless Ratios
Tipper magnitude
Z skew
Z ellipticity
Period (sec)

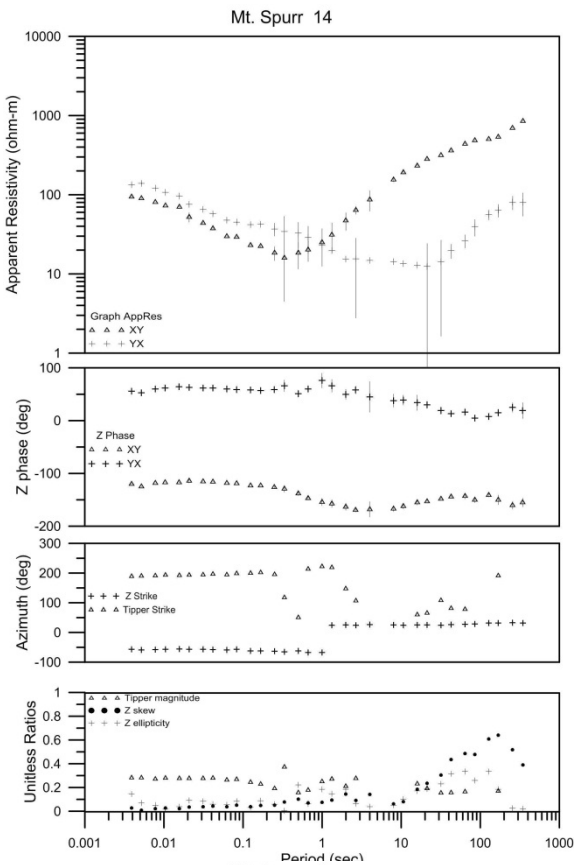
Mt. Spurr 14
Apparent Resistivity (ohm-m)
Graph AppRes
XY
YX
Z phase (deg)
Z Phase
XY
YX
Azimuth (deg)
Z Strike
Tipper Strike
Unitless Ratios
Tipper magnitude
Z skew
Z ellipticity
Period (sec)

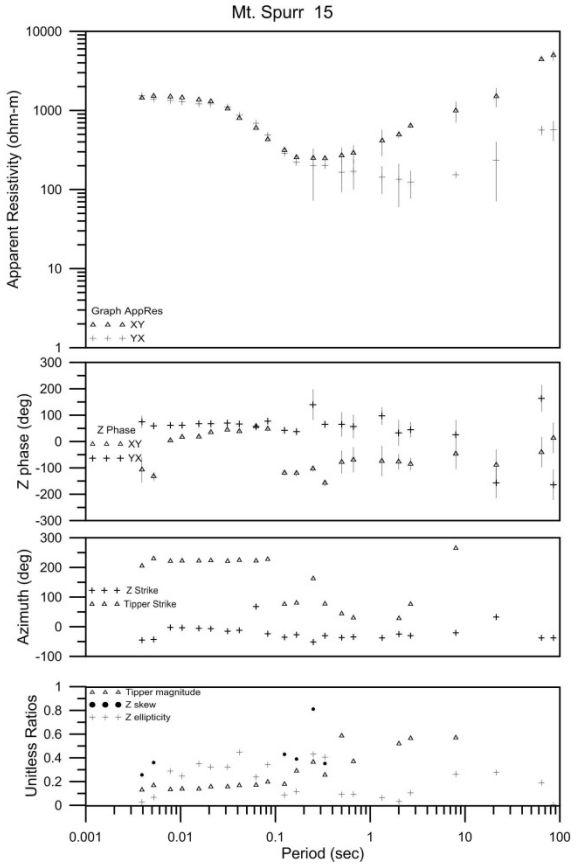
Mt. Spurr 15
Apparent Resistivity (ohm-m)
Graph AppRes
XY
YX
Z phase (deg)
Z Phase
XY
YX
Azimuth (deg)
Z Strike
Tipper Strike
Unitless Ratios
Tipper magnitude
Z skew
Z ellipticity
Period (sec)

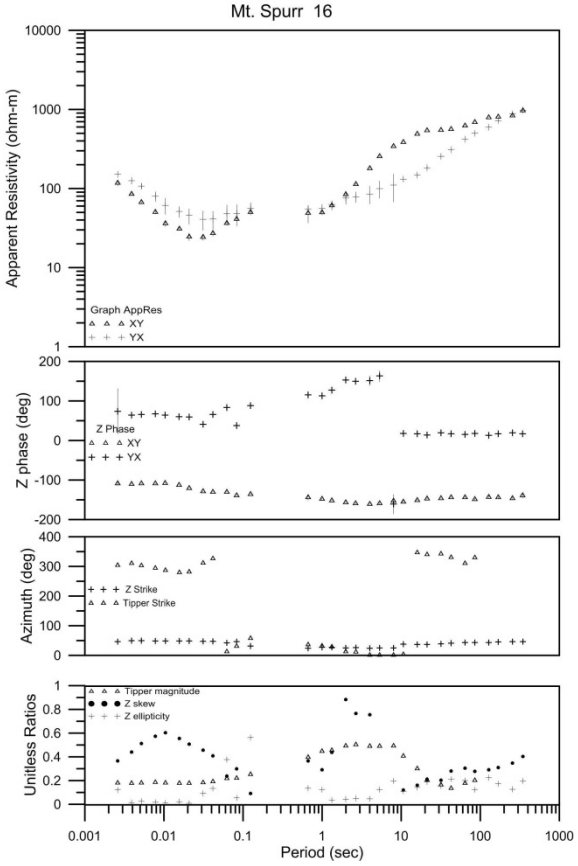
Mt. Spurr 16
Apparent Resistivity (ohm-m)
Graph AppRes
XY
YX
Z phase (deg)
Z Phase
XY
YX
Azimuth (deg)
Z Strike
Tipper Strike
Unitless Ratios
Tipper magnitude
Z skew
Z ellipticity
Period (sec)

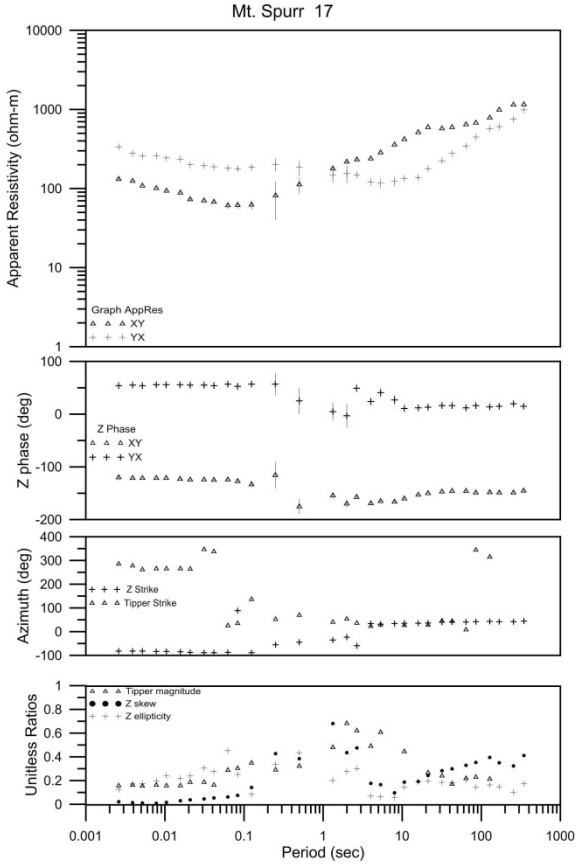
Mt. Spurr 17
Apparent Resistivity (ohm-m)
Graph AppRes
XY
YX
Z phase (deg)
Z Phase
XY
YX
Azimuth (deg)
Z Strike
Tipper Strike
Unitless Ratios
Tipper magnitude
Z skew
Z ellipticity
Period (sec)

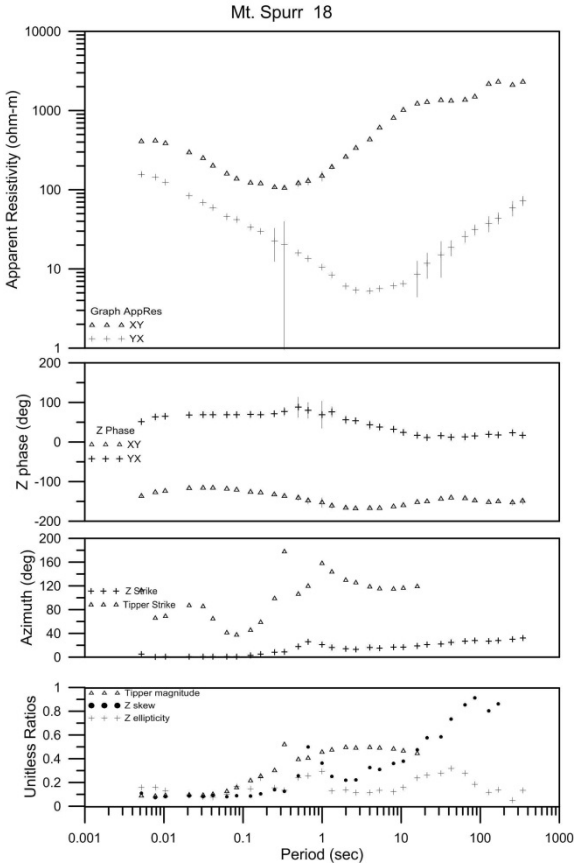
Mt. Spurr 18
Apparent Resistivity (ohm-m)
Graph AppRes
XY
YX
Z phase (deg)
Z Phase
Azimuth (deg)
Z Strike
Tipper Strike
Unitless Ratios
Tipper magnitude
Z skew
Z ellipticity
Period (sec)

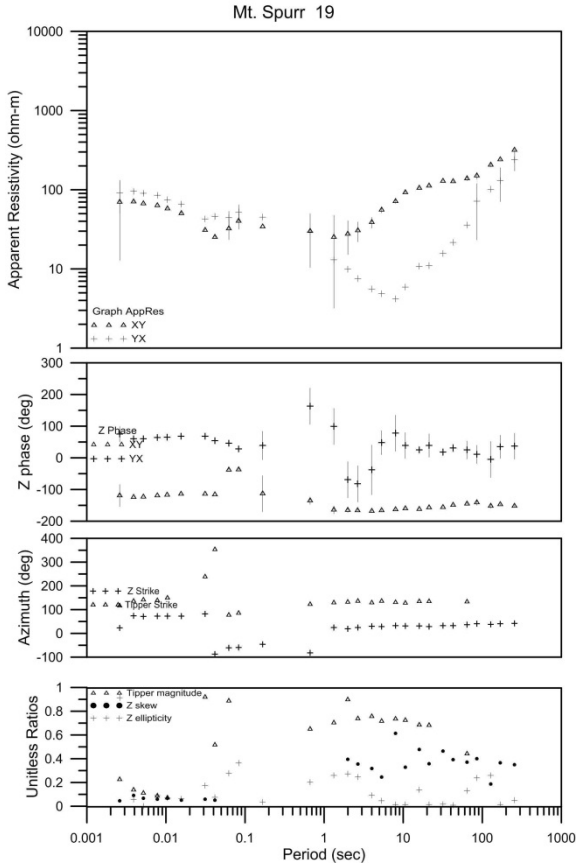
Mt. Spurr 19
Apparent Resistivity (ohm-m)
Graph AppRes
XY
YX
Z phase (deg)
Z Phase
Azimuth (deg)
Z Strike
Tipper Strike
Unitless Ratios
Tipper magnitude
Z skew
Z ellipticity
Period (sec)

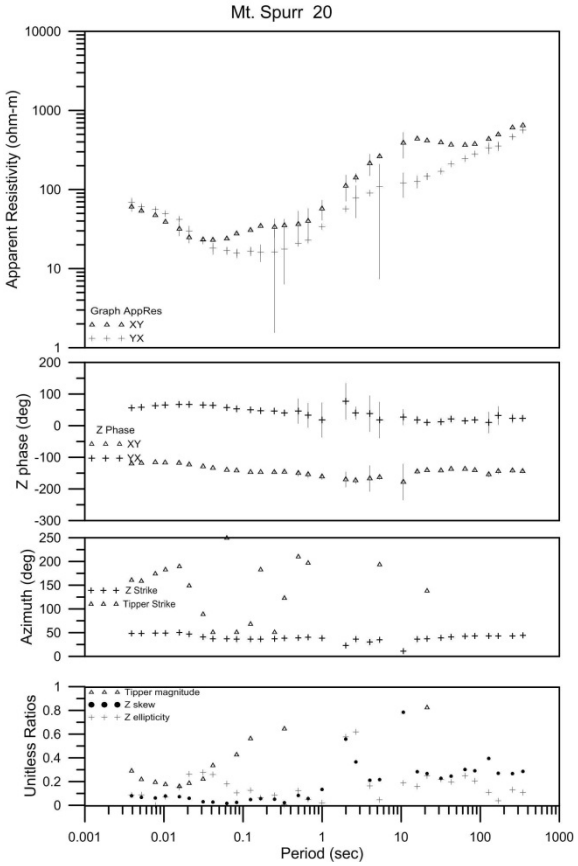
Mt. Spurr 20
Apparent Resistivity (ohm-m)
Graph AppRes
XY
YX
Z phase (deg)
Z Phase
Azimuth (deg)
Z Strike
Tipper Strike
Unitless Ratios
Tipper magnitude
Z skew
Z ellipticity
Period (sec)

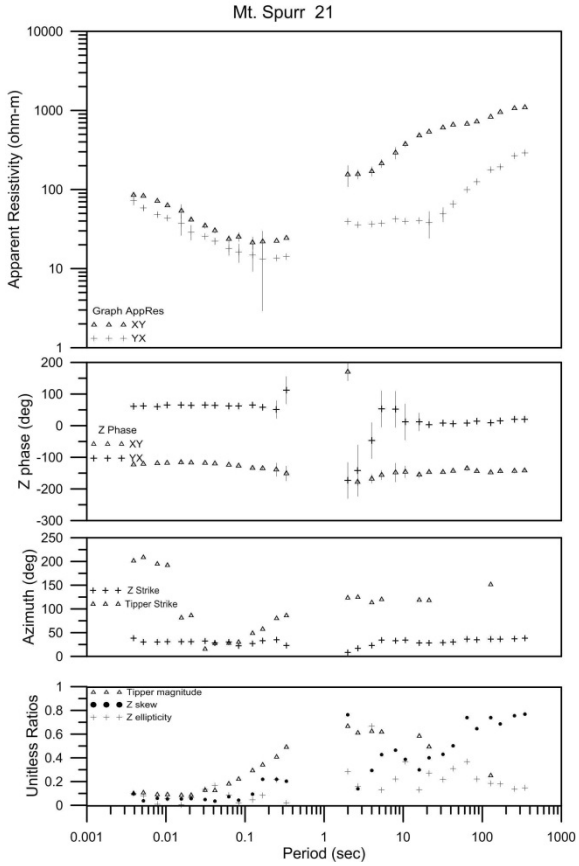
Mt. Spurr 21
Apparent Resistivity (ohm-m)
Graph AppRes
XY
YX
Z phase (deg)
Z Phase
Azimuth (deg)
Z Strike
Tipper Strike
Unitless Ratios
Tipper magnitude
Z skew
Z ellipticity
Period (sec)

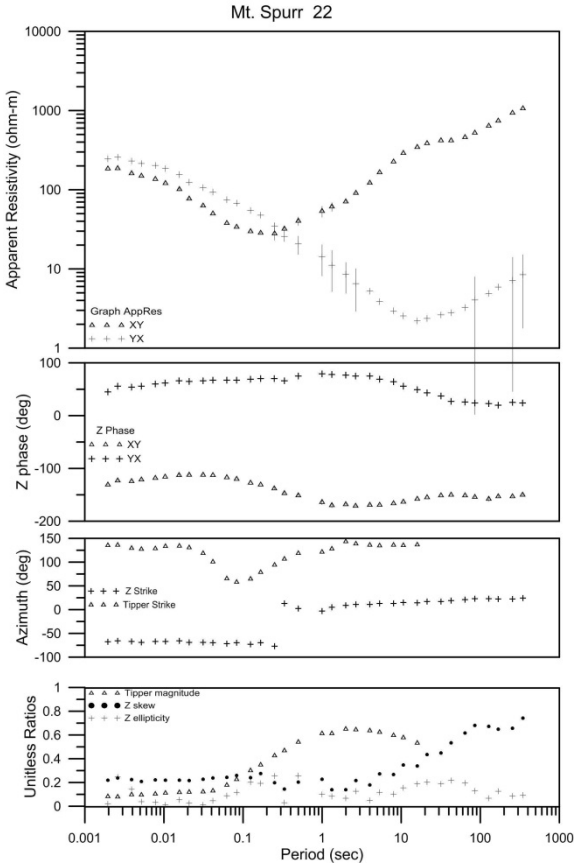
Mt. Spurr 22
Apparent Resistivity (ohm-m)
Graph AppRes
XY
YX
Z phase (deg)
Z Phase
XY
YX
Azimuth (deg)
Z Strike
Tipper Strike
Unitless Ratios
Tipper magnitude
Z skew
Z ellipticity
Period (sec)

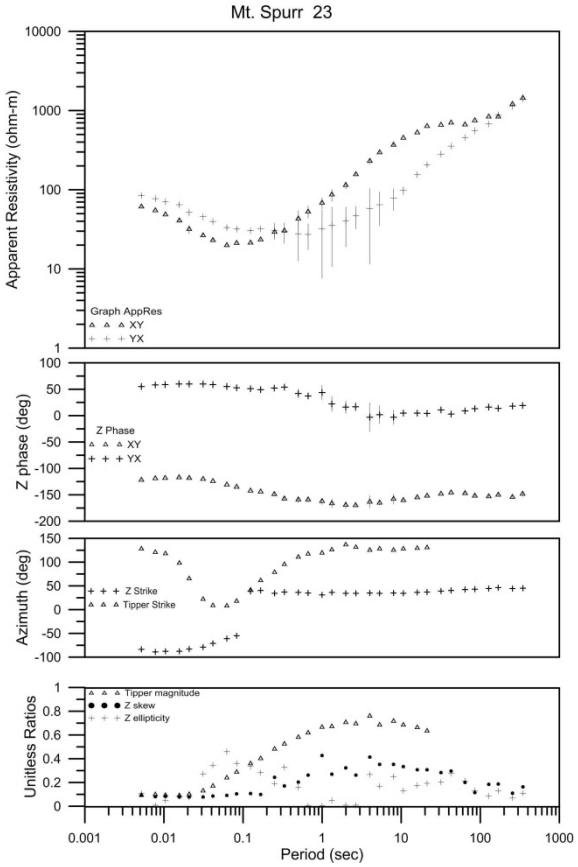
Mt. Spurr 23
Apparent Resistivity (ohm-m)
Graph AppRes
XY
YX
Z phase (deg)
Z Phase
XY
YX
Azimuth (deg)
Z Strike
Tipper Strike
Unitless Ratios
Tipper magnitude
Z skew
Z ellipticity
Period (sec)

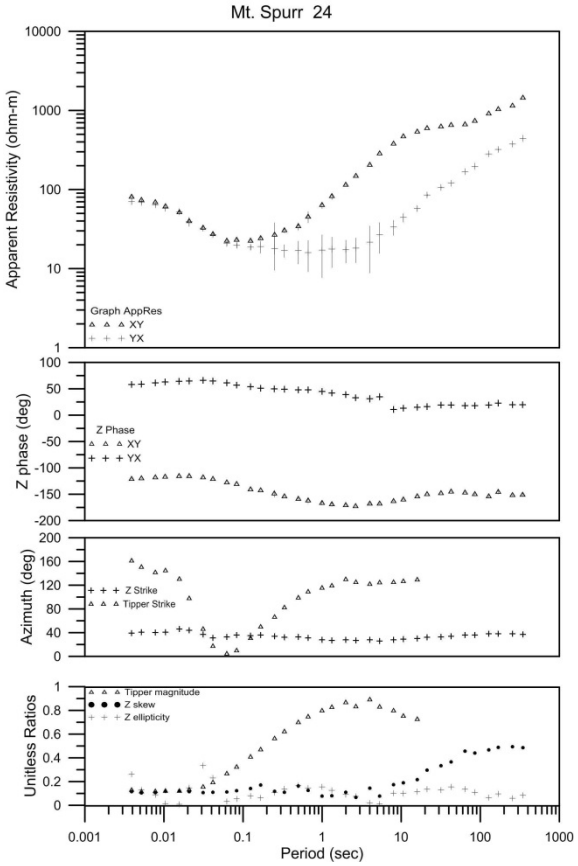
Mt. Spurr 24
Apparent Resistivity (ohm-m)
Graph AppRes
XY
YX
Z phase (deg)
Z Phase
XY
YX
Azimuth (deg)
Z Strike
Tipper Strike
Unitless Ratios
Tipper magnitude
Z skew
Z ellipticity
Period (sec)

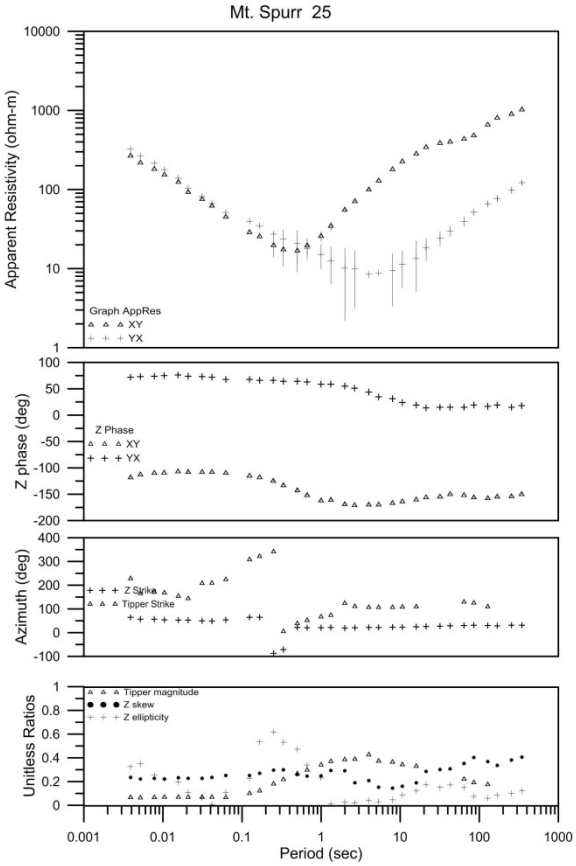
Mt. Spurr 25
Apparent Resistivity (ohm-m)
Graph AppRes
XY
YX
Z phase (deg)
Z Phase
XY
YX
Azimuth (deg)
Z Strike
Tipper Strike
Unitless Ratios
Tipper magnitude
Z skew
Z ellipticity
Period (sec)

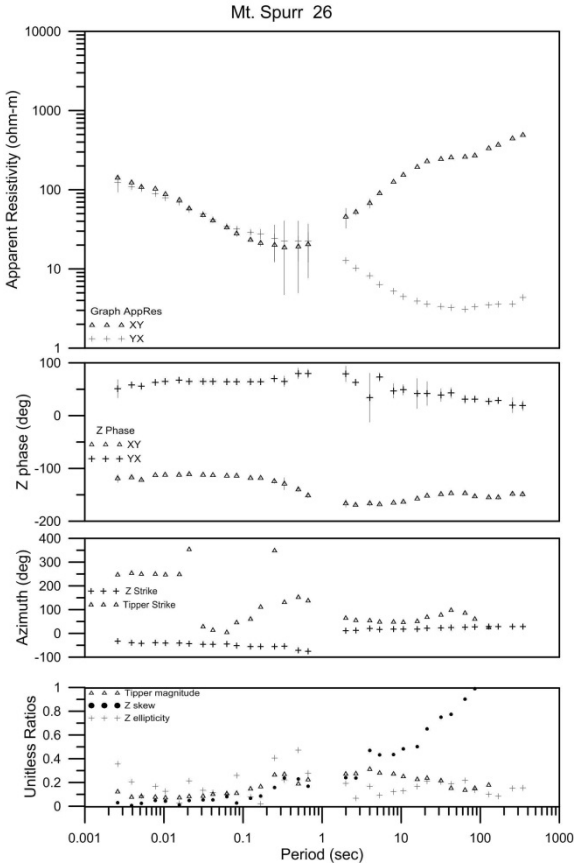
Mt. Spurr 26
Apparent Resistivity (ohm-m)
Graph AppRes
XY
YX
Z phase (deg)
Z Phase
Azimuth (deg)
Z Strike
Tipper Strike
Unitless Ratios
Tipper magnitude
Z skew
Z ellipticity
Period (sec)

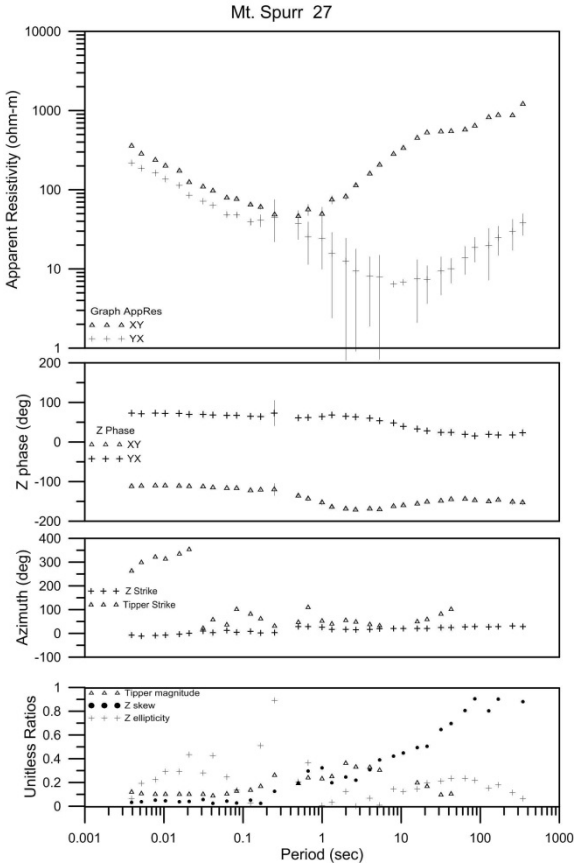
Mt. Spurr 27
Apparent Resistivity (ohm-m)
Graph AppRes
XY
YX
Z phase (deg)
Z Phase
Azimuth (deg)
Z Strike
Tipper Strike
Unitless Ratios
Tipper magnitude
Z skew
Z ellipticity
Period (sec)

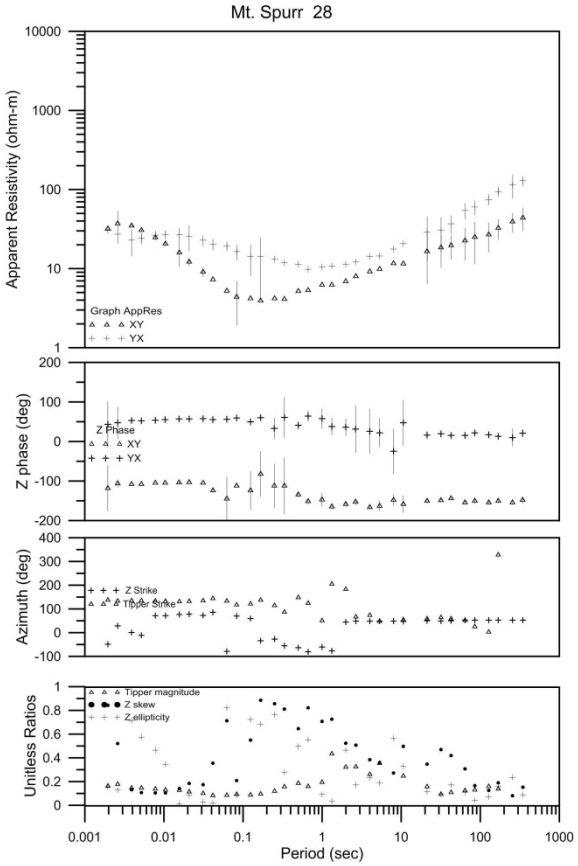
Mt. Spurr 28
Apparent Resistivity (ohm-m)
Graph AppRes
XY
YX
Z phase (deg)
Z Phase
Azimuth (deg)
Z Strike
Tipper Strike
Unitless Ratios
Tipper magnitude
Z skew
Z ellipticity
Period (sec)

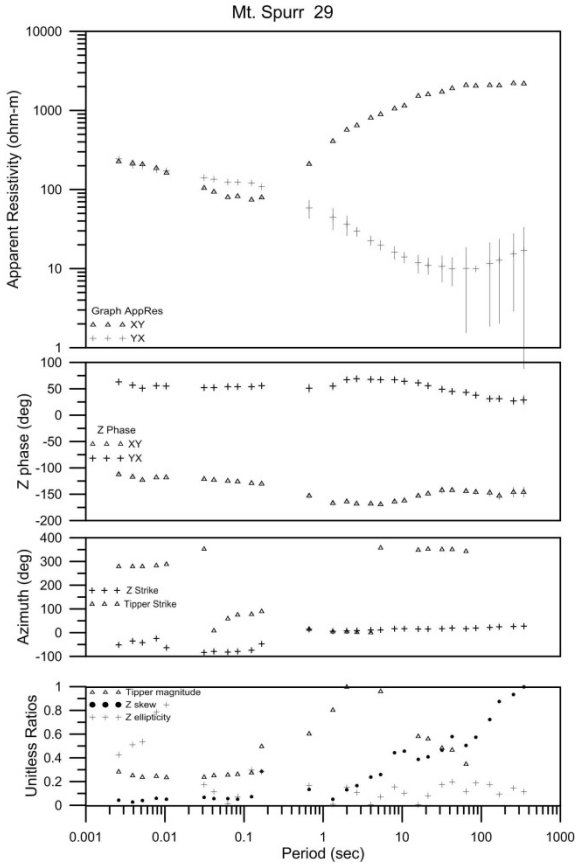
Mt. Spurr 29
Apparent Resistivity (ohm-m)
Graph AppRes
XY
YX
Z phase (deg)
Z Phase
Azimuth (deg)
Z Strike
Tipper Strike
Unitless Ratios
Tipper magnitude
Z skew
Z ellipticity
Period (sec)

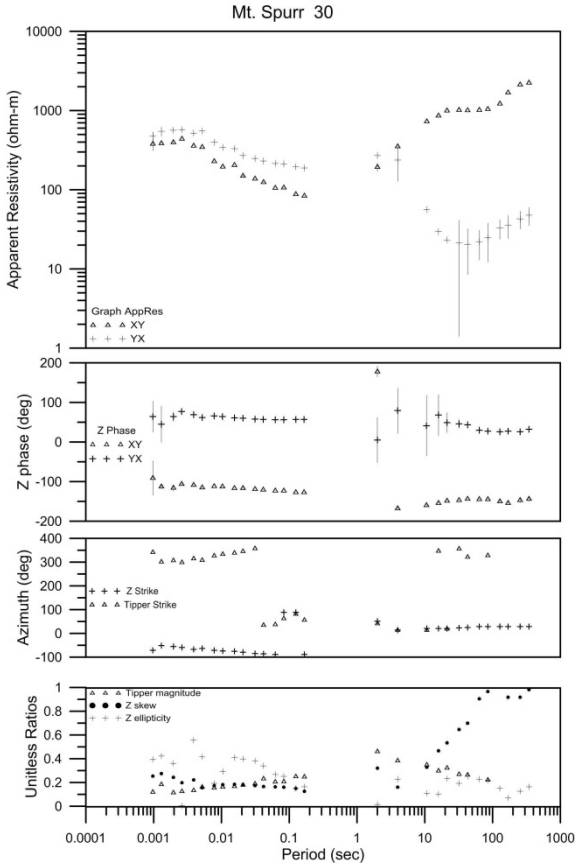
Mt. Spurr 30
Apparent Resistivity (ohm-m)
Graph AppRes
XY
YX
Z phase (deg)
Z Phase
Azimuth (deg)
Z Strike
Tipper Strike
Unitless Ratios
Tipper magnitude
Z skew
Z ellipticity
Period (sec)

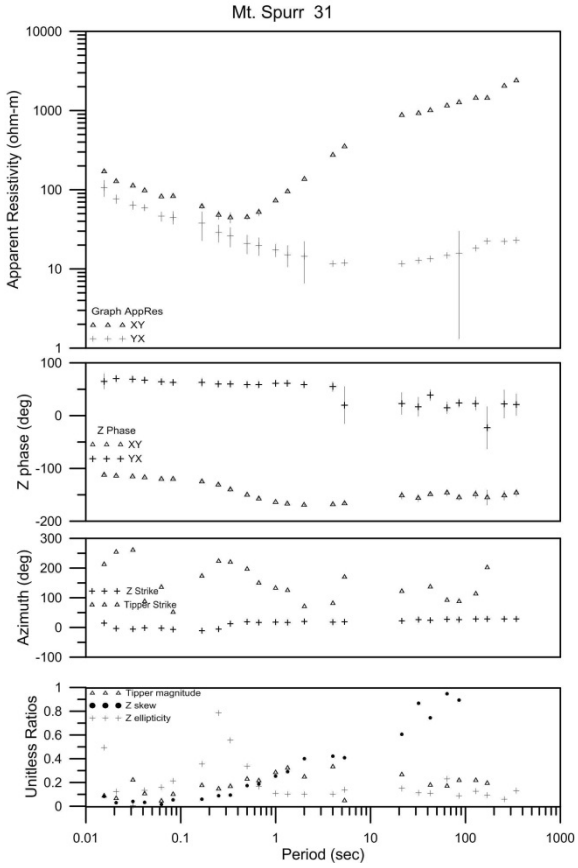
Mt. Spurr 31
Apparent Resistivity (ohm-m)
Graph AppRes
XY
YX
Z phase (deg)
Z Phase
Azimuth (deg)
Z Strike
Tipper Strike
Unitless Ratios
Tipper magnitude
Z skew
Z ellipticity
Period (sec)

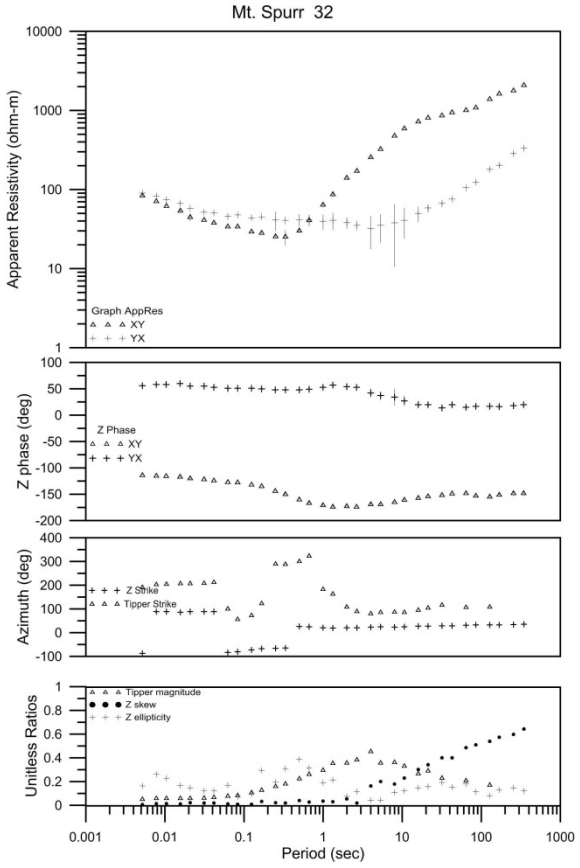
Mt. Spurr 32
Apparent Resistivity (ohm-m)
Graph AppRes
XY
YX
Z phase (deg)
Z Phase
Azimuth (deg)
Z Strike
Tipper Strike
Unitless Ratios
Tipper magnitude
Z skew
Z ellipticity
Period (sec)

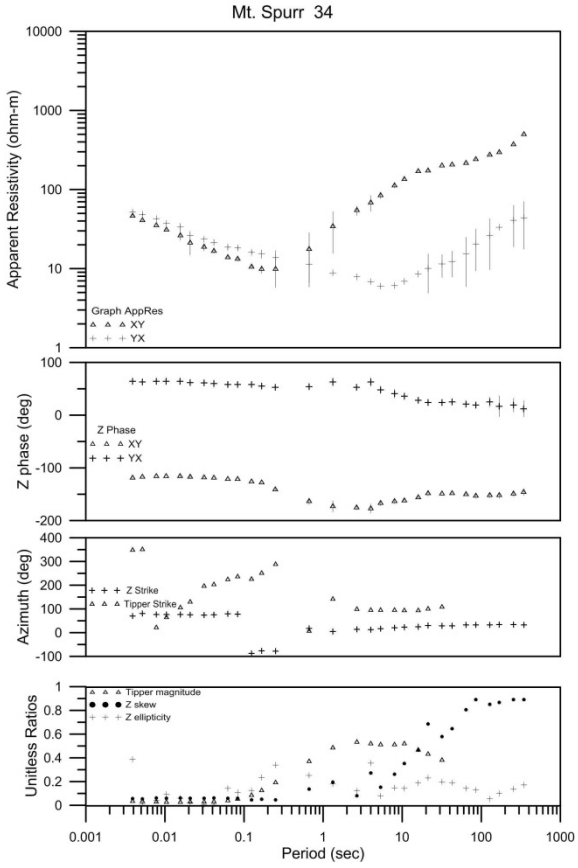
Mt. Spurr 34
Apparent Resistivity (ohm-m)
Graph AppRes
XY
YX
Z phase (deg)
Z Phase
Azimuth (deg)
Z Strike
Tipper Strike
Unitless Ratios
Tipper magnitude
Z skew
Z ellipticity
Period (sec)

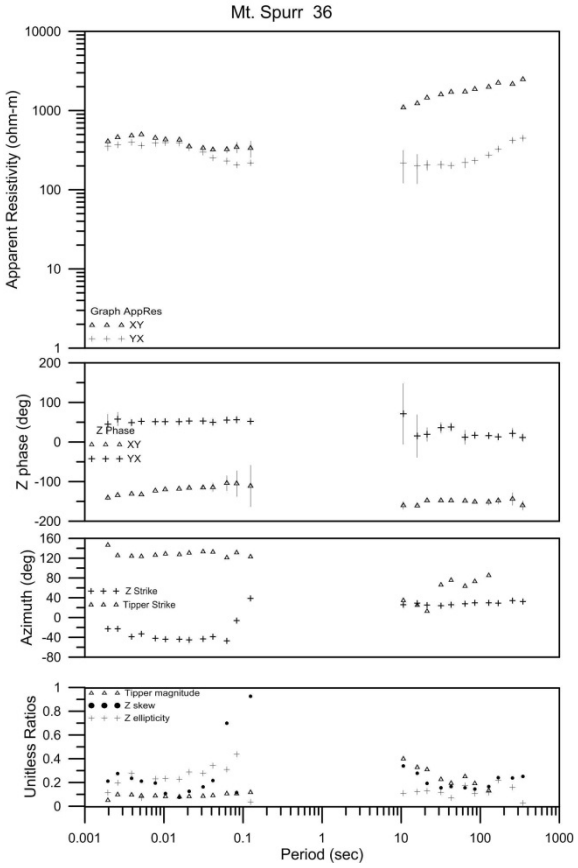
Mt. Spurr 36
Apparent Resistivity (ohm-m)
Graph AppRes
XY
YX
Z phase (deg)
Z Phase
Azimuth (deg)
Z Strike
Tipper Strike
Unitless Ratios
Tipper magnitude
Z skew
Z ellipticity
Period (sec)

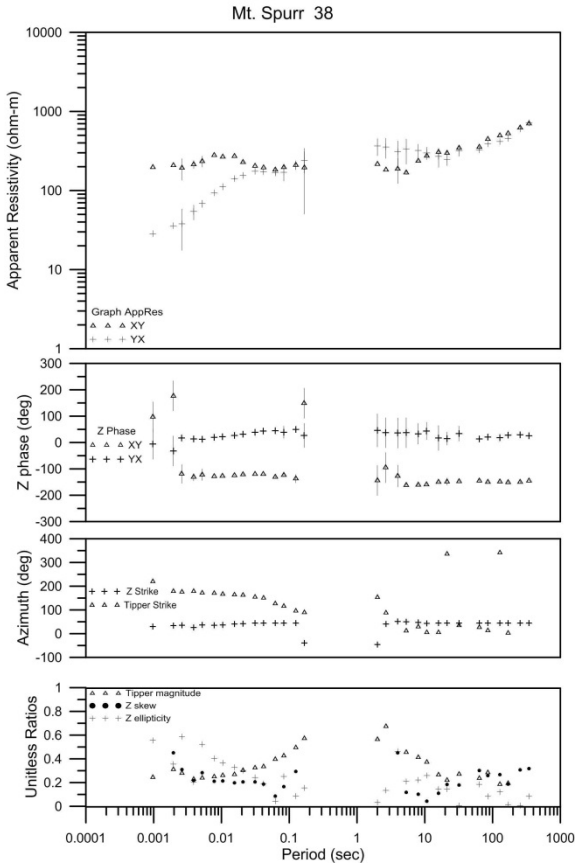
Mt. Spurr 38
Apparent Resistivity (ohm-m)
Graph AppRes
XY
YX
Z phase (deg)
Z Phase
Azimuth (deg)
Z Strike
Tipper Strike
Unitless Ratios
Tipper magnitude
Z skew
Z ellipticity
Period (sec)

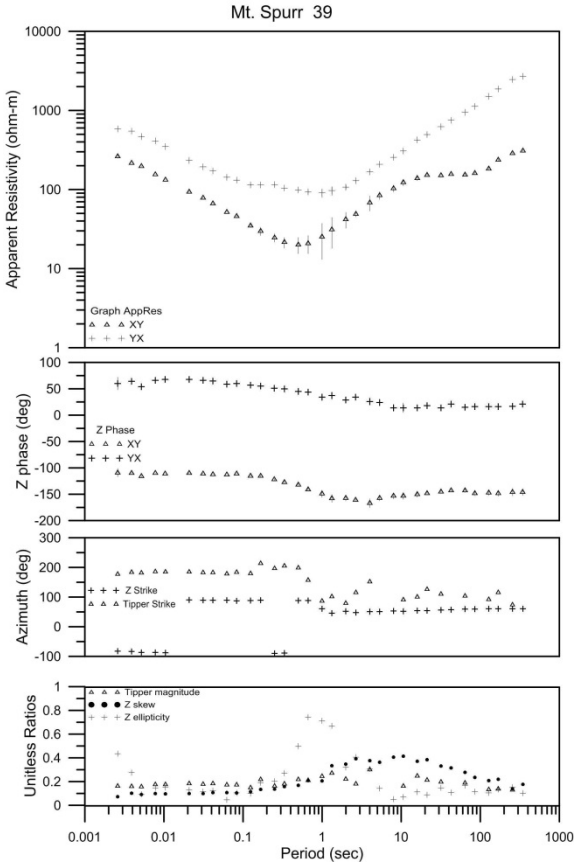
Mt. Spurr 39
Apparent Resistivity (ohm-m)
Graph AppRes
XY
YX
Z phase (deg)
Z Phase
Azimuth (deg)
Z Strike
Tipper Strike
Unitless Ratios
Tipper magnitude
Z skew
Z ellipticity
Period (sec)

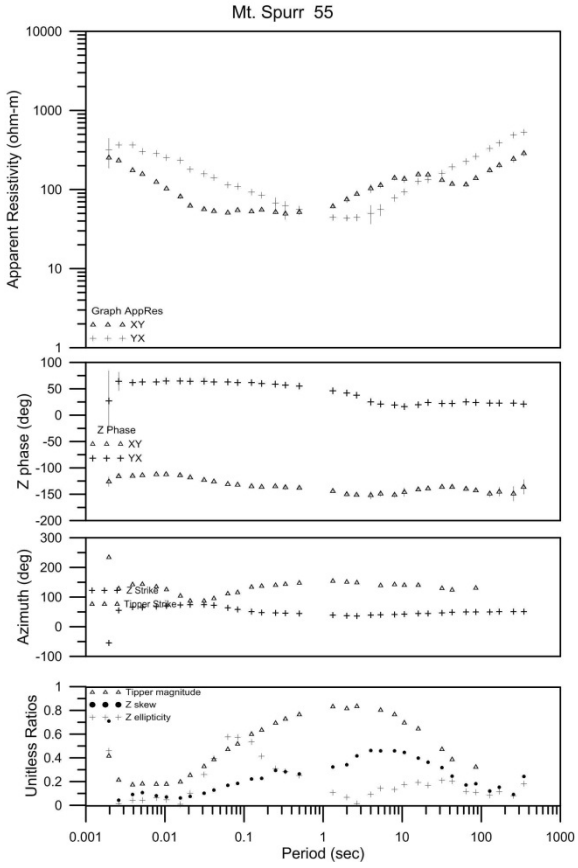
Mt. Spurr 55
Apparent Resistivity (ohm-m)
Graph AppRes
XY
YX
Z phase (deg)
Z Phase
Azimuth (deg)
Z Strike
Tipper Strike
Unitless Ratios
Tipper magnitude
Z skew
Z ellipticity
Period (sec)

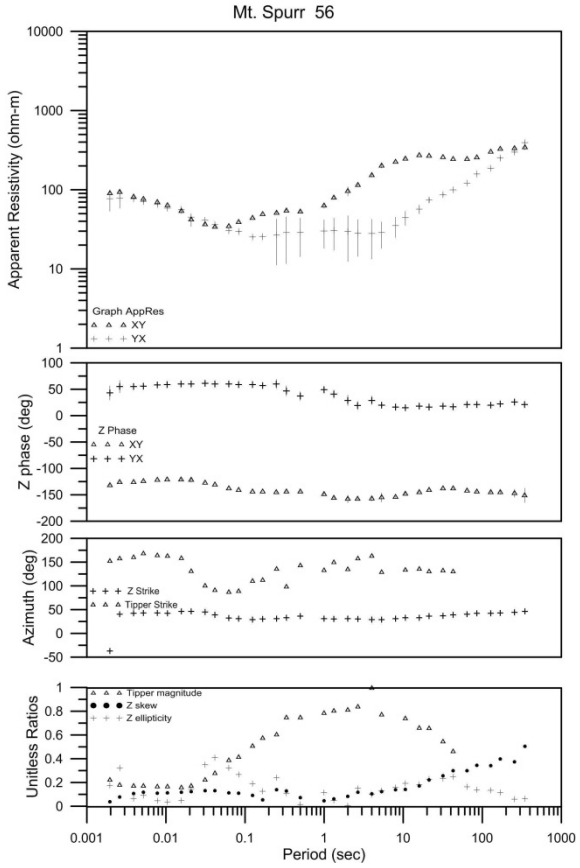
Mt. Spurr 56
Apparent Resistivity (ohm-m)
Graph AppRes
XY
YX
Z phase (deg)
Z Phase
Azimuth (deg)
Z Strike
Tipper Strike
Unitless Ratios
Tipper magnitude
Z skew
Z ellipticity
Period (sec)

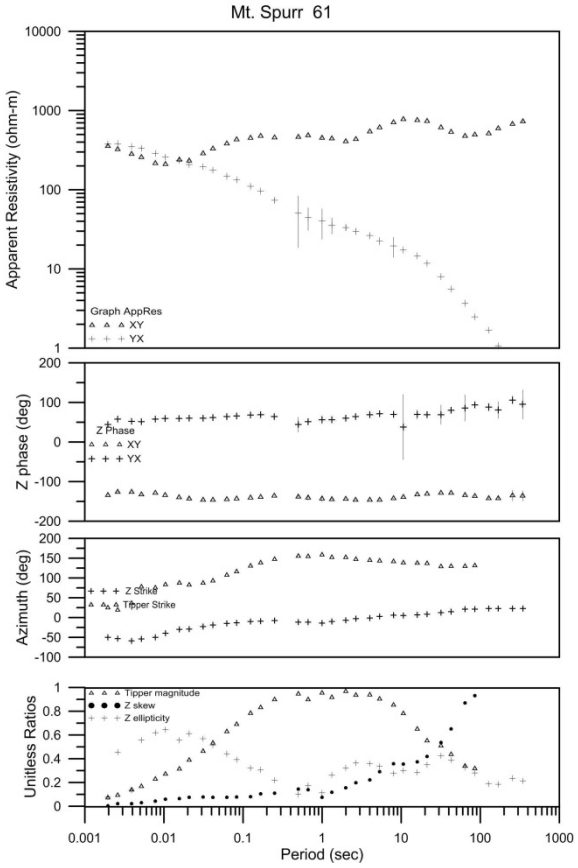
Mt. Spurr 61
Apparent Resistivity (ohm-m)
Graph AppRes
XY
YX
Z phase (deg)
Z Phase
Azimuth (deg)
Z Strike
Tipper Strike
Unitless Ratios
Tipper magnitude
Z skew
Z ellipticity
Period (sec)

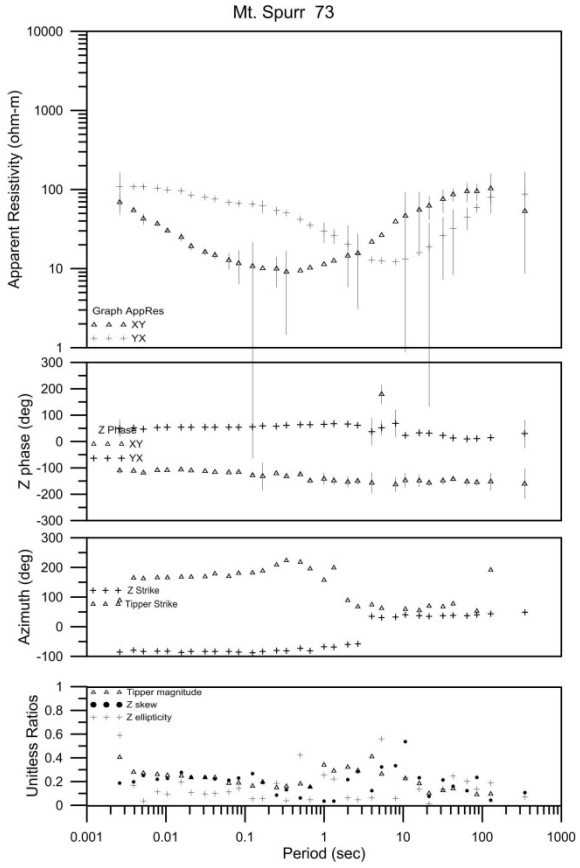
Mt. Spurr 73
Apparent Resistivity (ohm-m)
Graph AppRes
XY
YX
Z phase (deg)
Z Phase
Azimuth (deg)
Z Strike
Tipper Strike
Unitless Ratios
Tipper magnitude
Z skew
Z ellipticity
Period (sec)

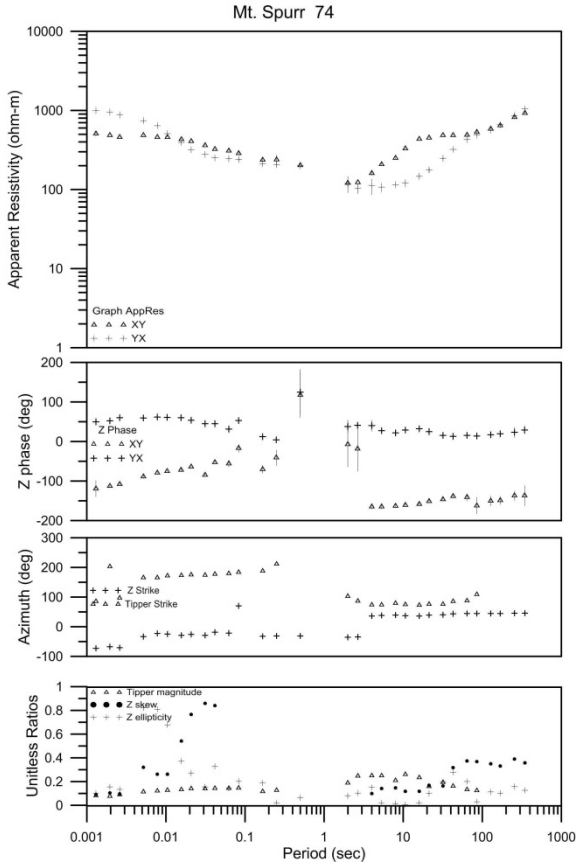
Mt. Spurr 74
Apparent Resistivity (ohm-m)
Graph AppRes
XY
YX
Z phase (deg)
Z Phase
Azimuth (deg)
Z Strike
Tipper Strike
Unitless Ratios
Tipper magnitude
Z skew
Z ellipticity
Period (sec)

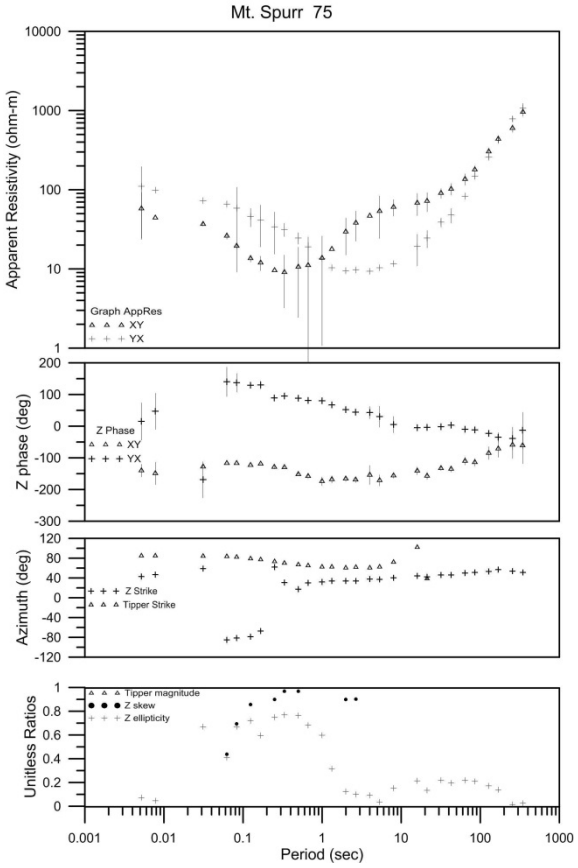
Mt. Spurr 75
Apparent Resistivity (ohm-m)
Graph AppRes
XY
YX
Z phase (deg)
Z Phase
Azimuth (deg)
Z Strike
Tipper Strike
Unitless Ratios
Tipper magnitude
Z skew
Z ellipticity
Period (sec)

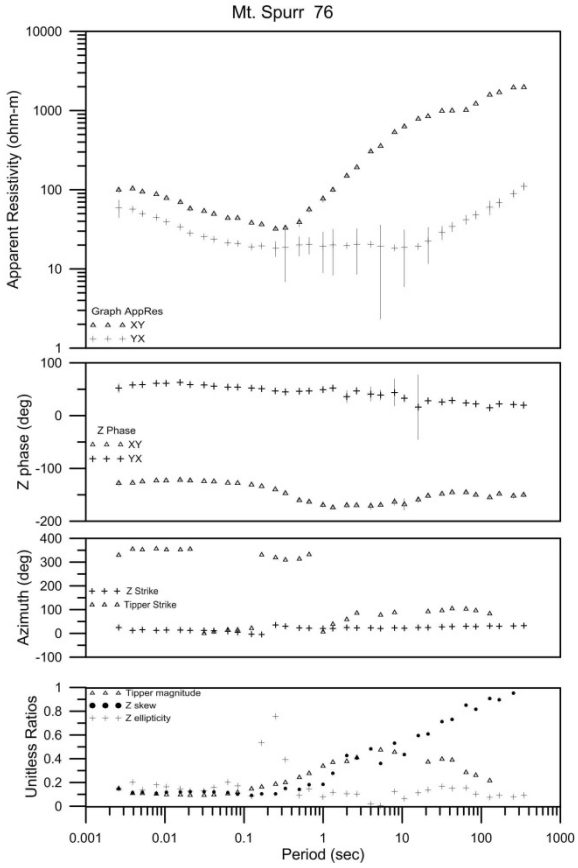
Mt. Spurr 76
Apparent Resistivity (ohm-m)
Graph AppRes
XY
YX
Z phase (deg)
Z Phase
Azimuth (deg)
Z Strike
Tipper Strike
Unitless Ratios
Tipper magnitude
Z skew
Z ellipticity
Period (sec)

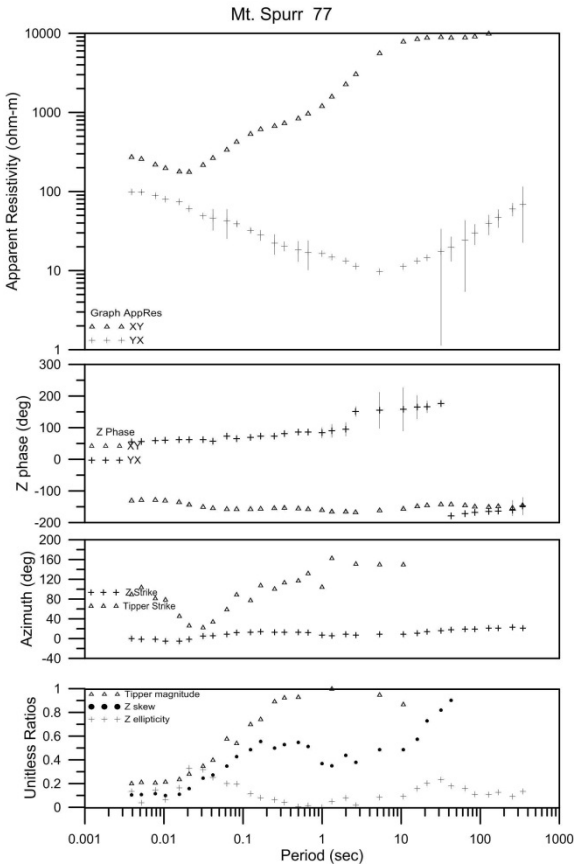
Mt. Spurr 77
Apparent Resistivity (ohm-m)
Graph AppRes
XY
YX
Z phase (deg)
Z Phase
Azimuth (deg)
Z Strike
Tipper Strike
Unitless Ratios
Tipper magnitude
Z skew
Z ellipticity
Period (sec)

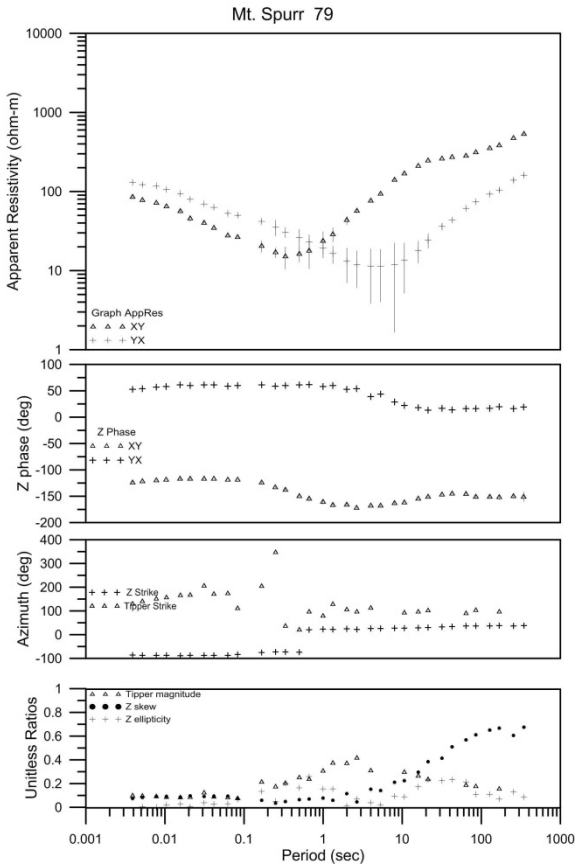
Mt. Spurr 79
Apparent Resistivity (ohm-m)
Graph AppRes
XY
YX
Z phase (deg)
Z Phase
Azimuth (deg)
Z Strike
Tipper Strike
Unitless Ratios
Tipper magnitude
Z skew
Z ellipticity
Period (sec)

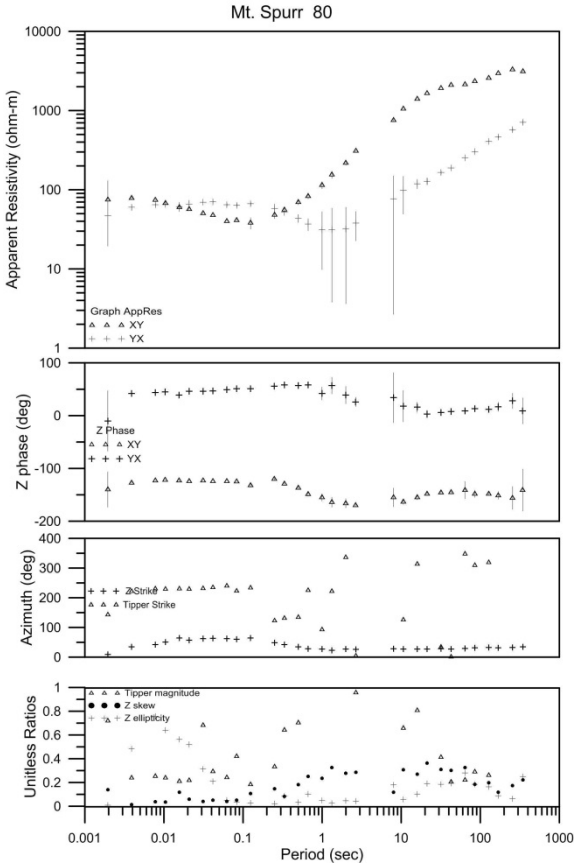
Mt. Spurr 80
Apparent Resistivity (ohm-m)
Graph AppRes
XY
YX
Z phase (deg)
Z Phase
Azimuth (deg)
Z Strike
Tipper Strike
Unitless Ratios
Tipper magnitude
Z skew
Z ellipticity
Period (sec)

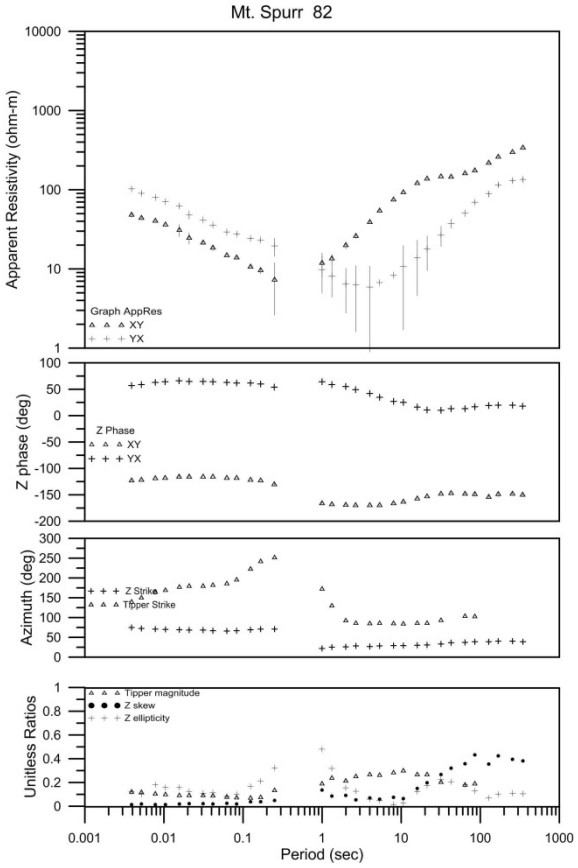
Mt. Spurr 82
Apparent Resistivity (ohm-m)
Graph AppRes
XY
YX
Z phase (deg)
Z Phase
Azimuth (deg)
Z Strike
Tipper Strike
Unitless Ratios
Tipper magnitude
Z skew
Z ellipticity
Period (sec)

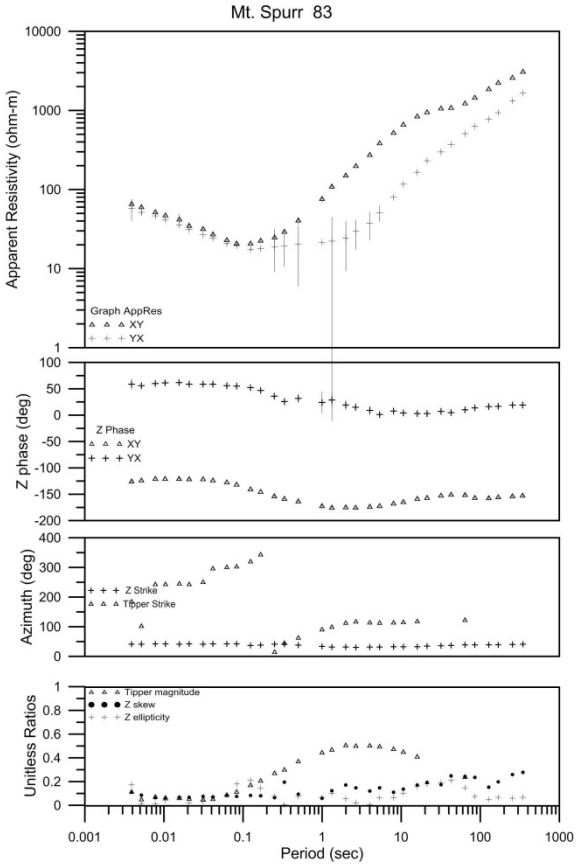
Mt. Spurr 83
Apparent Resistivity (ohm-m)
Graph AppRes
XY
YX
Z phase (deg)
Z Phase
Azimuth (deg)
Z Strike
Tipper Strike
Unitless Ratios
Tipper magnitude
Z skew
Z ellipticity
Period (sec)

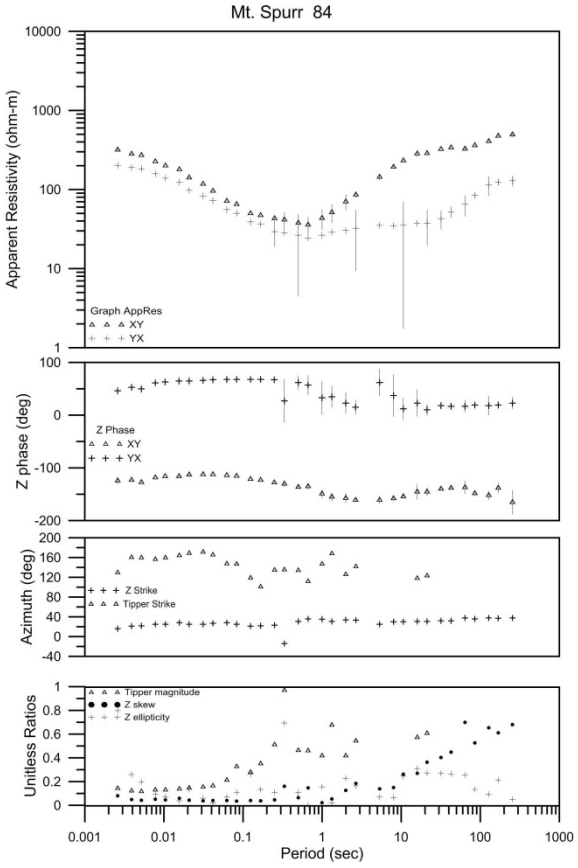
Mt. Spurr 84
Apparent Resistivity (ohm-m)
Graph AppRes
XY
YX
Z phase (deg)
Z Phase
Azimuth (deg)
Z Strike
Tipper Strike
Unitless Ratios
Tipper magnitude
Z skew
Z ellipticity
Period (sec)

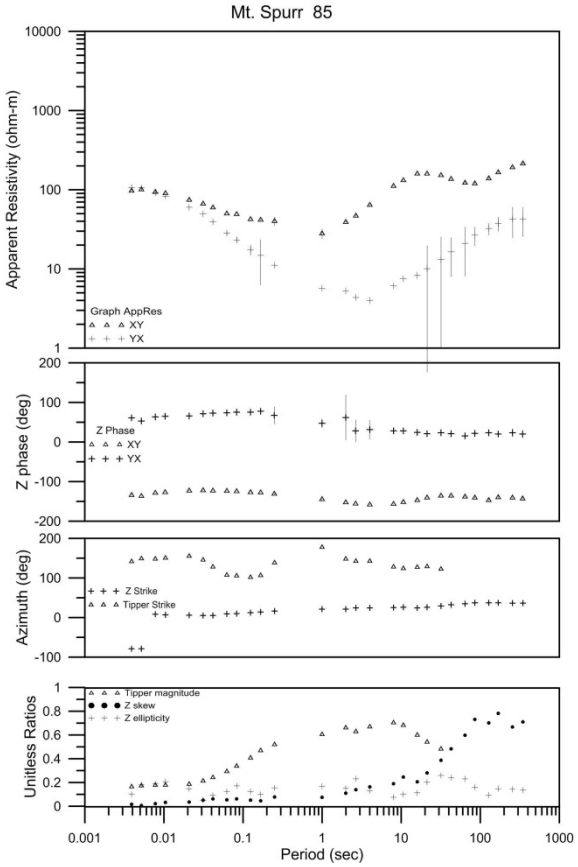
Mt. Spurr 85
Apparent Resistivity (ohm-m)
Graph AppRes
XY
YX
Z phase (deg)
Z Phase
Azimuth (deg)
Z Strike
Tipper Strike
Unitless Ratios
Tipper magnitude
Z skew
Z ellipticity
Period (sec)

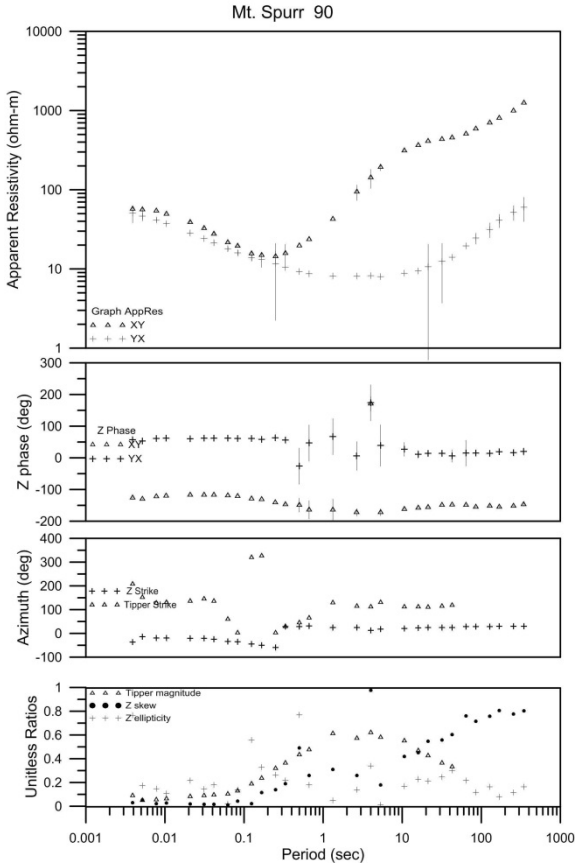
Mt. Spurr 90
Apparent Resistivity (ohm-m)
Graph AppRes
XY
YX
Z phase (deg)
Z Phase
Azimuth (deg)
Z Strike
Tipper Strike
Unitless Ratios
Tipper magnitude
Z skew
Z ellipticity
Period (sec)

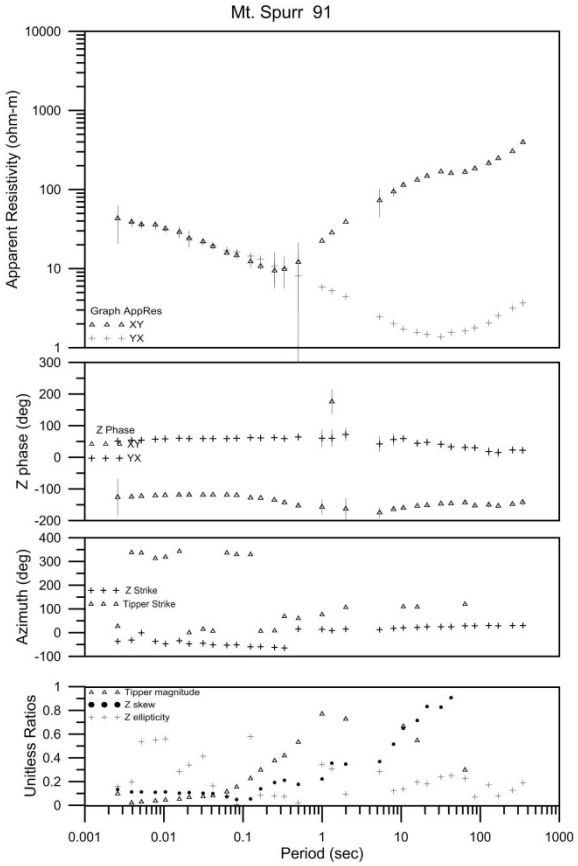
Mt. Spurr 91
Apparent Resistivity (ohm-m)
Graph AppRes
XY
YX
Z phase (deg)
Z Phase
Azimuth (deg)
Z Strike
Tipper Strike
Unitless Ratios
Tipper magnitude
Z skew
Z ellipticity
Period (sec)

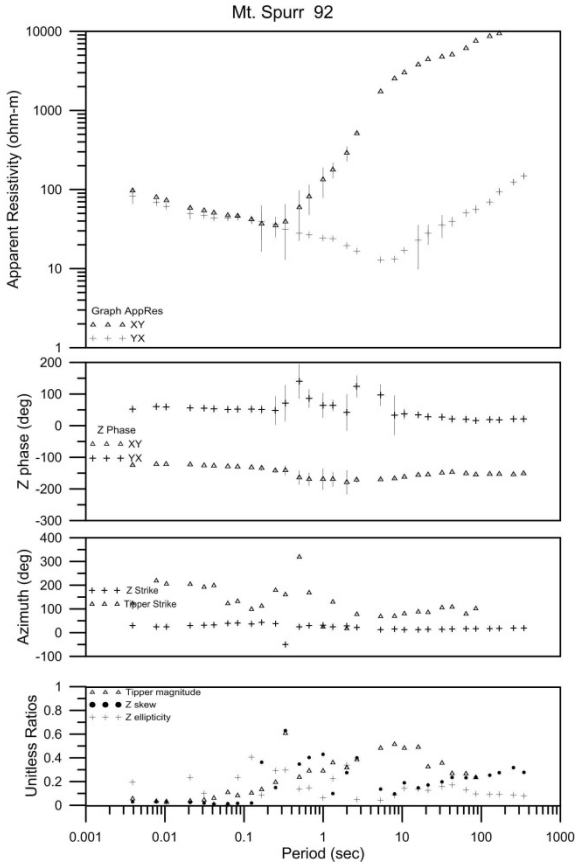
Mt. Spurr 92
Apparent Resistivity (ohm-m)
Graph AppRes
XY
YX
Z phase (deg)
Z Phase
Azimuth (deg)
Z Strike
Tipper Strike
Unitless Ratios
Tipper magnitude
Z skew
Z ellipticity
Period (sec)

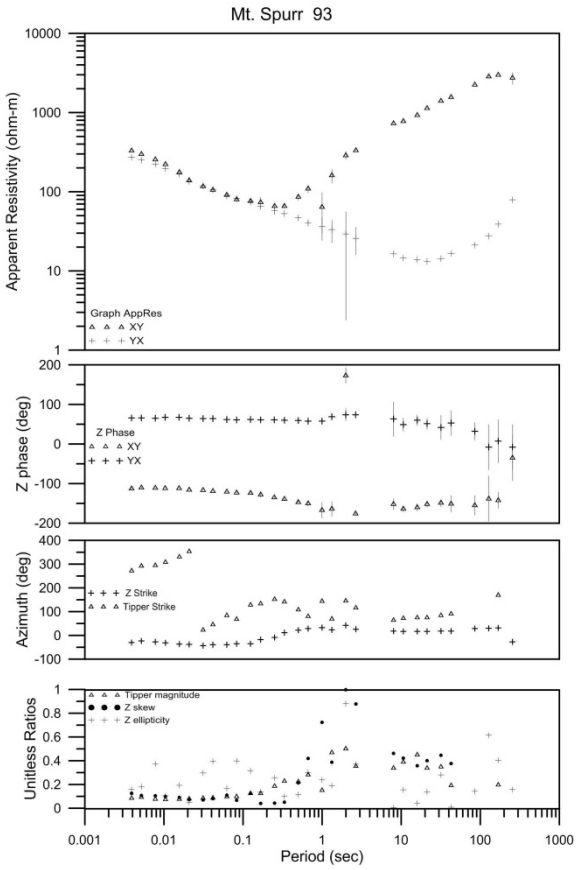
Mt. Spurr 93
Apparent Resistivity (ohm-m)
10000
1000
100
10
1
Graph AppRes
XY
YX
Z phase (deg)
200
100
0
-100
-200
Z Phase
XY
YX
Azimuth (deg)
400
300
200
100
0
-100
Z Strike
Tipper Strike
Unitless Ratios
1
0.8
0.6
0.4
0.2
0
Tipper magnitude
Z skew
Z ellipticity
0.001
0.01
0.1
1
10
100
1000
Period (sec)

APPENDIX C: Logistics

MT survey for Ormat Nevada, Inc.

Zonge Job # 2010.118

Location: Mt. Spurr, AK

Dates: 07/12/2010 – 08/31/2010

Personnel

Project Field Manager: Jerrod Davis.

Geophysicist: Sam Harworth

Field Technicians: J.T. Busby, Matt Church, Roy Santa Cruz.

Data Processing Geophysicist: Nicole Pendrigh.

Date	Time*	Daily Log	Comments
7/12		Crew mobilization.	All crew members – Jerrod Davis, Sam Harworth, J.T. Busby, Roy Santa Cruz & Brad Haddix arrived Anchorage
7/13		Safety Training with Alaskan Earth Sciences (AES).	
7/14		Training with AES.	
7/15		Crew mobilization from Anchorage to Tyonek.	Weather and ordnance found near camp delayed departure from Tyonek.
7/16		Crew mobilization from Tyonek to camp.	Reconnaissance flight of proposed survey area.
7/17	07:00-17:00	Weather delay in camp – helicopter unable to fly due to low visibility.	Crew set up station # 31 near camp for training purposes. Packed in equipment on foot. No data acquisition.
7/18	07:00-09:00	Morning weather delay. Set up at station # 28 and # 31.	Weather forced crews to walk back to camp from respective station locations.
7/19	07:00-17:00	Weather delay.	Crew worked at station # 31 to troubleshooting time series clipping issue found during first night of acquisition.
7/20	07:00-17:00	Weather delay.	Helicopter able to fly during short weather break to retrieve key components from station # 28. Helicopter waited with crew while equipment was retrieved.
7/21		Moved from station # 31 to # 26.	Reacquired data at station # 28 due to faulty

		Set up at station # 28 again.	piece of geophysical equipment found on 7/20.
7/22	07:00-09:30	Weather delay. Moved from station # 28 to # 25 and from # 26 to # 17.	Weather forced crews to walk back to camp from respective station locations.
7/23		Moved from station # 25 to # 21 and from # 17 to # 16.	
7/24	07:00-17:00	Weather delay.	
7/25	07:00-17:00	Weather delay.	Short flight around 15:00 to station # 15, but couldn't get in proximity to equipment to retrieve data or move equipment. Returned to camp.
7/26		Moved from station # 21 to 19 and from # 16 to # 27.	
7/27		Moved from station # 19 to #12 and from # 27 to # 29.	In field weather delayed moving equipment from station # 19.
7/28	07:00-09:15	Weather delay in camp. Moved from station # 12 to # 3 and from # 29 to # 30.	Intermittent weather delays in camp and in field complicated crew movements. Crew at station # 3 forced to spend night at site. Other crew able to walk back to camp from station # 30. Gravity crew also stuck out.
7/29	07:00-17:00	Weather delay in camp. Crew picked up at station # 3 and returned to camp 13:30. Gravity crew returned at 14:00.	Inclement weather all day in camp and in field. Helicopter pilot took only available opportunity to retrieve crews in field.
7/30		Moved from station # 30 to # 38. Set up again at station # 3.	Helicopter to Tyonek to get fuel during weather break. Camp low on fuel after several days of poor weather.
7/31	07:00-10:40	Weather delay at survey sites. Moved from station # 3 to # 4 and from # 38 to # 36.	Helicopter to Tyonek to pick up supplies for camp during morning weather delay.
8/1		Left equipment at sites # 4 and # 36 and set up a third unit 26 Km from camp to act as a remote reference. Trained interim operator to run equipment at station # 4 before leaving for remote reference site.	Set up new remote reference away from camp as part of continuing process of collecting best data possible given local conditions, i.e. topography, weather, noise. Short weather delay in camp mid-morning after crew returned to camp to mobilize to new site.
8/2	07:00-09:00	Weather delay in camp. Moved from station # 4 to # 55. Helicopter grounded due to weather at station # 36 most of day. Trained interim operator to run equipment at station # 36 before departing for new remote reference location.	Flew to new remote reference location with operator at earliest opportunity.
8/3		Equipment/noise issue testing at station # 55. Moved from station # 36 to # 3 with different	Could not get to new remote reference location due to weather in valley towards Tyonek.

		set of equipment for testing.	
8/4	07:00-17:00	Weather delay in camp.	
8/5	07:00-17:00	Weather delay in camp.	19:00 – retrieved equipment at remote reference site and moved to new location near Tyonek. Weather delay forced two crew members to stay night in Tyonek.
8/6	07:00-17:00	Weather delay in camp and in Tyonek.	Helicopter in Anchorage for 100 hour maintenance.
8/7	07:00-08:30	Helicopter returned from Anchorage to Tyonek. Returned one crew member to camp. One stayed in Tyonek to run remote reference for remainder of survey. Crews out to station # 55 and # 3.	Helicopter to Tyonek for supplies and fuel. Weather delay while in Tyonek. Did not return in time to move equipment. Reacquired data at station # 55 with new remote reference. Station # 3 could not be re-acquired as batteries dropped off at station # 4 earlier in day.
8/8	07:00-12:30	Weather delay in camp. Moved from station # 55 to # 56 and from # 3 to #4.	Re-acquired data at station # 4 with different set of equipment (see 7/31-8/1).
8/9	07:00-10:00	Weather delay in camp. Moved from station # 56 to # 2 and from # 4 to # 8.	Helicopter shutdown in field at station locations while equipment was being retrieved due to intermittent weather across entire survey site and in camp.
8/10	07:00-17:00	Weather delay in camp.	A few reconnaissance flights during day, but could not get to equipment. Gravity crew went out at 17:00 during small break in weather and helicopter unable to retrieve crew. Cutting crew also stuck out for night.
8/11	07:00-17:00	Weather delay in camp.	Reconnaissance flight at 07:00 to try to pick up gravity crew with MT crew on board. Whole survey site socked in. Retrieved gravity crew at 13:30.
8/12	07:00-10:30	Weather delay in camp. Moved from station # 2 to # 34 and # 8 to # 20.	Weather in field delayed moving from station # 8 to # 20.
8/13		Moved from station # 34 to # 23 and # 20 to # 14.	
8/14		Moved from station # 23 to # 24 and from #14 to # 7.	Weather in camp after first crews out delayed second MT crew. Helicopter to Tyonek.
8/15	07:00-12:00	Helicopter out to Anchorage for maintenance issue and to swap pilots. Moved from station # 24 to # 25 and from # 7 to # 26.	Reacquired data at stations # 25 and # 26 in emerging area of interest and due to time constraints due to shortened field day.
8/16	07:00-17:00	Weather delay in camp. Helicopter back to Anchorage for maintenance. Returned to camp after 17:00.	Crews walked to station # 25 and # 26 to retrieve data and pack up equipment to hasten move on next day.
8/17	07:00-16:30	Weather delay in camp. Moved equipment from # 25 to # 79 and	

		# 26 to # 78.	
8/18	07:00-09:00	Weather delay in camp. Moved from # 79 to # 77 and # 78 to # 80.	
8/19		Moved from station # 77 to # 20 and # 80 to # 15.	Re-acquired data at station # 20 with different set of equipment due to data quality issues with first acquisition.
8/20	07:00-08:00	Weather delay in camp. Moved from station # 20 to # 75 and # 15 to # 13.	
8/21		Moved from station # 75 to # 76 and # 13 to # 84.	
8/22		Moved from station # 76 to # 32 and # 84 to # 39.	
8/23		Moved from station # 84 to # 82 and # 39 to # 85.	
8/24		Moved from station # 82 to # 74 and # 85 to # 61.	
8/25		Moved from station # 74 to # 22 and # 61 to # 1.	
8/26		Moved from station # 22 to # 83 and # 1 to # 18.	
8/27	07:00-17:00	Weather delay in camp.	
8/28	07:00-08:00	Weather delay in camp. Moved from station # 83 to # 91 and # 18 to # 90.	
8/29		Moved from station # 91 to # 93 and # 90 to # 92.	Started flying equipment out to Tyonek.
8/30		Packed up remaining equipment. Moved equipment from camp to Tyonek and onto Anchorage. Crews arrived in Anchorage.	
8/31		Shipped equipment, left Anchorage.	

APPENDIX D: MT Station Locations

This appendix shows UTM locations for each of the 49 different MT stations and two remote reference stations in the Mt. Spurr MT survey. Coordinates are in meters using coordinate projection UTM Zone 5N NAD83.

Station Number	UTM Easting (m)	UTM Northing (m)	Altitude above mean sea level (m)	Date collected
1	544004	6789186	780	8/25
2	541973	6786131	295	8/09
3	541818	6788337	731	8/03
4	541991	6789997	923	8/08
7	543046	6790812	975	8/14
8	543250	6789031	740	8/09
12	543612	6787973	681	7/27
13	543581	6789838	796	8/20
14	544161	6791038	899	8/13
15	545404	6792654	1594	8/19
16	546312	6792870	1119	7/26
17	547437	6791655	858	7/23
18	545399	6788320	669	8/26
19	545198	6787373	630	7/26
20	546562	6786477	543	8/19
21	546915	6787950	643	7/23
22	546097	6788150	659	8/25
23	548192	6787203	458	8/13
24	548802	6786780	428	8/14
25	548053	6789396	972	8/15
26	548180	6790387	898	8/15
27	548201	6791038	978	7/26
28	550786	6791627	563	7/21
29	547959	6792810	779	7/27
30	548654	6791780	704	7/28
31	549563	6790065	758	7/19

32	550015	6789062	386	8/22
34	551627	6787651	355	8/12
36	551827	6790439	452	7/31
38	550832	6792917	913	7/30
39	541496	6790763	1232	8/22
55	540066	6787951	574	8/03
56	541347	6787836	438	8/08
61	540171	6786692	388	8/24
73	545923	6790669	805	8/17
74	545059	6790133	831	8/24
75	549931	6786453	406	8/20
76	550627	6788434	380	8/21
77	547847	6786063	271	8/18
79	547434	6789344	716	8/17
80	546529	6791678	1047	8/18
82	547138	6789838	751	8/23
83	548567	6788293	468	8/26
84	542531	6788614	711	8/21
85	542868	6787608	716	8/23
90	550188	6787221	392	8/28
91	551324	6786813	367	8/28
92	550729	6789609	403	8/29
93	549326	6790490	730	8/29
RR1	573995	6781143	431	8/01-8/07
RR2	591194	6775279	99	8/07-8/30

APPENDIX E: Instrument Specifications

GDP-32 Receiver

GDP-32 Receivers

- 1 to 16 channels, large case, user expandable
- 1 to 6 channels, small case, user expandable
- Alphanumeric keypad
- 386SX MPU, 387SL math coprocessor
- All programs resident in memory:
  Resistivity, Time/Frequency Domain IP, CR, CSAMT/MT, Harmonic Analysis CSAMT/MT (HACSAMT/MT), AMT, MT, TEM & NanoTEM®
- Screen graphics: plots of time-domain decay, resistivity and phase, complex plane plots, etc., on a 256 x 128 pixel LCD
- Internal humidity and temperature sensors
- Automatic time-schedule program for remote operation with the XMT-32 transmitter controller.
- Use as a data logger for analog data, borehole data, etc.
- 0.015625 Hz to 8 kHz frequency range standard, 0.0007 Hz minimum for MT
- One 16 bit A/D per channel for maximum speed and phase accuracy
- 1.5 MB ROM, up to 15 MB RAM for program execution
- 1 MB SRAM for data storage standard, stores several days' worth of data, expansion up to 4 MB SRAM plus optional hard disk
- Real-time data and statistics display
- Anti-alias, power line notch and telluric filtering
- Automatic SP buck out, gain setting and calibration
- Rugged, portable and environmentally sealed
- Modular design for upgrades and board replacement

ANT/4 MT Antenna

- Frequency Range: 0.0005 to 1000 Hz
- Sensitivity in Passband: 100 millivolts/gamma (100 mV/nT)
- Noise Level:
  - 100 microgamma (100 fT) per squareroot_Hz at 1 Hz
  - 20 microgamma (20 fT) per squareroot_Hz nominal > 1 Hz

- Tube diameter: 4.8 cm (1.875 in)
- Length: 138 cm (54.0 in)
- Weight: 6.2 kg (13.5 lb)

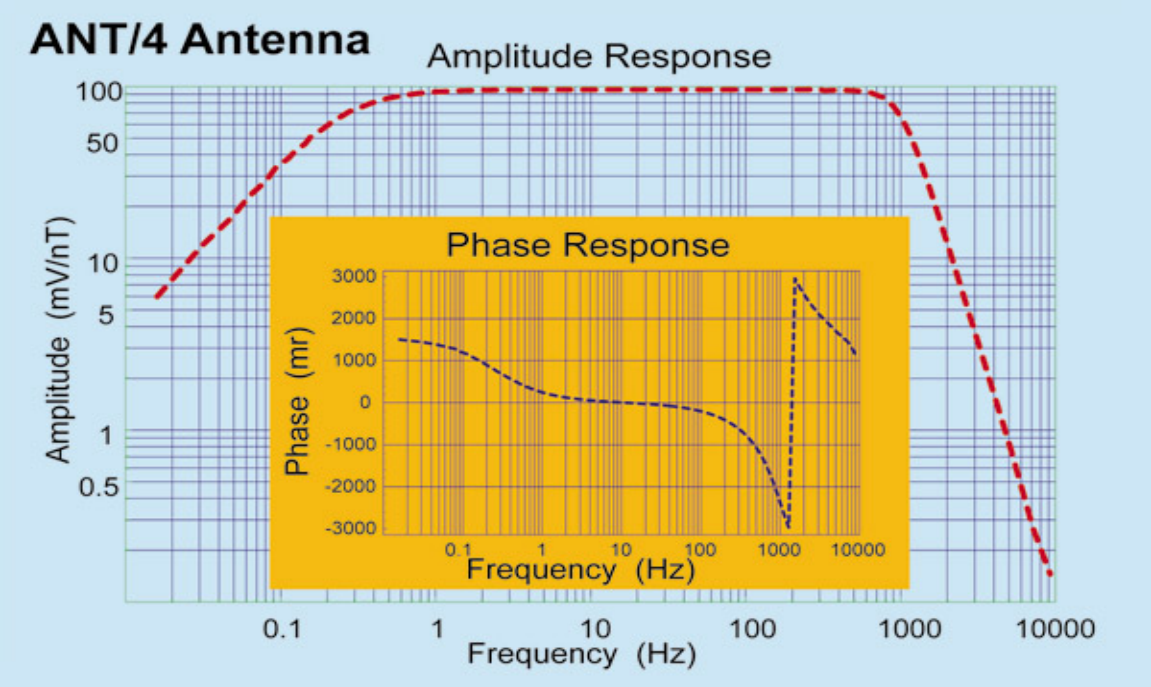

SC-8 *Signal conditioning preamplifier for MT/AMT measurements*

The SC-8 Signal Conditioner is used to amplify and filter electric and magnetic telluric signals prior to entering the GDP receiver system. Use of this device is recommended to provide low-noise amplification, radio-noise filtering, and limiting of low-frequency tellurics.

Electrical Specifications

Analog channels: 8.
Gain settings: x1, x8, x32, x128.
High pass filters 1, .1, .01, .001 Hz.
Low pass filter: 10 Hz.
Saturation detector: +/- 4.5 volts.
Noise: Less than 50 nV per squareroot-Hz at 1 Hz.
Batteries: One set of 12-volt batteries.

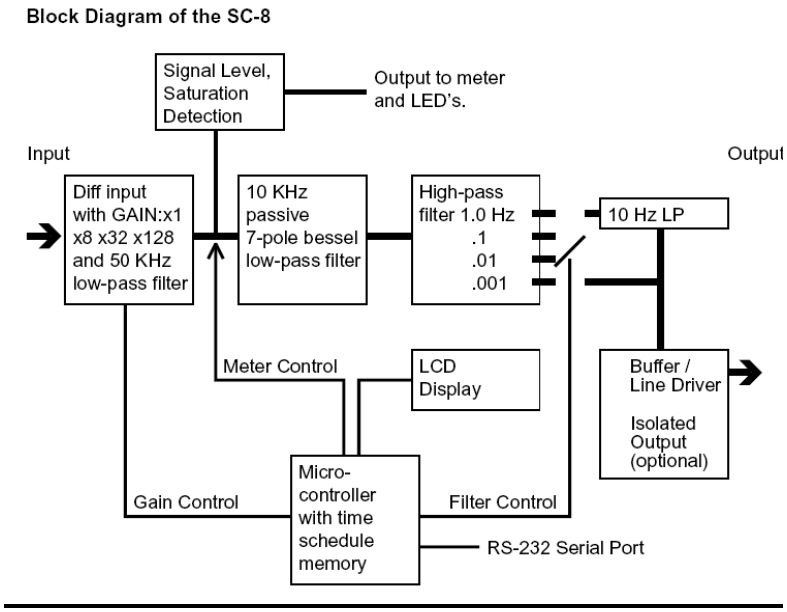

APPENDIX F: Overview of magnetotellurics

Electric currents within the earth produce the magnetotelluric signals that are measured by the Zonge AMT/MT System. The earth currents are induced by two types of natural electromagnetic activity above the earth's surface. Atmospheric electrical discharge, i.e., lighting from distant continents and nearby are the primary sources electromagnetic fields at frequencies above 3 Hz. These signals are channeled globally in the "waveguide" between the earth's surface and ionosphere. Below 3 Hz the electromagnetic sources are associated with the interaction between the earth's magnetosphere (several thousand kilometers above the earth's ionosphere) and the solar wind plasma. These magnetic fluctuations, in turn, induce horizontal electrical current circulation in the ionosphere and in the earth's crust and oceans.

These natural sources produce unpredictable daily variation in the magnitude of the source field used for magnetotelluric (MT) and audiomagnetotelluric (AMT) measurements, which occasionally make it desirable to re-occupy or extend the recording time at a station. For most areas and applications, a single over-night observation period is sufficient. (MT refers to measurements below approximately 300 Hz, AMT to measurements at frequencies from 10 to 10,000 Hz.)

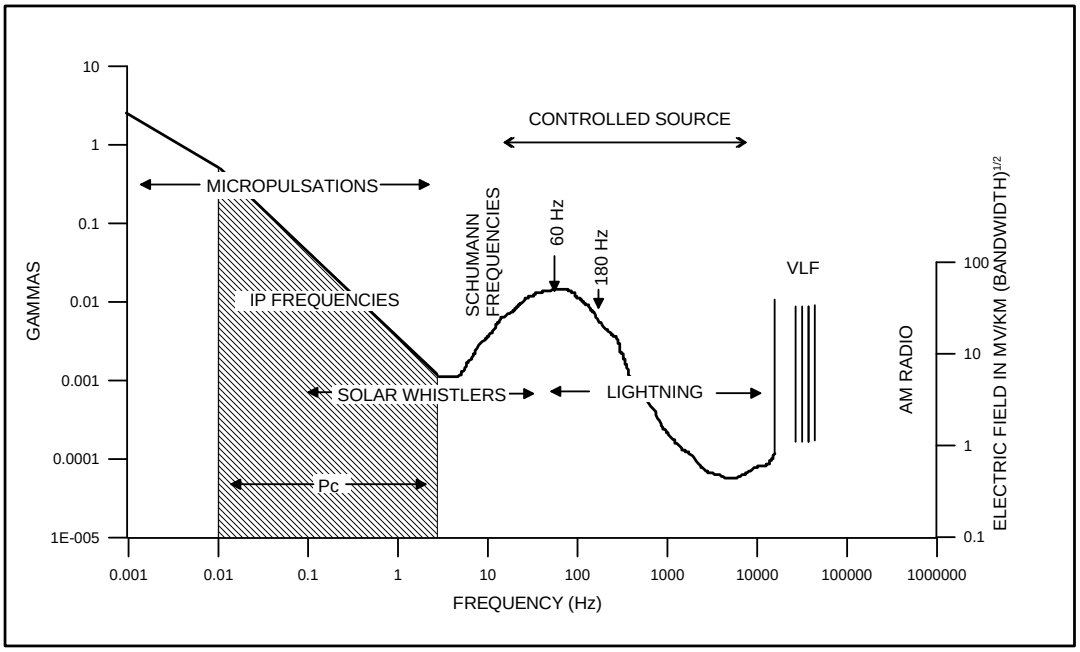

Figure D1: Natural Source AMT and MT, power spectra.

The theoretical foundations the MT/AMT methods and the practical interpretation of the field observation rest securely on several assumptions about the geometry of the electromagnetic source fields and the earth materials electrical properties over the range of frequencies employed.

- The natural EM (electromagnetic) fields are generated by large-scale current systems in the ionosphere or electrical discharges in the ionosphere-earth wave guide. These sources are typically far enough away from the Earth's surface that the observed fields can be treated as uniform, EM plane waves which are refracted into vertically propagating, horizontally uniform, electric and magnetic fields in the earth. Any locally uniform magnetic field variations originating above the surface will meet the plane wave assumption. This includes any natural or artificial electrical or magnetic source located at least six to eight horizontal earth skin-depths distance for the frequencies of interest. These source assumptions may breakdown for ionosphere sources near the equator and poles and very near lightning strikes.
- The measured magnetic fields exhibit multiple azimuths or polarizations. For full solution of the MT/AMT impedance Tensor, the direction of the surface horizontal magnetic field vector must exhibit at least two distinct azimuths or polarizations over the observation period in each frequency band. A change in source or direction to the source is not required, just a change in the azimuth or polarization of the observed field. Observing multiple polarizations in measurements during a standard length occupation period is rarely a problem.
- Earth materials behave as ohmic conductors rather than dielectrics over the frequency ranges employed. In other words time-varying electric currents (displacement currents) arising from earth material dielectric permittivity and macroscopic polarization effects (graphite coated fractures) are negligible in comparison with conduction currents at a given frequency and can be assumed to be zero in modeling. This assumption has two implications: the electric and magnetic fields induced in the earth are controlled by diffusion rather than electromagnetic wave propagation theory; and the earth can be modeled as an ohmic conductor, i.e. Ohm's law is obeyed: $j = \sigma E$ where j is current density in amps per square meter, σ is conductivity in siemens per meter, and E is the electrical field in volts per meter.
- Magnetic permeability's of the earth materials are well approximated by free-space permeability. This is a good approximation except over the most highly magnetic deposits.
- Surface normal or vertical electric current flow and electric fields at the earth's surface are zero. This is a very good approximation. Due to the high air-earth resistivity contrast, induced currents must flow surface parallel, so vertical currents and the vertical electric field are zero at the surface.
- Local measured electric fields are divergence free, which is equivalent to requiring that there are no electric current sources or drains (active electrodes) contributing to the magnetic and electric field measurements. This assumption can breakdown momentarily during lightning strikes within a few km of the measurements or near points of artificial current injection.

In the MT and AMT methods, the electric and magnetic fields generated by the electromagnetic sources discussed above are measured over a range of frequencies. The common recording range is 8000 Hz to 10^{-3} Hz. Regardless of the frequency the MT source field geometry is assumed to be planar. The electric field signal is sensed as a potential difference between two separated non-polarizable porous electrodes, connected by insulated wire to the receiver. The magnetic fields are detected using mu-metal cored induction magnetic field antennas. Different arrays can be used in the field to collect MT data, two examples of which are presented below in Figure D2. These include tensor and scalar setups:

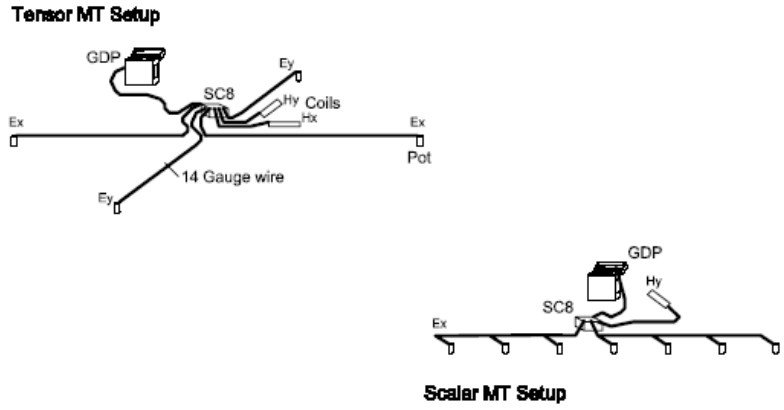

Figure D2. Tensor and scalar MT sensor setups.

The first step in the use of magnetotelluric information is to calculate impedance estimates for each pair if electric and magnetic fields. The scalar impedance, Z, is defined by E/H. This impedance can then be used to calculate the apparent resistivity:

$$\rho_{xy} = \frac{1}{5f}\left|\frac{Ex}{Hy}\right|^2 \text{ (ohm - meters)}$$

and phase:

$$\phi_{xy} = \arctan\left(\frac{\text{imag}(Z_{xy})}{\text{real}(Z_{xy})}\right),$$

where E_x is measured in mV/km and H_y is in nT.

The full impedance tensor $\overline{\overline{\mathbf{Z}}}$ relates horizontal electric and magnetic field components as

$$\begin{bmatrix} E_x \\ E_y \end{bmatrix} = \begin{bmatrix} Z_{xx} & Z_{xy} \\ Z_{yx} & Z_{yy} \end{bmatrix} \cdot \begin{bmatrix} H_x \\ H_Y \end{bmatrix}$$

or equivalently

$$E_x = Z_{xx} \cdot H_x + Z_{xy} \cdot H_y \text{ and } E_y = Z_{yx} \cdot H_x + Z_{yy} \cdot H_y .$$

The MT method is well suited for studying complicated geological environments because the electric and magnetic relations are sensitive to vertical and horizontal variations in resistivity. The method is capable of establishing whether the EM fields are responding to subsurface terranes of effectively 1-, 2-, or 3-dimensions. In a horizontally layered (1-D) earth diagonal impedance elements Z_{xx} and Z_{yy} are zero and the off diagonal terms are equal in magnitude and are related by $Z_{xy} = -Z_{yx}$. The impedance tensor Z is directionally independent in a 1-D earth. If resistivity decreases with depth, phase measurements will increase over 45^o; if resistivity increases with depth, phase measurements will dip below 45^o. An additional indicator of a 1-D earth is when the ratio H_z/H_x (Tipper) is a small number. H_z measured at the earth's surface should be zero for a 1-D earth.

For a 2-D earth, the diagonal elements of the impedance tensor are zero if sensors are aligned parallel and perpendicular to the structural strike, and in that case the off-diagonal elements correspond to the impedances of the two principal coupling modes, which are known as transverse electric (TE) and transverse magnetic (TM). For a y-directed strike direction, Z_{yx} (electric field parallel and magnetic field perpendicular to strike) would be the TE mode, and Z_{xy} (electric field perpendicular and magnetic field parallel to strike) would be the TM mode. If the dominant strike direction is unclear or unknown, Z_{xx} and Z_{yy} will be non-zero, but it is possible to apply mathematical rotation to make them zero (or nearly zero) and thus define the TE and TM directions. Mode identification is important to direct interpretational processing. Both 1-D and 2-D inversion algorithms require the identification and input of data in the TE and TM modes.

In a 2-D environment, inversion on the TM mode is usually superior to TE mode inversion, since the TM mode is more sensitive to lateral conductivity changes than is the TE mode. Wannamaker et al. (1984) has demonstrated that inversion of the 2-D TM mode in many

circumstances can be a suitable approximation to model data in a 3-D environment. However, 2-D inversions of 3-D electrical structures can sometimes produce conductivity artifacts. In particular, conductivities can be estimated too low, and conductive blobs or dike-like bodies may appear in the 2-D inversion model. This same effect can be caused by electrical anisotropy. In addition, charges can build up on vertical conductivity contacts, and this can produce significant frequency independent static shifts, which appear as offsets in the apparent resistivity curves. If not identified and corrected, static shifts can lead to order-of-magnitude inaccuracies in the inverted model.

Data are often collected in an orientation that is not aligned to geological strike of the target structure. Data at Mt Spurr were acquired with a consistent orientation of sensors with x = 90^o, i.e. due east. For a 3-D earth, pure TE and TM modes do not exist, and the simplicity of analysis by mode separation is reduced. In this case, all components of Z are present, and can have similar magnitudes.

Tipper

The vertical component of the magnetic field H_z is linearly related to the horizontal components by the relation

$$H_z = T_x H_x + T_y H_y.$$

In general, all quantities in the above equation are complex and frequency dependent. The quantities T_x and T_y are called tippers because they have the effect of tipping the horizontal components of the H fields slightly into the vertical plane, creating a usually small H_z component.

H_z is generated by lateral gradients in conductivity or sharp conductivity discontinuities, and quantities derived from H_z are therefore important in assessing 2-D or 3-D MT environments. Tipper magnitude |T| is defined as sqrt($|T_x|^2 + |T_y|^2$), and is directly proportional to the lateral conductivity gradient. In a purely layered earth, there are no lateral gradients, thus $H_z = 0$, as are the tipper components and tipper magnitude.

In a 2-D earth, the tipper is associated with only the TE mode, and T_y and T_x have the same phases, so that and T_y/T_x is a real number. In this case, it is possible to determine the strike direction of a 2-D contact by computing ϕ where

$$\phi = \arctan (T_y/T_x) .$$

This quantity is referred to as tipper strike.

It is also possible to infer the conductive vs the resistive side of a contact by analyzing the tipper magnitude and phase across the contact.

In a 3-D earth, the phases of T_x and T_y are different, and more complicated definitions for ϕ are required. One definition involves finding the value of ϕ that maximizes the cross-power of horizontal and vertical components. In this way a dominant strike direction may be found under favorable conditions.

Tipper magnitudes and directions can be combined to make induction arrow maps. Induction arrows can be used to infer the presence or absence of lateral conductivity gradients, and can be used to identify 3-D conductors in the earth as they will point toward the conductor (or away from it, depending on convention used).

APPENDIX G: Geomagnetic Indices

Geomagnetic indices K and A are indicators of geomagnetic activity over periods of three hours or a day, respectively. The K index measures geomagnetic fluctuations at a geomagnetic observatory during three hours intervals. It ranges from a K-value of 0 (0-5 nT variance) to a K-value of 9 (>500 nT variance). The A-scale is non-linear function of the eight daily K-values. A zero K-value corresponds to a zero A-value. A K-value of 9 corresponds to an A-value of 400. (Source: http://en.wikipedia.org/wiki/K-index)

2010_DGD.txt Issued: 1900 UT 07 Jan 2011: NOAA, Space Weather Prediction Center

	Middle Latitude - Fredericksburg -									High Latitude ---- College ----									Estimated --- Planetary ---								
Date	A	K-indices								A	K-indices								A	K-indices							
2010 07 15	10	5	2	1	2	1	1	1	1	13	3	3	2	4	4	2	1	1	10	4	3	1	2	2	2	1	2
2010 07 16	2	0	0	1	1	2	1	0	1	5	0	1	1	4	1	0	0	0	4	1	1	1	1	1	1	0	2
2010 07 17	1	0	0	0	0	1	1	0	1	0	0	0	0	0	0	0	0	0	2	1	0	0	0	1	1	0	1
2010 07 18	2	0	0	0	1	1	1	1	1	0	0	0	0	0	0	0	0	0	3	1	0	0	0	0	1	1	2
2010 07 19	2	0	0	0	1	1	1	1	1	1	0	0	0	0	0	2	1	0	4	1	0	0	1	1	2	1	2
2010 07 20	3	1	0	2	1	1	1	1	1	2	0	1	2	0	0	0	1	1	5	2	1	2	1	2	1	2	2
2010 07 21	3	1	2	0	1	1	1	1	1	4	1	2	1	1	1	1	1	1	5	2	2	0	1	1	2	2	1
2010 07 22	4	0	1	1	1	1	1	2	2	7	1	1	3	3	2	1	1	1	5	1	1	1	1	2	1	2	2
2010 07 23	6	1	1	2	1	1	2	2	3	9	1	2	2	2	3	3	3	1	8	2	2	2	1	2	2	2	3
2010 07 24	4	2	1	1	0	1	1	2	2	2	1	1	1	0	0	1	1	1	5	2	1	1	0	1	1	2	2
2010 07 25	5	2	1	1	1	2	1	2	2	7	3	1	1	1	4	0	1	1	6	3	1	1	1	2	1	1	2
2010 07 26	5	2	2	1	1	1	1	2	2	3	2	2	1	0	0	1	1	1	6	2	2	1	1	1	2	1	3
2010 07 27	11	2	3	3	2	2	2	3	3	23	3	5	4	4	4	4	2	2	19	3	3	4	4	3	3	4	3
2010 07 28	10	4	2	2	2	2	2	2	2	25	4	3	3	6	5	2	2	1	14	4	3	3	3	3	2	3	3
2010 07 29	5	1	2	2	2	2	1	1	1	9	2	2	2	4	3	1	1	1	7	2	3	2	2	2	1	1	2
2010 07 30	5	2	1	0	1	1	2	2	2	8	2	2	1	4	2	2	1	1	7	2	1	1	2	1	2	2	3
2010 07 31	4	2	1	0	1	2	2	1	0	7	3	2	0	2	3	2	1	1	6	2	1	1	1	2	2	2	2
2010 08 01	2	0	0	1	0	1	1	1	2	4	1	1	1	2	1	1	1	1	4	0	1	1	1	1	1	1	2
2010 08 02	5	1	2	1	1	2	2	1	2	5	2	1	2	2	2	2	0	1	5	1	2	1	1	1	2	1	2
2010 08 03	14	1	3	2	1	1	3	3	5	14	2	2	2	2	1	3	3	5	20	2	3	2	1	1	2	5	6
2010 08 04	26	5	4	3	4	4	2	4	4	-1	5	5	2	-1	-1	-1	-1	-1	42	6	5	3	5	4	4	6	4
2010 08 05	7	3	3	0	1	2	1	2	2	10	4	3	1	2	3	2	1	1	10	4	3	0	1	1	2	2	2
2010 08 06	6	1	3	2	1	1	1	2	2	9	1	4	2	2	3	1	1	1	8	2	3	2	1	2	1	3	2
2010 08 07	4	1	1	1	1	1	1	2	1	4	1	1	2	3	1	1	0	0	5	1	2	1	1	1	1	1	1
2010 08 08	2	0	0	0	1	1	1	2	1	1	0	0	0	0	0	1	2	0	4	1	0	0	1	1	1	2	2
2010 08 09	7	2	3	2	1	2	2	1	2	7	1	3	2	1	2	2	2	1	10	3	4	2	1	2	2	2	3
2010 08 10	7	2	2	3	1	2	1	1	2	6	2	2	2	1	2	1	1	2	8	2	2	2	1	1	1	2	3
2010 08 11	9	4	2	4	1	0	2	0	1	16	3	3	5	3	3	3	1	0	10	3	3	3	2	2	1	1	1
2010 08 12	3	1	1	1	1	1	0	1	1	5	0	1	2	2	3	0	1	1	4	2	2	1	1	1	0	0	1
2010 08 13	3	1	2	0	1	1	1	1	1	1	1	1	0	0	0	0	0	0	4	1	2	0	1	1	1	1	1
2010 08 14	2	1	0	0	0	1	1	1	1	2	1	0	0	1	1	0	1	1	3	1	0	0	1	1	1	1	2
2010 08 15	5	2	2	0	1	2	1	2	2	4	1	1	0	1	3	0	1	1	5	2	2	0	1	1	1	1	2
2010 08 16	4	2	2	1	1	1	1	1	1	8	1	2	2	3	3	2	1	1	7	2	3	1	2	2	2	2	2
2010 08 17	3	1	1	1	0	1	1	1	1	3	1	1	1	1	2	1	0	1	5	1	1	1	1	2	1	2	2
2010 08 18	3	1	3	1	0	1	0	0	0	3	1	2	1	1	2	0	0	0	5	2	2	1	1	2	1	2	1
2010 08 19	3	0	1	1	2	2	1	0	0	2	1	1	1	2	0	0	0	0	5	1	2	1	2	0	1	2	1
2010 08 20	1	0	0	0	0	1	1	0	1	2	1	0	0	1	2	0	1	0	4	1	0	0	0	2	2	2	2
2010 08 21	3	0	1	1	1	1	1	1	1	0	0	0	0	0	0	0	0	0	3	1	1	0	0	2	1	1	1
2010 08 22	0	0	0	0	0	0	0	0	0	0	0	0	0	0	1	0	0	0	4	1	0	0	0	1	2	2	2
2010 08 23	5	0	0	0	1	1	1	1	4	2	0	0	0	0	1	1	1	1	7	1	0	0	0	1	2	2	4
2010 08 24	13	3	3	2	2	3	2	2	4	47	3	5	5	6	7	4	2	2	18	4	4	3	3	4	3	2	4
2010 08 25	15	4	5	2	2	2	2	2	2	31	4	4	3	6	5	4	2	3	20	5	5	2	3	3	2	2	3
2010 08 26	11	3	2	3	1	2	1	4	2	18	4	3	4	5	3	2	1	0	11	3	4	3	2	2	2	2	2
2010 08 27	10	2	2	3	3	2	2	1	3	20	2	3	3	6	3	3	1	2	14	2	3	3	4	3	3	2	4
2010 08 28	5	3	1	2	1	1	1	1	1	15	3	2	3	5	4	1	1	1	7	3	2	3	1	2	1	1	2
2010 08 29	2	1	0	1	0	0	0	1	1	1	1	0	1	0	0	0	0	1	2	2	0	1	0	0	0	0	1
2010 08 30	0	0	0	0	0	0	0	0	0	0	0	0	0	0	0	0	0	1	2	1	0	0	0	0	0	0	1
2010 08 31	2	0	0	0	1	2	1	1	1	1	0	0	0	0	0	1	1	0	2	1	0	0	0	1	0	1	1

APPENDIX H: .avg File Structure

```
$Rx.GdpStn=450
$Rx.Stn=450
$Rx.Length=100 m
$Rx.Cmp=Zxy
Z.mwgt, Z.pwgt, Freq,   Tx.Amp, Z.mag,  Z.phz,   ARes.mag, SRes,   Z.%err, Z.perr, ARes.%err, Coher
1,      1,      0.125,  *,      14.674, -2323.3, 344.5,    344.5,  8.2,    166.2,  16.5,      0.89
1,      1,      0.1875, *,      16.713, -2377.5, 297.95,   297.95, 8.2,    165.3,  16.4,      0.85
1,      1,      0.25,   *,      16.649, -2460.8, 221.74,   221.74, 5.9,    118.5,  11.8,      0.9
1,      1,      0.375,  *,      19.129, -2573.2, 195.16,   195.16, 2.7,    53.4,   5.3,       0.95
1,      1,      0.5,    *,      21.656, -2677.9, 187.59,   187.59, 2.7,    53.9,   5.4,       0.98
1,      1,      0.75,   *,      23.043, -2649.2, 141.6,    141.6,  9.8,    196.9,  19.6,      0.98
1,      1,      1,      *,      23.739, -2729.4, 112.71,   112.71, 1.4,    27.1,   2.7,       0.99
1,      1,      1.5,    *,      27.166, -2725.9, 98.396,   98.396, 2.6,    52.5,   5.2,       0.97
1,      1,      2,      *,      27.301, -2709.9, 74.536,   74.536, 2.5,    50.2,   5,         0.97
1,      1,      3,      *,      28.885, -2659,   55.624,   55.624, 9.4,    188.9,  18.8,      0.97
1,      1,      4,      *,      31.581, -2600.7, 49.869,   49.869, 12.8,   257.5,  25.5,      0.98
1,      1,      6,      *,      36.457, -2476.8, 44.305,   44.305, 0.8,    15.7,   1.6,       0.99
1,      1,      8,      *,      42.918, -2458.7, 46.05,    46.05,  0.4,    9,      0.9,       1
```

Sample AMT/MT .AVG File

Z.mwgt: Electric field weight, -1 indicates polarity flip.
Z.pwgt: Magnetic field weight, -1 indicates polarity flip.
Freq: Frequency (hertz).
Tx.Amp: Square wave current (amperes), none in AMT/MT.
Z.mag: Impedance magnitude (km/sec).
Ares.mag: Cagniard apparent resistivity magnitude (ohm-m).
SRes: Static-corrected apparent resistivity added by ASTATIC (ohm-m).
Z%err: Relative |Z| error (%).
Z.perr: Phase(Z) error (mrad).
Ares.%err: Relative apparent resistivity error (%).
Coher: Coherence, or spectral ratio, of cross-correlated electric and magnetic fields (dimensionless), where 1 denotes perfect signal coherence between the fields.